



Girling, Kathryn (2011) *Heterogeneously catalysed isomerisation of allylbenzene*. MSc(R) thesis.

<http://theses.gla.ac.uk/2399/>

Copyright and moral rights for this thesis are retained by the author

A copy can be downloaded for personal non-commercial research or study, without prior permission or charge

This thesis cannot be reproduced or quoted extensively from without first obtaining permission in writing from the Author

The content must not be changed in any way or sold commercially in any format or medium without the formal permission of the Author

When referring to this work, full bibliographic details including the author, title, awarding institution and date of the thesis must be given



University  
of Glasgow

# Heterogeneously Catalysed Isomerisation of Allylbenzene

**Kathryn Girling**  
**BSc Hons**

Submitted in fulfilment of the requirements for the degree of  
MSc

**University of Glasgow**  
**Department of Chemistry**

**September 2010**

© Kathryn Girling 2010

## ABSTRACT

The current method for the isomerisation of aromatic alkenes involves super stoichiometric quantities of liquid base (KOH) in higher alcohols [1-7]. Acid catalysis of such transformations produces a cis:trans ratio near to one [8]. It is well documented that solid bases catalyse double bond migration through the abstraction of an allylic proton forming an anionic intermediate [9-11]. Solid bases hold a significant advantage over acid catalysis as they promote double bond migration without carbon-carbon bond interruption [12]. In addition, solid base catalysts provide an environmentally benign method of producing a mixture of cis/trans isomers, which could potentially find application in the pharmaceutical [13] and perfumery industries [14].

Activated potassium carbonate supported on alumina was found to be active at 50°C for the isomerisation of allylbenzene. Where isomerisation of aliphatic alkenes has reportedly given high cis:trans ratios, the isomerisation of aromatic alkenes appears to favour the formation of the trans-isomer. The formation of the trans-isomer suggests that the thermodynamic stability of this isomer controls the outcome of the reaction.

The optimum  $K_2CO_3$  loading was found to be 15% with higher loadings leading to pore blockage and reduced surface areas. Spray impregnation was found to produce an active catalyst that produced high conversions, which however rapidly became deactivated. The alumina supplier had a significant effect on the product alkene selectivity. Engelhard AL-3992E was found to produce a catalyst that allowed for high product selectivity.

Catalyst deactivation occurred via two processes. BET analysis showed a 25% reduction in surface area post reaction which, served as evidence of coke formation. Additionally, TGA-DSC analysis showed that under thermal treatment benzene was desorbed from the catalyst post reaction. It is thought that aromatic reactants/products act as poisons. Chemisorption through multiple bonds and back-bonding [15] causes aromatic species to block active sites required for further reaction. It was also noted that with increasing LHSV, the deactivation of the catalyst increased. This led to the determination of a negative first order of reaction, with respect to the concentration of allylbenzene.

## **ACKNOWLEDGEMENTS**

Firstly I would like to thank my supervisor Professor S. D. Jackson for his unyielding advice and support. Thank you for having faith in me as a chemist.

To Ron Spence, thank you for fixing everything that mysteriously stopped functioning. Thank you for all of your help.

A big thank you must go to Andy Monaghan for putting up with my constant badgering and for helping me with all of my analysis.

I would also like to thank other members of the research group, namely Fiona Wigzell and Lynsey Pugh for proof reading and general advice.

Finally, I'd like to thank my friends and family for putting up with me, especially while I was writing up. To Gavin McCutcheon I owe many a thank you and probably a large drink! Also to Daniel, thank you for your words of encouragement and for bullying me towards the end to get finished, I couldn't have done it without you!

## **AUTHOR'S DECLARATION**

I declare that, except where explicit reference is made to the contribution of others, that this thesis is the result of my own work and has not been submitted for any other degree at the University of Glasgow or any other institution.

Signature \_\_\_\_\_

Printed Name \_\_\_\_\_

# CONTENTS

<b>A</b>	<b>FIGURES</b>	<b>9</b>
<b>B</b>	<b>TABLES</b>	<b>13</b>
<b>1.</b>	<b>BACKGROUND</b>	<b>15</b>
<b>2.</b>	<b>INTRODUCTION</b>	<b>19</b>
<b>2.1</b>	<b>Catalysis</b>	<b>19</b>
<b>2.2</b>	<b>Heterogeneous versus Homogeneous Catalysis</b>	<b>20</b>
<b>2.2.1</b>	<b>Adsorption</b>	<b>20</b>
<b>2.3</b>	<b>Solid Catalysts</b>	<b>22</b>
<b>2.3.1</b>	<b>Metals</b>	<b>22</b>
<b>2.3.2</b>	<b>Metal Loading</b>	<b>23</b>
<b>2.3.3</b>	<b>Oxides</b>	<b>23</b>
<b>2.3.4</b>	<b>Zeolites</b>	<b>24</b>
<b>2.3.5</b>	<b>Solid Acids</b>	<b>24</b>
<b>2.3.6</b>	<b>Solid Bases</b>	<b>24</b>
<b>2.4</b>	<b>Catalyst Deactivation</b>	<b>25</b>
<b>2.4.1</b>	<b>Poisoning</b>	<b>25</b>
<b>2.4.2</b>	<b>Carbon lay-down</b>	<b>25</b>
<b>2.4.3</b>	<b>Sintering</b>	<b>26</b>
<b>2.5</b>	<b>Basic Catalysis</b>	<b>27</b>
<b>2.6</b>	<b>Potassium Carbonate</b>	<b>31</b>
<b>2.7</b>	<b>Alumina</b>	<b>32</b>
<b>2.8</b>	<b>Project</b>	<b>34</b>

<b>3.</b>	<b>AIM</b>	<b>35</b>
<b>4.</b>	<b>EXPERIMENTAL</b>	<b>37</b>
4.1	Catalyst Preparation	37
4.2	Catalyst Characterisation	39
4.2.1	Surface Area Determination	39
4.2.2	Thermo-gravimetric analysis	39
4.2.3	X-ray Diffraction	40
4.2.3.1	High Temperature <i>in-situ</i> XRD	40
4.2.4	Raman Spectroscopy	42
4.3	Materials	42
4.4	Trickle Bed Reactor	43
4.5	Experimental Procedure	44
4.5.1	Calcination	44
4.5.2	Activation	44
4.5.3	Set up	45
4.5.4	Standard Solutions	46
4.5.5	GC Analysis	47
4.5.6	Regeneration	47
4.5.7	Deactivation	48
4.5.7.1	Guard Bed	48
4.5.7.2	Water Addition	48
4.5.7.3	Effect of Concentration	49
4.5.8	Caesium	49
4.5.9	Post-mortem analysis	49
4.5.9.1	XRD	49
4.5.9.2	TGA-DSC	49
4.5.9.3	BET	50

<b>5.</b>	<b>RESULTS</b>	<b>51</b>
<b>5.1</b>	<b>Catalyst Characterisation</b>	<b>51</b>
<b>5.1.1</b>	<b>Surface area determination</b>	<b>51</b>
<b>5.1.2</b>	<b>TGA-DSC profiles</b>	<b>52</b>
<b>5.1.2.1</b>	<b>Alumina</b>	<b>52</b>
<b>5.1.2.2</b>	<b>Potassium Carbonate</b>	<b>53</b>
<b>5.1.2.3</b>	<b>Inert Decomposition</b>	<b>56</b>
<b>5.1.2.4</b>	<b>Calcination</b>	<b>59</b>
<b>5.1.2.5</b>	<b>Activation</b>	<b>61</b>
<b>5.1.3</b>	<b>High Temperature <i>in-situ</i> XRD</b>	<b>63</b>
<b>5.1.4</b>	<b>Raman Spectroscopy</b>	<b>64</b>
<b>5.2</b>	<b>Catalyst Testing</b>	<b>67</b>
<b>5.2.1</b>	<b>Alumina</b>	<b>68</b>
<b>5.2.2</b>	<b>Preparation Methods</b>	<b>68</b>
<b>5.2.3</b>	<b>K<sub>2</sub>CO<sub>3</sub> Loading</b>	<b>73</b>
<b>5.2.4</b>	<b>Alumina Supplier</b>	<b>77</b>
<b>5.3</b>	<b>Regeneration</b>	<b>79</b>
<b>5.4</b>	<b>Deactivation</b>	<b>80</b>
<b>5.4.1</b>	<b>Water Addition</b>	<b>80</b>
<b>5.4.2</b>	<b>Guard Bed</b>	<b>81</b>
<b>5.5</b>	<b>Caesium</b>	<b>82</b>
<b>5.6</b>	<b>Effect of Concentration</b>	<b>84</b>
<b>5.7</b>	<b>Post Reaction Analysis</b>	<b>86</b>
<b>5.7.1</b>	<b>TGA-DSC</b>	<b>86</b>
<b>5.7.1.1</b>	<b>Glove Box</b>	<b>86</b>
<b>5.7.1.2</b>	<b>Air</b>	<b>92</b>
<b>5.7.2</b>	<b>XRD</b>	<b>95</b>
<b>5.7.3</b>	<b>BET</b>	<b>96</b>

<b>6.</b>	<b>DISCUSSION</b>	<b>97</b>
<b>6.1</b>	<b>Catalyst Characterisation</b>	<b>97</b>
<b>6.1.1</b>	<b>Surface area determination</b>	<b>97</b>
<b>6.1.2</b>	<b>TGA-DSC Analysis</b>	<b>98</b>
<b>6.1.2.1</b>	<b>Support</b>	<b>98</b>
<b>6.1.2.2</b>	<b>Potassium Carbonate</b>	<b>98</b>
<b>6.1.2.3</b>	<b>Inert Atmosphere</b>	<b>99</b>
<b>6.1.2.4</b>	<b>Calcination</b>	<b>101</b>
<b>6.1.2.5</b>	<b>Activation</b>	<b>103</b>
<b>6.1.3</b>	<b>XRD Analysis</b>	<b>105</b>
<b>6.1.4</b>	<b>Raman Spectroscopy</b>	<b>105</b>
<b>6.2</b>	<b>Post Reaction Analysis</b>	<b>109</b>
<b>6.2.1</b>	<b>XRD</b>	<b>109</b>
<b>6.2.2</b>	<b>TGA-DSC</b>	<b>109</b>
<b>6.3</b>	<b>Deactivation</b>	<b>111</b>
<b>6.3.1</b>	<b>Poisoning</b>	<b>111</b>
<b>6.3.2</b>	<b>Coke Formation</b>	<b>112</b>
<b>6.4</b>	<b>Regeneration</b>	<b>114</b>
<b>6.5</b>	<b>Preparation Methods</b>	<b>115</b>
<b>6.6</b>	<b>K<sub>2</sub>CO<sub>3</sub> Loading</b>	<b>118</b>
<b>6.7</b>	<b>Alumina Supplier</b>	<b>118</b>
<b>6.8</b>	<b>Caesium</b>	<b>121</b>
<b>6.9</b>	<b>Product Distribution</b>	<b>122</b>
<b>6.10</b>	<b>Future Work</b>	<b>123</b>
<b>7.</b>	<b>CONCLUSIONS</b>	<b>125</b>
<b>8.</b>	<b>REFERENCES</b>	<b>127</b>

## **A. FIGURES**

<b>Figure 1.1: Isomerisation of alkenyl aromatics</b>	<b>15</b>
<b>Figure 1.2: Isomerisation of Eugenol</b>	<b>16</b>
<b>Figure 1.3: Isomerisation of Estragole</b>	<b>16</b>
<b>Figure 2.1: Energy Profile</b>	<b>19</b>
<b>Figure 2.2: Catalytic Processes</b>	<b>21</b>
<b>Figure 2.3: Representation of coke formation and poisoning</b>	<b>26</b>
<b>Figure 2.4: Crystallite migration and atomic migration</b>	<b>27</b>
<b>Figure 2.5: Strength of solid base catalysts</b>	<b>29</b>
<b>Figure 2.6: Isomerisation of 1-butene with anionic intermediates</b>	<b>30</b>
<b>Figure 2.7: Reaction of <math>K_2CO_3</math> with Brønsted acid sites on <math>\gamma</math>-alumina</b>	<b>32</b>
<b>Figure 2.8: Different Forms of Alumina</b>	<b>33</b>
<b>Figure 2.9: Examples of alumina hydroxyl groups</b>	<b>33</b>
<b>Figure 3.1: Isomerisation of Allylbenzene</b>	<b>35</b>
<b>Figure 4.1: The BET equation</b>	<b>39</b>
<b>Figure 4.2: Schematic of hot-stage XRD chamber</b>	<b>41</b>
<b>Figure 4.3: The Scherrer Equation</b>	<b>41</b>
<b>Figure 4.4: Trickle Bed Reactor</b>	<b>44</b>
<b>Figure 4.5: Calibration for Allylbenzene</b>	<b>47</b>
<b>Figure 5.1: TGA profile of support in <math>O_2/Ar</math></b>	<b>52</b>
<b>Figure 5.2: TGA-DSC profiles of support in <math>O_2/Ar</math></b>	<b>53</b>
<b>Figure 5.3: TGA profile of Potassium Carbonate</b>	<b>54</b>
<b>Figure 5.4: TGA-DSC profiles for Potassium Carbonate</b>	<b>54</b>
<b>Figure 5.5: Mass Spectrometry data m/e 18</b>	<b>55</b>
<b>Figure 5.6: Mass Spectrometry data m/e 44</b>	<b>56</b>
<b>Figure 5.7: TGA - Inert Decomposition of P2013</b>	<b>57</b>

<b>Figure 5.8: TGA-DSC Inert Decomposition of P2013</b>	<b>57</b>
<b>Figure 5.9: Inert Decomposition Mass Spectrometry Data m/e 18</b>	<b>58</b>
<b>Figure 5.10: Inert Decomposition Mass Spectrometry Data m/e 44</b>	<b>58</b>
<b>Figure 5.11: P2030 TGA weight profile in oxygen</b>	<b>59</b>
<b>Figure 5.12: P2030 TGA-DSC profiles in oxygen</b>	<b>60</b>
<b>Figure 5.13: P2030 Mass Spectrometry data m/e 18</b>	<b>60</b>
<b>Figure 5.14: P2030 Mass Spectrometry data m/e 44</b>	<b>61</b>
<b>Figure 5.15: TGA profile for activation of calcined P2008</b>	<b>62</b>
<b>Figure 5.16: TGA-DSC profile for activation of calcined P2008</b>	<b>62</b>
<b>Figure 5.17: XRD of Catalyst P2026 at room temperature and 500°C</b>	<b>63</b>
<b>Figure 5.18: Raman Spectrum of K<sub>2</sub>CO<sub>3</sub></b>	<b>64</b>
<b>Figure 5.19: Raman Spectrum for Engelhard AL-3992E Alumina</b>	<b>65</b>
<b>Figure 5.20: Raman Spectrum of Catalyst P2013 at room temperature</b>	<b>65</b>
<b>Figure 5.21: Raman Spectra for calcination of catalyst P2013</b>	<b>66</b>
<b>Figure 5.22: Catalyst P2013 post-calcination Raman Spectrum</b>	<b>67</b>
<b>Figure 5.23: Isomerisation of Allylbenzene</b>	<b>67</b>
<b>Figure 5.24: (P2008) Conversion of allylbenzene against time</b>	<b>69</b>
<b>Figure 5.25: (P2015) Conversion of allylbenzene against time</b>	<b>69</b>
<b>Figure 5.26: (P2030) Conversion of allylbenzene against time</b>	<b>70</b>
<b>Figure 5.27: Deactivation Constants</b>	<b>71</b>
<b>Figure 5.28: Yield of trans-β-methyl styrene for P2008/P2015/P2030</b>	<b>72</b>
<b>Figure 5.29: Conversion for loadings 12%, 15%, 18% and 20%</b>	<b>74</b>
<b>Figure 5.30: Yield of trans- isomer for loading catalysts</b>	<b>75</b>
<b>Figure 5.31: 15%/20% Engelhard Alumina Catalysts</b>	<b>76</b>
<b>Figure 5.32: % Conversion against time for each alumina supplier</b>	<b>77</b>
<b>Figure 5.33: % Yield of TBMS for each alumina supplier</b>	<b>78</b>
<b>Figure 5.34: Concentration of trans-β-methyl styrene</b>	<b>79</b>
<b>Figure 5.35: Conversion of allylbenzene plus water over P2013</b>	<b>80</b>

<b>Figure 5.36: Conversion of allylbenzene over P2013 plus guard bed</b>	<b>81</b>
<b>Figure 5.37: Conversion of allylbenzene against time on stream (Cs)</b>	<b>83</b>
<b>Figure 5.38: Conversion against WHSV at 90 minutes on stream</b>	<b>84</b>
<b>Figure 5.39: Determination of kinetic order with respect to concentration of feed solution (-0.672) at 90 minutes on stream</b>	<b>85</b>
<b>Figure 5.40: TGA profile P2023 in Oxygen</b>	<b>87</b>
<b>Figure 5.41: TGA-DSC Profile P2023 in Oxygen</b>	<b>87</b>
<b>Figure 5.42: Mass Spectrometry Data P2023 in Oxygen m/e 18</b>	<b>88</b>
<b>Figure 5.43: Mass Spectrometry Data P2023 in Oxygen m/e 44</b>	<b>89</b>
<b>Figure 5.44: Mass Spectrometry Data P2023 in Oxygen m/e 78</b>	<b>89</b>
<b>Figure 5.45: Mass Spectrometry Data for P2023 in Oxygen m/e 118</b>	<b>90</b>
<b>Figure 5.46: Possible fragmentation of ethylbenzene</b>	<b>91</b>
<b>Figure 5.47: TGA profile for P2023 in Oxygen</b>	<b>92</b>
<b>Figure 5.48: TGA-DSC profile for P2023 in Oxygen</b>	<b>93</b>
<b>Figure 5.49: Mass Spectrometry data m/e 18</b>	<b>93</b>
<b>Figure 5.50: Mass Spectrometry data m/e 44</b>	<b>94</b>
<b>Figure 5.51: Mass Spectrometry data m/e 78</b>	<b>94</b>
<b>Figure 5.52: Mass Spectrometry data m/e 118</b>	<b>95</b>
<b>Figure 5.53: XRD for Catalyst P2023 post-reaction</b>	<b>96</b>
<b>Figure 6.1: Weight loss profile for Potassium Carbonate</b>	<b>99</b>
<b>Figure 6.2: Weight loss profile of P2013 in Argon (~100°C)</b>	<b>100</b>
<b>Figure 6.3: Weight loss profile of P2013 in Argon (200-400°C)</b>	<b>101</b>
<b>Figure 6.4: Weight loss profile of P2030 in Oxygen (~100°C)</b>	<b>102</b>
<b>Figure 6.5: Weight loss profile for calcined P2008</b>	<b>104</b>
<b>Figure 6.6: Raman Spectrum of Caesium Carbonate</b>	<b>105</b>
<b>Figure 6.7: Raman Active Vibrations</b>	<b>106</b>
<b>Figure 6.8: Bands Observed in Raman Spectrum of K<sub>2</sub>CO<sub>3</sub></b>	<b>107</b>

<b>Figure 6.9: TGA-DSC analysis of Catalyst P2023 from Glove box</b>	<b>110</b>
<b>Figure 6.10: Proposed mechanism for coke formation</b>	<b>112</b>
<b>Figure 6.11: Conversion of Allylbenzene against time on stream for P2008, P2015 and P2030</b>	<b>115</b>
<b>Figure 6.12: Conversion of Allylbenzene against time on stream</b>	<b>119</b>
<b>Figure 6.13: Isomerisation of allylbenzene via anionic intermediate</b>	<b>123</b>

## B TABLES

<b>Table 4.1:</b>	<b>Catalysts prepared</b>	<b>37</b>
<b>Table 4.2:</b>	<b>Alumina Surface Area Measurements</b>	<b>38</b>
<b>Table 4.3:</b>	<b>List of Materials</b>	<b>42</b>
<b>Table 5.1:</b>	<b>Surface Area Measurements</b>	<b>51</b>
<b>Table 5.2:</b>	<b>Catalysts formed by different Preparation Methods</b>	<b>68</b>
<b>Table 5.3:</b>	<b>Selectivity of cis/trans- isomers</b>	<b>71</b>
<b>Table 5.4:</b>	<b>Comparison of catalysts with different nominal K<sub>2</sub>CO<sub>3</sub> loading</b>	<b>73</b>
<b>Table 5.5:</b>	<b>Selectivity of cis/trans- isomers</b>	<b>74</b>
<b>Table 5.6:</b>	<b>Selectivity of cis/trans- isomers</b>	<b>76</b>
<b>Table 5.7:</b>	<b>Catalysts prepared using alumina support material provided by different suppliers</b>	<b>77</b>
<b>Table 5.8:</b>	<b>Selectivity of cis/trans- isomers</b>	<b>78</b>
<b>Table 5.9:</b>	<b>Deactivation constants</b>	<b>81</b>
<b>Table 5.10:</b>	<b>Selectivity of cis-/trans- isomers</b>	<b>82</b>
<b>Table 5.11:</b>	<b>Product selectivity for Cs<sub>2</sub>CO<sub>3</sub>/AL-3992E and K<sub>2</sub>CO<sub>3</sub>/AL-3992E</b>	<b>83</b>
<b>Table 5.12:</b>	<b>Determination of kinetic order with respect to concentration of allylbenzene at 90 minutes on stream</b>	<b>84</b>
<b>Table 5.13:</b>	<b>Comparison of surface area determination analysis pre/post reaction P2023</b>	<b>96</b>
<b>Table 6.1:</b>	<b>Surface Area Measurements</b>	<b>97</b>
<b>Table 6.2:</b>	<b>Bands Observed (cm<sup>-1</sup>) in Raman Spectra of K<sub>2</sub>CO<sub>3</sub>/Al<sub>2</sub>O<sub>3</sub></b>	<b>108</b>
<b>Table 6.3:</b>	<b>Product Selectivity for Loading Catalysts</b>	<b>110</b>
<b>Table 6.4:</b>	<b>Surface area measurements for Catalyst P2023</b>	<b>114</b>
<b>Table 6.5:</b>	<b>Surface Area Measurements</b>	<b>116</b>

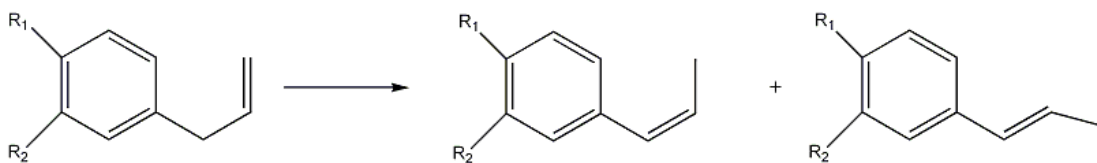
<b>Table 6.6:</b>	<b>Product Alkene Selectivity</b>	<b>116</b>
<b>Table 6.7:</b>	<b>Surface area measurements for % K<sub>2</sub>CO<sub>3</sub> catalysts</b>	<b>118</b>
<b>Table 6.8:</b>	<b>Surface area measurements for Alumina Supplier Catalysts</b>	<b>119</b>
<b>Table 6.9:</b>	<b>Surface area catalyst: surface area of alumina</b>	<b>120</b>
<b>Table 6.10:</b>	<b>Product Alkene selectivity for Alumina Supplier Catalysts</b>	<b>121</b>

## 1. BACKGROUND

The isomerisation of alkenyl aromatics is an important transformation with the corresponding iso-compounds finding application in the pharmaceutical and fragrance industries [16, 17].

This type of transformation involves the migration of the double bond from the terminal position to a position conjugated with the benzene ring. Such a reaction can be highly desirable if readily available alkenyl aromatics can be used to produce less accessible and often more valuable products [17]. The isomerisation of these compounds always produces a mixture of cis- and trans- compounds with the trans- isomer being the more thermodynamically stable of the two [1]. The isomerisation of some alkenyl aromatic compounds is shown in figure 1.1.

**Figure 1.1: Isomerisation of alkenyl aromatics**



where  $R_1, R_2 = H$  is allylbenzene;

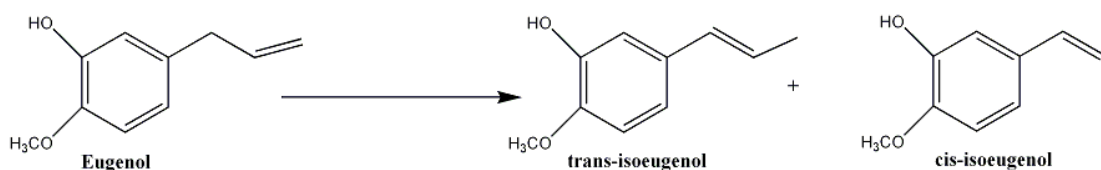
$R_1, R_2 = CH_3O$  is dimethoxyallylbenzene (4-allyl-1, 2-dimethoxybenzene);

$R_1 = OH, R_2 = CH_3O$  is eugenol (2-methoxy-4- (2-propenyl) phenol);

and  $R_1 = CH_3O, R_2 = H$  is estragole (4-allylanisole).

The isomerisation of eugenol, for example as shown in figure 1.2, produces its corresponding alkenyl alkoxybenzene, isoeugenol which finds application in pharmaceuticals [13] and in a wide variety of blossom compositions in fragrances [14].

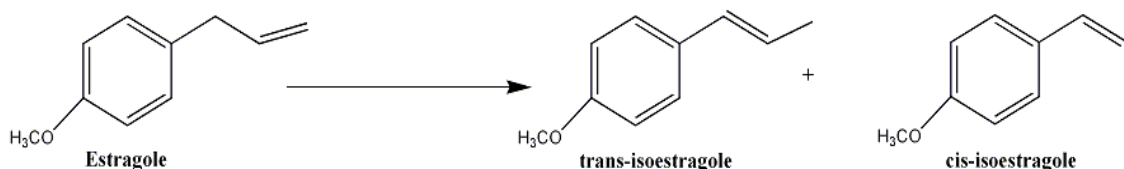
**Figure 1.2: Isomerisation of Eugenol**



The current methodology for this type of transformation involves an alkaline base catalyst [2-7]. Such reactions are catalysed at high temperatures by means of KOH in alcoholic solutions [1]. However, these bases are often used in super-stoichiometric quantities in relation to the compound to be isomerised. The result is unacceptably large quantities of caustic waste streams, which poses handling problems. Post-synthesis work up and separation of spent KOH solution from liquid products also make this method unfavourable.

Solutions of KOH are also used, as a liquid base, for the isomerisation of 1-methoxy-4-(2-propen-1-yl) benzene (Estragole), which is shown in figure 1.3.

**Figure 1.3: Isomerisation of Estragole**



The isomerisation of estragole produces a mixture of trans-isoestragole and cis-isoestragole. The main component in many ethereal oils is trans-isoestragole which is used widely in the perfume and cosmetic industries. Trans-isoestragole is also used in large quantities in the alcoholic beverage industry and in the formulation of oral hygiene products. Contrastingly, the cis-isomer has yet to find any significant use due to its toxicity, burning taste and disagreeable odour [12].

It has been well documented that olefinic hydrocarbons possessing allylic hydrogen atoms undergo isomerisation under catalytic influence of strong bases [18, 19]. Such bases reported are potassium amide, lithium-ethylene-diamine systems and organosodium compounds [20]. It has also been proven that the stronger the base, the easier the double

bond migration [18]. Base catalysis promotes a high cis/trans ratio whereas reactions catalysed by acids have ratios close to one [21]. Various test reactions have been used to identify the acid/base character of a catalyst, the most common of them being the isomerisation of but-1-ene to cis and trans-butenes, where the cis/trans ratio varies with acid-base character [21].

Although solid acids have been extensively studied [22-28] in literature as an environmentally friendly alternative to acids such as HF or H<sub>2</sub>SO<sub>4</sub>, solid bases have not been studied to the same extent. There are, however, several advantages to the application of a solid base over a liquid base. For instance, there are fewer disposal problems when a solid base catalyst is used since neutralisation is not required [29]. In addition, they are non-corrosive and make the separation and recovery of products, catalysts and solvent easier [24]. Thus, solid base catalysts present an environmentally benign and economical pathway for the synthesis of fine chemicals [30].

There are, however, some drawbacks associated with the use of a supported base catalyst for a given reaction. One of the reasons why the studies of heterogeneous basic catalysts are not as extensive as those of heterogeneous acidic catalysts is the requirement for severe pre-treatment conditions for active basic catalysts [18]. At relatively low temperatures the surface of these catalysts are covered with carbon dioxide, water, and oxygen and show no activity for base-catalysed reactions. The generation of basic sites requires high-temperature pre-treatment in order to remove carbon dioxide, water and in some cases oxygen [24, 31]. The removal of these adsorbed species from the surface is essential to reveal the oxide surface. Another reason for the limited use of heterogeneous basic catalysts arises from a rapid deactivation while being handled in the atmosphere. It is, therefore, desirable to pre-treat catalysts at high temperatures and handle them in the absence of air prior to use for the reaction [18].

Recently, a study explored the use of K<sub>2</sub>CO<sub>3</sub>/alumina catalyst in the isomerisation of allylbenzene, dimethoxy-allylbenzene, estragole and eugenol [32]. It was reported that K<sub>2</sub>CO<sub>3</sub>/alumina catalyst was active at 303K but rapidly deactivated, however, through the deposition of carbonaceous species. Interestingly, cis:trans ratios were reported to be in favour of the thermodynamically stable trans- isomer.

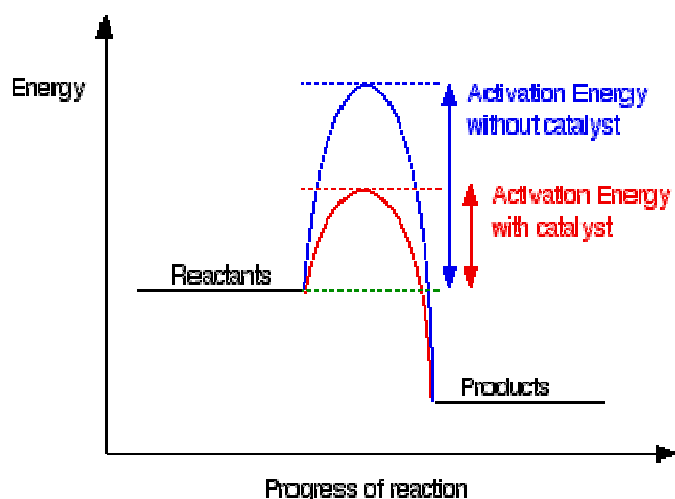
In this study, the isomerisation of allylbenzene, the simplest aromatic alkenyl compound, was investigated. Various  $K_2CO_3$ /alumina catalysts were used to determine the optimum metal loading required to produce a desirable yield and product distribution. Alumina supplier was also considered. Alumina from four different suppliers were used, namely Condea, Engelhard, La Roche and Alcoa.

## 2. INTRODUCTION

### 2.1 Catalysis

Sir Humphrey Davy first observed the phenomenon of catalysis during the development of the mine safety lamp in 1816. It was not until 1836, however, that Jakob Berzelius defined the term catalyst. A catalyst is a substance that increases the rate at which a chemical reaction will reach equilibrium without it itself being consumed in the process [33]. The action of the catalyst is called *catalysis* and it comes from two Greek words: the prefix *cata-* that meaning down and the verb *lysein* which means to split or break. Catalysts provide an alternative reaction pathway with the benefit of lower activation energy as shown in figure 2.1.

**Figure 2.1: Energy Profile [34]**



The use of a catalyst provides a higher reaction rate at the same given temperature. It does not however affect the equilibrium of the reaction; the rate of the forward reaction is increased thus the rate of the back reaction is also increased. Hence the energy profile for a catalysed reaction and an uncatalysed reaction differ only in the height of the activation curve.

Examples may be found in nature in the form of enzymes that act as highly selective catalysts for the innumerable chemical reactions that take place within organisms, subsequently sustaining the activities of life. Industrially, it is reported that catalysts contribute to one-sixth of the value of all manufactured goods. Today over 90% of the

chemical manufacturing processes employed worldwide utilise a catalyst in one form or another [35].

Two main factors govern the choice of a particular catalyst for a specific reaction: the activity and the selectivity required [36]. The activity of a catalyst is a measure of the rate at which a compound *A* can be converted to compound *B*. Whereas, the selectivity can be defined as the sum of the rate by which the desired product is produced divided by the rate by which all other products are produced as shown below:

$$\text{Selectivity} = (\text{rate}_{\text{dp}} / \sum(\text{rate}_{\text{op}}))$$

If a catalyst exhibits a high selectivity for a desired product then the rate at which it is formed is greater than the rate at which all other products are formed.

Before a catalyst is chosen for a given reaction these factors must be addressed and the following also considered: type of catalyst, the desired product(s) and the preferred reaction conditions. The type of catalyst is very important as some materials will show no activity for a given reaction and/or even react themselves.

## **2.2 Heterogeneous versus Homogenous Catalysis**

There are two main forms in which a catalyst may exist, namely heterogeneous or homogeneous. Homogeneous catalysts exist in the same phase as that of the reactants whereas the former describes a system in which the catalyst exists in a different phase than that of the reactants. Typically heterogeneous catalysts exist in solid form while reactants are liquids/gases. As this study focuses on the use of a solid catalyst and liquid reactants, the processes associated with heterogeneous catalysis will be discussed further. Before a reaction can take place on the catalyst surface, the reactants must firstly associate with it via a process called adsorption.

### **2.2.1 Adsorption**

Adsorption comprises of two processes that is chemisorption and physisorption. Physisorption is a term given to the action of reactant molecules associating with a catalyst

surface by weak van der Waals forces. Chemisorption, in contrast, involves the formation of chemical bonds. In a solid catalyst, covalent bonds exist between atoms however the atoms at the surface do not have their full complement of atomic neighbours resulting in one or more free valencies [33]. The interaction of reactant molecules with these free valencies can cause a formal chemical bond to be formed. This process is involved in catalysis and is referred to as chemisorption.

In heterogeneous catalysis the reactant molecules adsorb on the surface of the catalyst where the reaction takes place and then product molecules desorb from the surface as shown in figure 2.2.

**Figure 2.2: Catalytic Processes [37]**

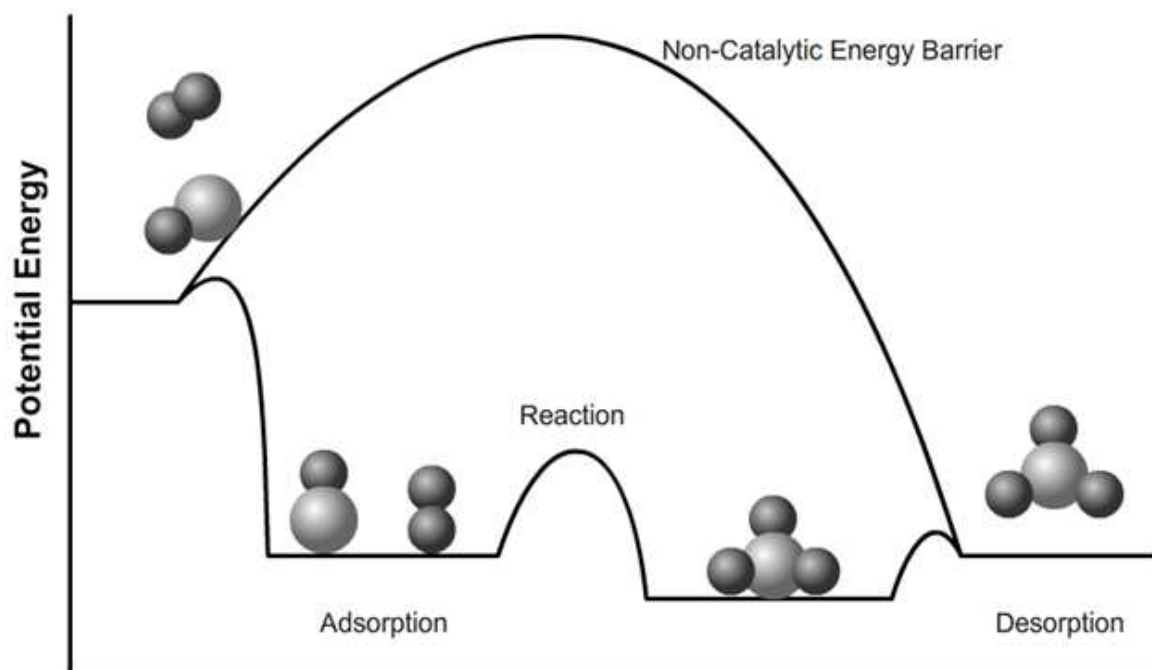


Figure 2.2 illustrates the process of adsorption, reaction and finally desorption of products in relation to potential energy. Since the catalyst's surface provides a reaction site the chemical and physical properties of such a surface are of great importance.

## 2.3 Solid Catalysts

Heterogeneous catalysts come in many forms but all have an active phase. The active phase can be equivalent to the bulk of the catalyst or it may be supported on a separate matrix.

### 2.3.1 Metals

Metal catalysts can be supported or unsupported. An important example of an unsupported metal is the skeletal metal Raney Nickel. Skeletal metal catalysts are prepared by the removal of one component of a bimetallic or polymetallic alloy or inter-metallic compound. The remaining material has a high surface area and microscopic spongy network of pores [38]. Raney Nickel is prepared by the action of sodium hydroxide on a powdered nickel aluminium alloy that leaves behind a high surface area nickel having a porous, sponge-like microstructure. Raney Nickel has found application in a range of catalytic transformations [39] for example the hydrogenation of monosaccharide (glucose, xylose etc.) and disaccharides (maltose, lactose etc.) aldoses to their respective alditols [40].

Noble metals are frequently used as the active phase in catalysts however they are expensive and so must be prepared as very small particles having a large surface to volume ratio. Although these particles are easily accessible, for example as colloidal dispersions, it is often more convenient to produce fine metal particles on a support in the form of supported catalysts [41]. The most common application for supported metal catalysts is the hydrogenation reactions [42, 43] however they are also used for hydrogenolysis reactions [44-46].

The primary role of a support material is to disperse the active phase providing a larger surface area and therefore improving the catalytic ability of the substance. In addition, the support also provides mechanical strength, thermal stability and gives the catalyst its shape. Support materials are often highly porous solids with very high surface areas, such as alumina ( $100\text{-}300\text{m}^2\text{g}^{-1}$ ), silica gel ( $300\text{-}800\text{m}^2\text{g}^{-1}$ ) [47] or activated carbon ( $610\text{-}$

1000m<sup>2</sup>g<sup>-1</sup>) [48]. As all of the catalysts that feature in this study are supported on alumina, this support material will be discussed further in a later section.

### **2.3.2 Metal Loading**

The fundamental characteristic of a successful supported catalyst is good dispersion of active phase over the surface of the support. Good dispersion allows for a high available surface area and therefore effective use of the catalytic metal. Monolayer dispersion is the optimum dispersion which can be achieved through maximising the surface:bulk ratio of the catalyst. To achieve this it is beneficial to aim for a low volume of crystals of micron size and instead try to achieve crystals of nano-size. Higher loadings of active phase can result in the formation of larger crystals through clustering of smaller particles. For a supported catalyst the active phase often constitutes 0.1-20 per cent by weight of the total catalyst [33], normally it exists in the form of very small crystallites (1 to 50nm in diameter), giving a high surface:bulk ratio.

### **2.3.3 Oxides**

Oxides generally belong in two categories, insulators or semiconductors. Insulator oxides such as alumina, silica and magnesia, which do not have redox properties, are poor oxidation catalysts. However, these materials find application as solid acids [49], solid bases and in other catalytic transformations such as dehydration [50, 51]. Semiconductor oxides are used in oxidations and are often metal species, which can exist in two different positive oxidation states [38]. Many oxides, such as Fe<sub>2</sub>O<sub>3</sub> and TiO<sub>2</sub>, are excellent oxidation catalysts because they possess redox properties, which allow them to interact with oxygen and indeed other molecules [38, 52]. Similarly, metal sulphides act as catalysts for reactions involving sulphur-containing reactants [53].

### **2.3.4 Zeolites**

Oxides such as alumina and silica can be used to form aluminosilicate crystalline materials called zeolites. These catalysts consist of about 10% alumina dispersed throughout a silica matrix [54]. Neither oxide exhibits a strong acidic character, however the resulting zeolite species exhibits marked acidity. Zeolites are used to catalyse hydrocarbon reactions that proceed via a carbonium-ion mechanism, for example in paraffin cracking [55]. Zeolites are often used as highly selective catalysts. The pore structure allows the catalyst to act as a molecular sieve and selectively catalyse reactions such as disproportionation of toluene [56, 57]. The size and shape of diffusing substrates and/or products are often closely matched to the pore diameter of the catalyst. This is referred to as molecular shape-selectivity. Aluminosilicate compounds tend to be microporous ( $<10\text{\AA}$ ) however newer zeolites such as aluminium phosphates have larger pores [47].

### **2.3.5 Solid acids**

Solid acids have been the most extensively studied of all heterogeneous catalysts [24-28]. This is mainly because they find application within the petroleum refinery industry. Following intensive research undertaken in 1950's and the realisation that heterogeneous cracking catalysts were acidic in nature, the study of supported acid catalysts has dominated within the field of heterogeneous catalysis [18]. Solid acids can be characterised by the presence of co-ordinately unsaturated cationic centres or protons on the surface. This leads to Brønsted or Lewis activity. Brønsted acids have the ability to donate a proton while Lewis acids possess the ability to accept a pair of electrons. Solid acid catalysts are used in a range of industrial processes such as catalytic cracking [9], paraffin isomerisation [8] and disproportionation of toluene [58].

### **2.3.6 Solid Bases**

The observation that sodium metal deposited on alumina acted as an effective catalyst for the isomerisation of olefins triggered much research in the field of solid base catalysis [19]. They offer several advantages over the use of liquid bases and are useful in the fine chemical industry. Solid base catalysts will be discussed more fully later.

## **2.4 Catalyst Deactivation**

Catalysts possess a finite lifetime due to catalyst deactivation. There are several processes by which a catalyst will experience a loss in activity or selectivity and inevitably, over time become deactivated. Some of these processes include catalyst poisoning, carbon lay-down (coking) and sintering.

### **2.4.1 Poisoning**

When a substance becomes adsorbed and retained on a catalyst surface, blocking active sites required by reactant molecules, the substance is referred to as a catalyst poison. A poison can be an impurity present in the feed stream, an intermediate formed during the reaction or the products themselves. If indeed the poison is a reaction product, the reaction can be termed as self-poisoned or self-inhibited [59]. The process of poisoning can be reversible or irreversible. If it is described as reversible, the impurity is often referred to as an inhibitor.

In addition, it is possible that the impurity present could serve as a catalyst for an undesirable reaction occurring simultaneously on the catalyst's surface [60]. Some selective poisons adsorb to specific sites on a catalyst so can be added to catalytic systems in order to control product selectivity [61]. Metallic catalysts are very sensitive to poisons; compounds containing sulphur and nitrogen are often found to poison metal catalysts. These compounds contain lone pairs of electrons that form strong donor bonds to the metal surface [62].

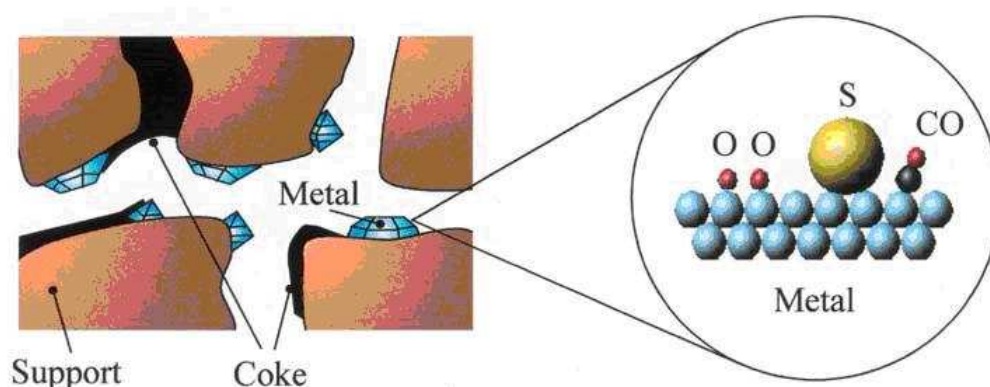
### **2.4.2 Carbon Lay-down**

Carbon lay-down describes a physical blockage (figure 2.3) caused by carbonaceous deposits (coke) on the catalyst surface. Often catalyst activity returns on the removal of the coke by burning. The rate and extent of carbon deposition can be affected by the structure of the hydrocarbon reactant. The more unsaturated the hydrocarbon the more willing it is to bond strongly to the surface of metal catalysts [63]. This is due to an

increase in carbon-metal bonds formed as soon as the molecule becomes chemisorbed. Aromatics compounds are well known for forming carbon on metal catalyst surfaces [64].

Additionally, unsaturated molecules can participate in multiple bonding, which can lead to undesirable transformations such as polymerisation and the production of carbon chains [63].

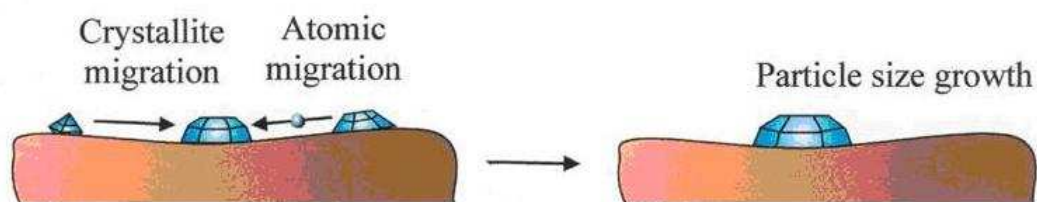
**Figure 2.3: Representation of coke formation and poisoning [65]**



### 2.4.3 Sintering

Thermal degradation or sintering is a common form of catalyst deactivation. Sintering is an irreversible physical process during which the effective catalytic area is reduced. In non-supported catalysts, sintering can cause a reduction in area and for supported catalysts it can cause growth of metal crystallites. The growth of metal crystallites can occur when metal crystals unite forming larger crystals with a lower surface area than that of the sum of the smaller crystals. There are three mechanisms for metal crystallite growth; crystallite migration, atomic migration and vapour transport [15]. Crystallite migration and atomic migration are shown in figure 2.4.

**Figure 2.4: Crystallite migration and atomic migration [65]**



Additionally, sintering can result in a loss of support area due to support collapse and a reduction of catalytic surface area due to pore collapse on crystallites of the active phase. The temperature at which sintering will occur can be affected by the strength of the interaction between metal and support, the nature of the support material and by metal loading.

## **2.5 Basic Catalysis**

The focus of this study is the use of a solid base catalyst therefore the definition and mechanisms of base catalysis will be discussed in detail in this section.

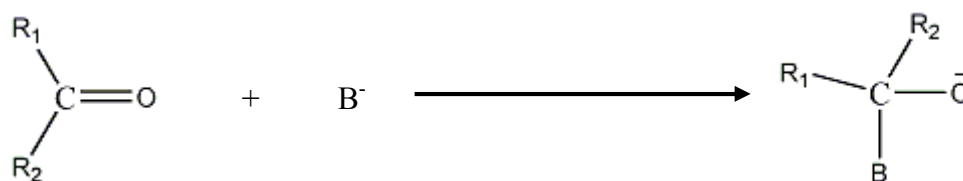
A solid base, following Brønsted and Lewis definitions, tends to accept a proton or donate an electron pair. Hence on the surface of a solid base catalyst there must be specific centres which function as base. The role played by these specific sites can be one of three depending on the combination of reactants and catalyst.

(1) Basic sites abstract protons from the reactant molecule forming carbanions ( $A^-$ ).



The isomerisation of 2, 3-dimethylbut-1-ene, for example, proceeds through the abstraction of a proton producing an anionic intermediate [10]. In this example, the basic site acts as a Brønsted base.

(2) In the case for reactants that are not activated by the abstraction of protons, such as aldehydes and ketones, the basic sites may act as Lewis Bases.



KF/Al<sub>2</sub>O<sub>3</sub> is effective for this type of reaction. The same surface site can equally act as a Brønsted base as well as a Lewis base depending on the nature of the reactant.

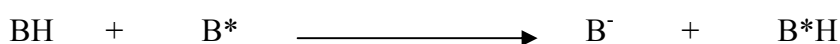
(3) Cooperative action of acidic and basic sites

One example of a catalyst that portrays this mechanism is magnesium oxide. It is active for the hydrogenation of 1, 3-butadiene and it is assumed heterolytic dissociation of hydrogen occurs in the presence of coordinatively unsaturated Mg<sup>2+</sup> and oxide ion [9, 18]. Adsorption of hydrogen then proceeds as follows:



In this case the magnesium ion acts as the acidic site and the oxygen ion acts as the basic site.

A suitable solid base must have the appropriate base strength for the specific reaction. If the removal of a proton is the initial reaction step then the acidity of the proton involved is also important. The base strength of solid base catalysts can be measured by the titration of adsorbed indicators having a wide range of pK<sub>a</sub> values [66]. For a reaction of an acid indicator (BH) with a solid base (B\*)

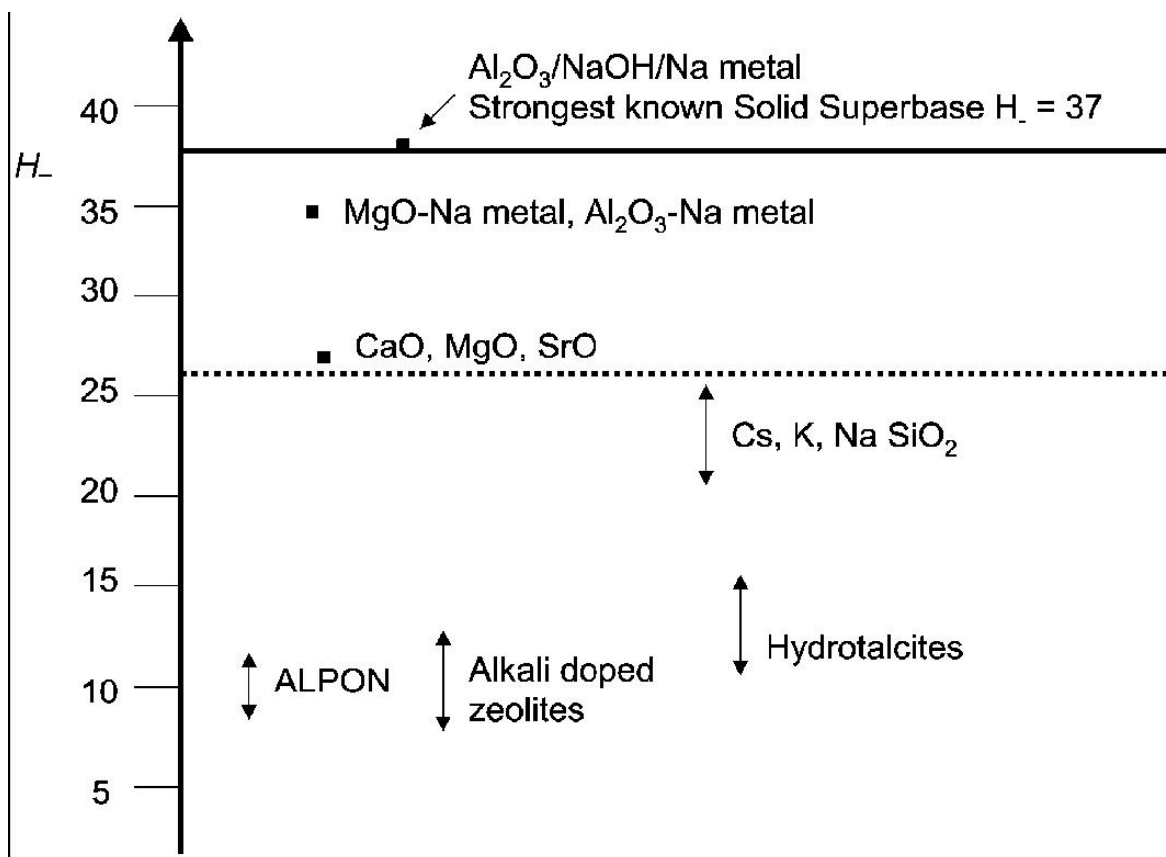


the Hammett basicity function, H<sub>-</sub>, is defined by

$$\text{H}_- = \text{pK}_a + \log [\text{B}^-]/[\text{BH}]$$

where [BH] is the concentration of the indicator and [B<sup>-</sup>] is the concentration of its conjugate form. Figure 2.5 gives an indication the strength of some solid base catalysts.

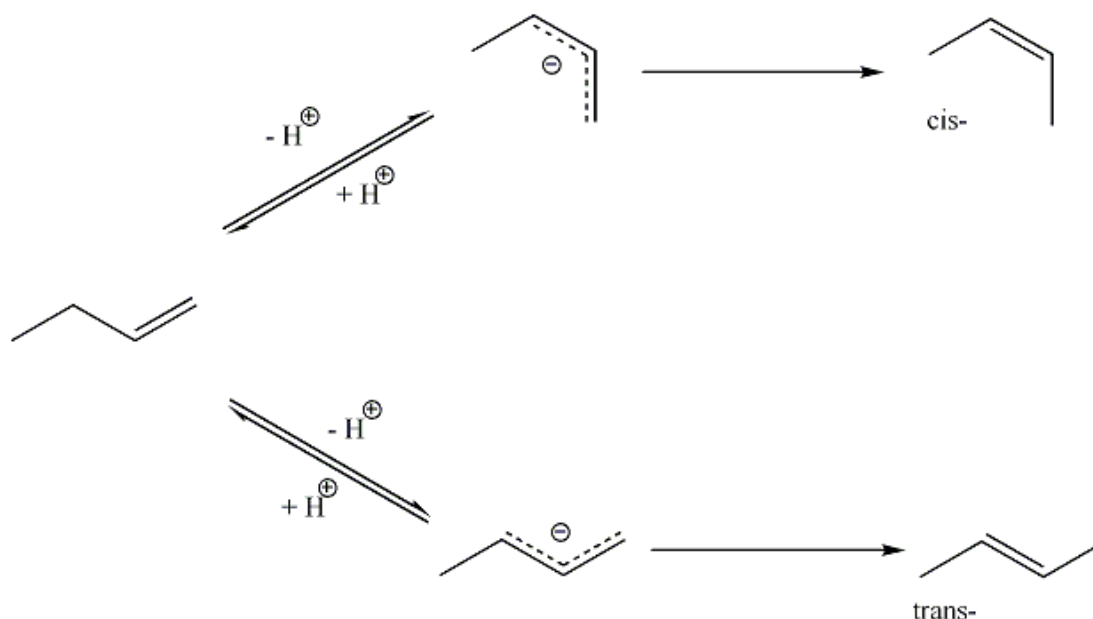
**Figure 2.5: Strength of solid base catalysts [67]**



Mild base materials are generally found in the region of  $H_0 = 5-10$  and include hydrotalcites and alkali doped zeolites. Materials which could be described as strongly basic belong in the region of  $H_0 = 20-25$ . Finally, superbasic materials such as alkaline metal based catalysts, like Na/NaOH/Al<sub>2</sub>O<sub>3</sub>, and alkaline earth oxides, like calcium oxide, have base strengths of  $H_0 > 26$ .

The isomerisation of an alkene using a solid base proceeds in stages forming anion intermediates by the removal of allylic proton [9] as shown in figure 2.6. Alkenes have high pK<sub>a</sub> values (pK<sub>a</sub> for propene = 38 [68]) so catalysts used are strongly basic [10].

**Figure 2.6: Isomerisation of 1-butene with anionic intermediates**



Strong base catalysts are often characterised by high catalytic activity for alkene isomerisation at relatively low temperatures [69]. In particular, alkali metal compounds are found to be very strong bases when supported on alumina. For instance, potassium compounds such as  $KNO_3$ ,  $KHCO_3$  and  $K_2CO_3$  on alumina, once heated at high temperature, have been shown to be highly active for the isomerisation of 1-butene (figure 2.6) at 273 K [70].

KF/alumina is another example of a solid base catalyst. It is thought that the basic nature of the catalyst arises from the hard  $F^-$  anion present on the surface [31]. In order to differentiate between KF/alumina and oxide catalysts, such as alkaline earth oxides, the performance of KF/alumina can be measured using a test reaction, namely the isomerisation of pentene. KF/alumina often undergoes a drying pre-treatment under  $200^\circ C$ , however this allows for a high probability that  $CO_2$  and  $H_2O$  molecules still exist on the surface, blocking the active sites. Hence pre-treatment of the catalyst at higher temperatures, above  $300^\circ C$ , is required to develop active sites capable of catalysing the double bond migration of 1-pentene to cis- and trans- 2-pentenes. At  $350^\circ C$  the catalyst shows maximum activity but by  $450^\circ C$  all activity has been lost. Cis- and trans-2-pentene were the only products and a high cis/trans ratio was observed with a conversion of 90%. It has been well documented that solid base catalysts exhibit a high selectivity for cis-2-olefin during 1-olefin isomerisation, as the more stable form of allylic anion is the cis-isomer [9]. With oxide type solid base catalysts, such as alkaline earth oxides, the product distribution appears close to equilibrium at a high conversion. This is due to rotational isomerisation between cis- and trans-2-olefins [31, 71]. Since, KF/alumina exhibits a high

cis/trans ratio and a high conversion of 1-pentene it is concluded that rotational isomerisation is slow on KF/alumina.

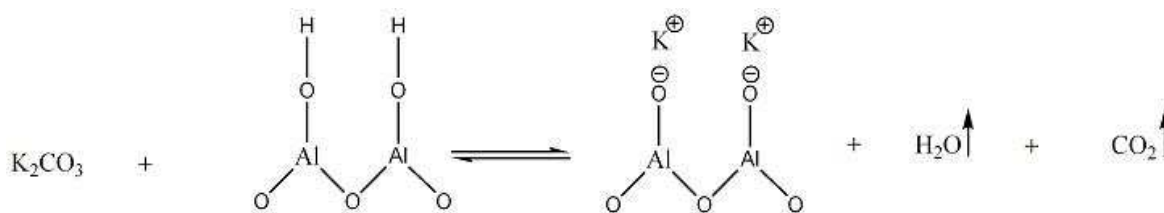
## 2.6 Potassium Carbonate

The catalysts used within this study were potassium carbonate supported on alumina. Potassium carbonate, in the solid phase, can be described as a hygroscopic compound, which means it easily attracts water molecules from its environment via adsorption.

Potassium carbonate supported on  $\gamma$ -alumina catalysts are often used for carbonyl sulphide (COS) hydrolysis [72] and they are active in the water gas shift reaction [73]. Previous studies suggest that potassium carbonate interacts strongly with the surface of alumina forming AlOK groups during thermal decomposition of supported potassium carbonate [74]. It was found that with increasing temperature potassium penetrates into the sub-layers of the lattice. Between temperatures of 247-297°C, CO<sub>2</sub> evolution occurs upon thermal decomposition. It is believed that simultaneously, OH groups once associated with K<sup>+</sup> are lost as water molecules.

Dotzel et al. [75] reported the reaction of K<sub>2</sub>CO<sub>3</sub> with  $\gamma$ -alumina releasing carbon dioxide at 284°C and 608°C. NH<sub>3</sub>-TPD (temperature programmed desorption) measurements indicated the presence of two different kinds of acid site. However, from the site that represented the Brønsted acid site, OH-groups were lost during TPD. It was therefore assumed that K<sub>2</sub>CO<sub>3</sub> reacts with the Brønsted acids sites as shown in figure 2.7.

**Figure 2.7 Reaction of  $K_2CO_3$  with Brønsted acid sites on  $\gamma$ -alumina**



It has also been suggested that potassium carbonate modifies the acid-base properties of alumina and can influence physical properties such as surface area, density and pore volume of activated aluminas [76].

## 2.7 Alumina

The support material used in this study was alumina. Alumina typically has a surface area of  $1-300\text{m}^2\text{g}^{-1}$  and is naturally weakly basic; however various suppliers can offer acidic, basic and neutral forms [47]. Alumina supports can be made by thermal dehydration of  $Al(OH)_3$  (Gibbsite or Bayerite) or  $AlOOH$  (Boehmite). Naturally, aluminium is found in the form of an ore (Bauxite) consisting of aluminium hydroxides, silica and other oxides. It is extracted from the ore by treatment with  $NaOH$  and produces  $Na_2Al_2O_4$  solution from which Gibbsite is obtained through crystallisation. Hence the alumina formed contains alkali metal, in this case sodium, co-crystallised within the structure. For alkali-free alumina the process involves hydrolysis of aluminium alcoholate, e.g.  $Al(OC_2H_5)_3$ , which yields a gelatinous form of boehmite, also referred to as pseudo-boehmite [77]. Figure 2.8 shows the different forms of alumina, the starting materials used to form the different types and the characteristics for each type.

**Figure 2.8: Different Forms of Alumina [77]**

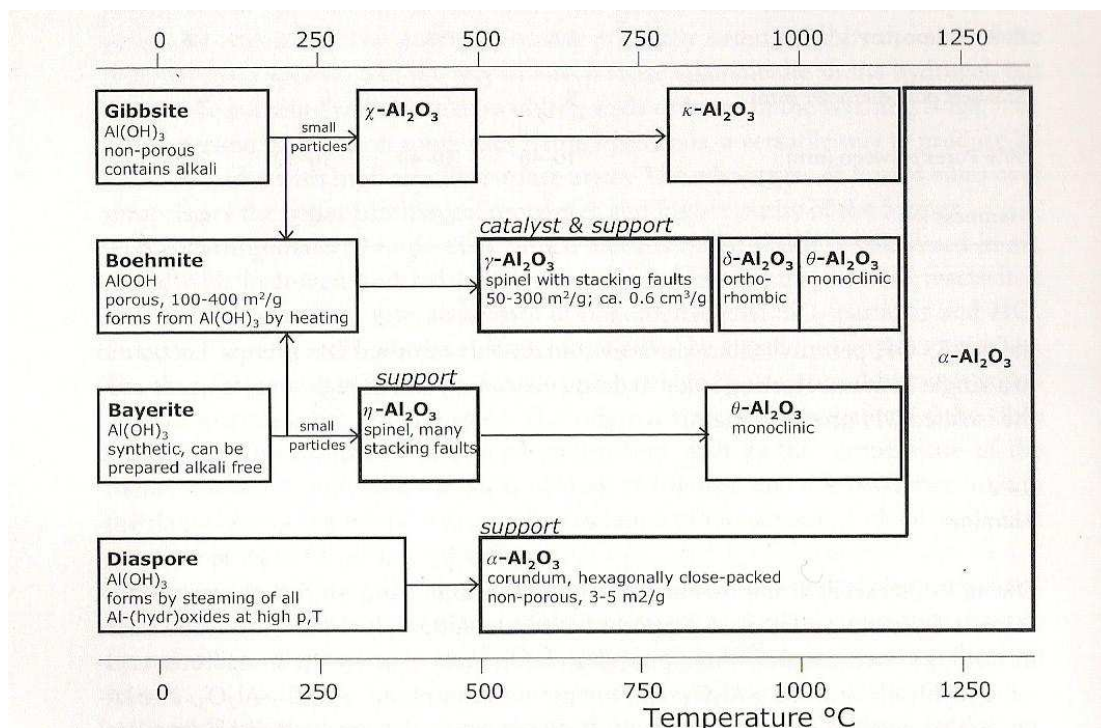
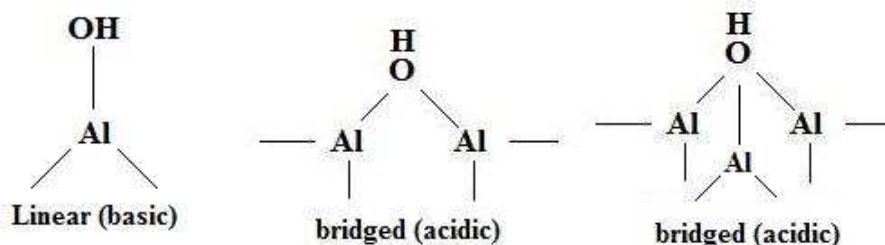


Figure 2.8 also shows the temperatures at which the different types of alumina will experience a phase change and the type of alumina that would be formed.

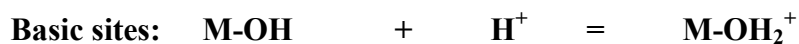
Alumina supports contain several types of hydroxyl groups that play a very important role in catalyst preparation. They represent anchoring sites where catalyst precursors can be attached to the support. Figure 2.9 illustrates some of the different types of alumina hydroxyl groups.

**Figure 2.9: Examples of alumina hydroxyl groups**



The surface of alumina can contain several hydroxyl groups; between 10 and 15 per nm<sup>2</sup>, the linear ones act as Brønsted bases (H<sup>+</sup> acceptors) and the bridged ones Brønsted acids (H<sup>+</sup> donors) [77].

In water, the hydroxyls react with protons and OH<sup>-</sup> groups, giving the surface ionic character. The following equilibria occur:



## 2.8 Project

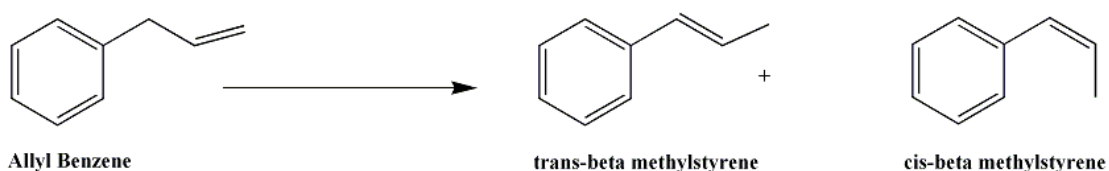
This project seeks to investigate the use of a solid base as an alternative to the current method for the isomerisation of aromatic alkenyls. Acid catalysis of aliphatic alkene isomerisation has been reported to produce cis:trans ratios close to one [21] and high cis:trans ratios have been reported through the use of a base catalyst [18, 19, 78]. Previous studies found KF/Al<sub>2</sub>O<sub>3</sub> catalysts [31, 79] and hydrotalcites [1] to be active for this transformation however high reaction temperatures were required. A recent study of the isomerisation of allylbenzene, dimethoxyallylbenzene, eugenol and estragole over a K<sub>2</sub>CO<sub>3</sub>/Al<sub>2</sub>O<sub>3</sub> reported activity at 303K with conversions of ~36% [32]. In contradiction with previous studies of base catalysed isomerisation of alkenes, such as butene [11, 70] and pentene [31], the more thermodynamically stable trans- isomer was the predominant product.

### 3. AIM

The aim of this study was to investigate the activity and the selectivity of potassium carbonate on alumina catalyst in the isomerisation of alkenyl aromatic compounds. It was decided that the simplest alkenyl aromatic (allylbenzene) would be used to minimise potential complications with reactive side groups.

This study will focus on the isomerisation of allylbenzene to a mixture of cis- and trans- $\beta$ -methyl styrene.

**Figure 3.1: Isomerisation of Allylbenzene**



As this was the first systematic study of these systems, we investigated 4 basic parameters.

#### i Preparation method

A series of catalysts were used to investigate firstly the effect the preparation method employed in the production of the catalyst had on the activity and selectivity of the catalyst.

#### ii % $K_2CO_3$ Loading

The percentage base loading was also varied and reactions were conducted to investigate the effect this had on catalyst deactivation and the overall yield of aromatic alkenyl isomers.

### **iii Alumina**

Finally, the alumina used in the preparation of these catalysts was sourced from a number of suppliers, each employing a different method for production of alumina support material. Reactions were conducted to explore the effect of different alumina supplies had on catalyst stability and selectivity.

### **iv Concentration of allylbenzene**

Reactions were conducted to investigate the effect of the concentration of the feed solution on the activity of the catalyst. A direct relationship between the concentration of allylbenzene feed solution and the rate of deactivation allowed for the determination of the order of reaction.

## 4. EXPERIMENTAL

### 4.1 Catalyst Preparation

A series of potassium carbonate supported on alumina catalysts were used throughout this project. All catalysts were prepared by the wetting of alumina with aqueous solutions of potassium carbonate to result in the desired nominal % w/w  $K_2CO_3$  loading. The method employed to produce the catalysts in the table below include wet impregnation, incipient wetness and spray impregnation. S. Watson prepared all of the catalysts shown in table 4.1.

**Table 4.1: Catalysts prepared**

Catalyst Code	Nominal $K_2CO_3$ loading / % w/w	Supplier and Supplier Code	Preparation method
P2008	15	Condea M-1206	Wet Impregnation
P2015	15	Condea M-1206	Incipient Wetness
P2030	15	Condea M-1206	Spray Impregnation
P2026	12	Condea M-1206	Incipient Wetness
P2023	15	Condea M-1206	Incipient Wetness
P2027	18	Condea M-1206	Incipient Wetness
P2019	20	Condea M-1206	Incipient Wetness
P2017	20	Engelhard AL-3992E	Incipient Wetness
P2013	15	Engelhard AL-3992E	Incipient Wetness
P2014	15	Alcoa CSS-200	Incipient Wetness
P2015	15	Condea M-1206	Incipient Wetness
P2016	15	La Roche 55-1 (ICI)	Incipient Wetness

The procedure of impregnation as a preparation method for a heterogeneous catalyst involves a certain volume of solution containing the precursor of the active phase. This is brought into contact with the solid support material and then dried to remove the solvent. There are two ways in which the solution can be contacted with the solid support material. One method involves using an excess quantity of solution and after a certain time the excess solvent is removed through drying. This method is called wet impregnation. The other method of impregnation is called incipient wetness and for this a solution of appropriate concentration, equal to if not slightly less than the pore volume of the solid, is used. This operation requires a level of control in which measurements must be precise and often applications need to be repeated. The solubility of the precursor in the solution therefore limits the maximum loading [80].

For catalysts prepared by wet impregnation, a solution of the correct amount of  $K_2CO_3$  in excess de-ionised water (500ml) was prepared. A round-bottomed flask was charged with alumina and the  $K_2CO_3$  solution. The flask was then attached to a Büchi Rotor-Vap and allowed to rotate in a water bath at  $60^\circ C$  until all of the water had evaporated (~ 20 hours). The sample was then dried in an oven at  $110^\circ C$  for 16 hours.

The second method, incipient wetness, was much the same as the first preparation method. However, rather than an excess of de-ionised water being used, the exact amount required to fill the pores of the alumina was used. The solution was added to alumina in a round-bottomed flask and the procedure for the previous method followed.

The following table shows the surface area measurements for the alumina support materials.

**Table 4.2: Alumina Surface Area Measurements**

Supplier and Supplier Code	Surface Area ( $m^2 g^{-1}$ )	Pore Diameter (nm)	Pore Volume ( $cm^3 g^{-1}$ )
Engelhard AL-3992 E	186	13.39	0.63
Alcoa CSS-200	201	7.86	0.39
Condea M-1206	220	10.27	0.57
La Roche 55-1 (ICI)	313	4.78	0.37

This means that preparation of 100g of 15% metal catalyst via incipient wetness would require 85g alumina support material and 15g of metal. The amount of water used would then depend on the pore volume of the support material. If for instance the support material used was Engelhard AL-3992 E (pore volume  $0.63 cm^3 g^{-1}$ ) then the maximum amount water that should be used is 135ml.

Finally, spray impregnation involved the preparation of a solution of  $K_2CO_3$  wherein the correct amount of  $K_2CO_3$  with the exact amount of de-ionised water required to saturate the pores of the alumina was used. A Pascall Mixer tumbling vessel was charged with alumina and the vessel rotated slowly. The  $K_2CO_3$ /de-ionised water solution was then sprayed as a fine mist into the vessel using a SG-1 Teflon sprayer. This process took about 15 minutes. The wet pellets were then allowed to rotate for one hour and then the sample dried in an oven at  $110^\circ C$  for 16 hours.

## 4.2 Catalyst Characterisation

Catalyst characterisation was conducted prior to reaction. For each catalyst, fines were produced and used in BET surface area measurements, thermo-gravimetric analysis and powder x-ray diffraction.

### 4.2.1 Surface Area Determination

The surface area and pore size for each catalyst was determined using a Micrometrics Gemini III 2375 Surface Area Analyser. Approximately 0.04g of the catalyst sample was weighed into a glass tube and degassed in a flow of N<sub>2</sub> overnight at 110°C before the measurement was carried out. Determining the number of molecules needed to form a monolayer is the underlying principle in surface area measurements. In practice however, the molecules may absorb to form multi-layers. The surface area was calculated using the BET (Brunauer-Emmett-Teller) equation:

**Figure 4.1: The BET equation**

$$\frac{P}{V(P_0 - P)} = \frac{1}{V_m C} + \frac{(C-1)P}{V_m C P_0}$$

Where

- V = volume of gas adsorbed at equilibrium pressure P,
- V<sub>m</sub> = volume necessary to form a monolayer,
- P<sub>0</sub> = saturated vapour pressure of the adsorbent gas at the temperature of measurement and
- C = constant.

For a supported catalyst, the BET method yields the total surface area of support and metal [77].

### 4.2.2 Thermo-gravimetric Analysis

Thermo-gravimetric analysis of each catalyst was performed on pre-reaction samples. The instrument used was a SDT Q600 series combined TGA, DSC instrument with online ESS Evolution Mass Spectrometer. Approximately 0.005g of sample was used. Each sample

was heated from room temperature to 700°C under an O<sub>2</sub>/Ar atmosphere with a flow rate of 100ml.min<sup>-1</sup> and a heating rate of 10°C.min<sup>-1</sup>. Species monitored with m/e equal to 18, 28, 44, which usually correspond to H<sub>2</sub>O, CO, and CO<sub>2</sub>. Samples for catalysts pre reaction were also heated from room temperature to 700°C under a N<sub>2</sub> atmosphere using the same flow and heating rate as before. The same species were monitored.

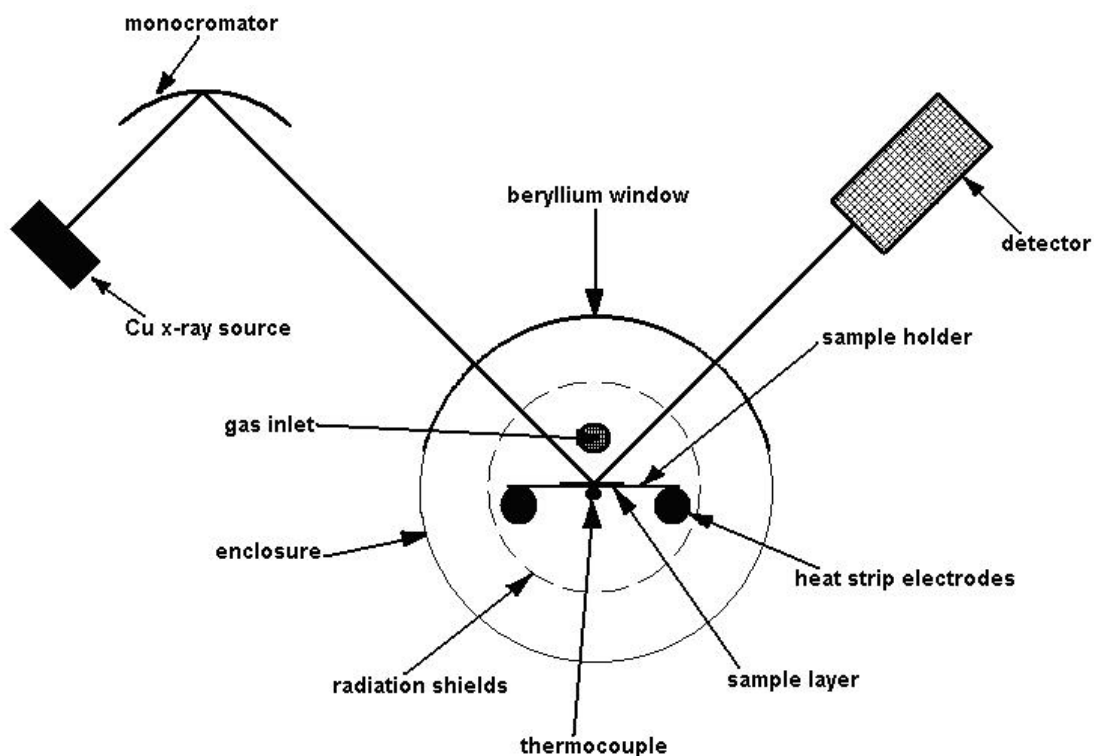
### **4.2.3 X-ray Diffraction**

XRD analysis was conducted on all catalysts pre- reaction. The apparatus used throughout was a Siemens D5000 X-ray Diffractometer (40kV, 40mA) using a monochromatised CuK<sub>α</sub> x-ray source (wavelength 1.5418Å). The scanning range used was 5° < 2θ < 80° with a step range size of 0.02° and counting time of 1 sec per step. Analysis was carried out at room temperature (25°C) and at 500°C.

#### **4.2.3.1 High Temperature *in-situ* XRD**

*In-situ* hot-stage XRD was performed under an argon atmosphere using an Anton Par XRK 900 heated reaction chamber. The unit comprises of a water-cooled, vacuum tight, stainless steel chamber with a beryllium window, shown in Figure 4.2.

**Figure 4.2: Schematic of hot-stage XRD chamber [81]**



The temperature programme used increases the temperature from ambient with a heating rate of  $12^{\circ}\text{C}\cdot\text{min}^{-1}$  to a maximum of  $700^{\circ}\text{C}$ , dwelling for 1 hour at  $100^{\circ}\text{C}$  intervals, starting at  $100^{\circ}\text{C}$ . A scan (scan speed 1) was taken after each dwell time in an  $\text{O}_2/\text{Ar}$  gas mix.

From the broadening of the peaks, it is possible to determine an average crystallite size by measuring the full width at half maximum (FWHM) of a peak, then applying the Scherrer equation:

**Figure 4.3: The Scherrer Equation**

$$t = K\lambda / \beta \cos\theta$$

Where:  $t$  = Average crystallite size

$K$  = Scherrer constant (0.87-1.0, normally taken to be 1.0)

$\lambda$  = the wavelength of the x-ray ( $1.5418 \text{ \AA}$ )

$\beta$  = the breadth of a reflection in radians  $2\theta$  (FWHM)

This is only an approximation as the results can be influenced by various factors such as lattice distortion and instrumental parameters.

#### 4.2.4 Raman Spectroscopy

Raman Spectroscopy was conducted on potassium carbonate and catalyst P2013 using a Horiba Jobin Yvon LabRAM HR. The laser used was a Kimmon IK series He-Cd laser. The wavelength used was 532.17nm, the objective x10 and the grating 600. A total of 5 samples were taken at a time with an exponential of 10 seconds, through a 100 $\mu$ m hole and at 50% power.

A sample of potassium carbonate and a sample of catalyst P2013 were heated from room temperature to 500°C under an O<sub>2</sub>/Ar atmosphere and measurements were taken every 100°C. The sample was then allowed to cool and a final measurement at ambient temperature was taken.

#### 4.3 Materials

The following materials were used throughout this project without further purification.

**Table 4.3: List of Materials**

<b>Material</b>	<b>Supplier</b>	<b>Purity</b>
Allylbenzene	Sigma-Aldrich	98%
Cis- $\beta$ -methylstyrene	Sigma-Aldrich	95%
Trans- $\beta$ -methylstyrene	Sigma-Aldrich	99%
4-Allyl-1,2-dimethoxybenzene	Sigma-Aldrich	99%
Cis/trans mixture 1,2-Dimethoxy-4-(1-propenyl)benzene	Sigma-Aldrich	99%
Eugenol	Sigma-Aldrich	99%
Isoeugenol cis/trans mixture	Sigma-Aldrich	98%
4-Allylanisole (Estragole)	Sigma-Aldrich	98%
Trans-anethole	Sigma-Aldrich	97%
Toluene	Fisher Scientific	99.99%
Acetone	VWR	100%
n-Decane	Avocado	99%
N <sub>2</sub>	BOC	99.98%
2% O <sub>2</sub> / Argon	BOC	99.95%
Potassium Carbonate	Sigma-Aldrich (ACS reagent)	$\geq$ 99.0%
Caesium Carbonate	Alfa Aesar	99.9%

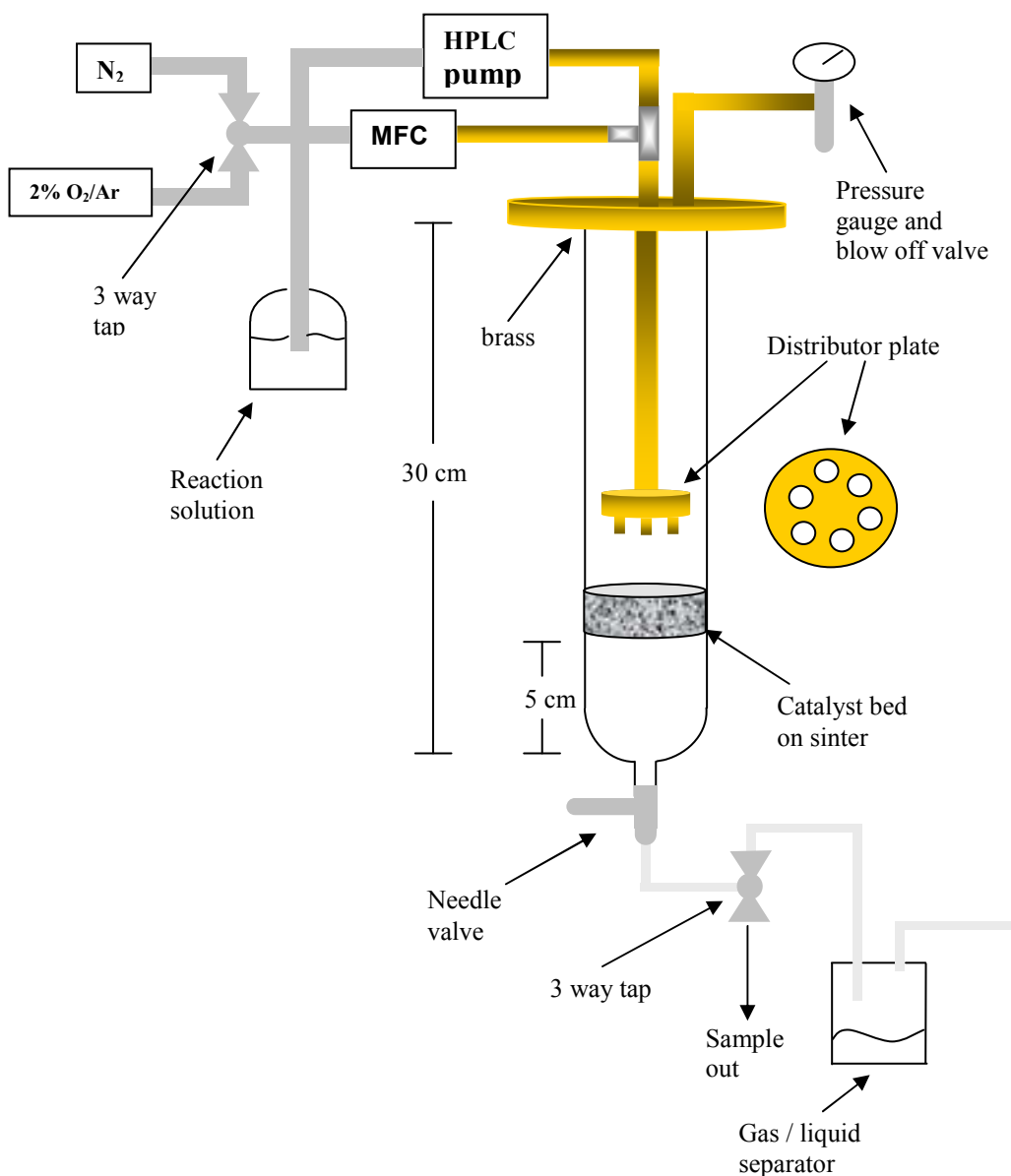
#### **4.4 Trickle bed reactor**

The trickle bed reactor employed for use in all experiments was 30cm in length with an internal diameter of 2.5cm and a sinter 5cm from the bottom of the reaction vessel. The gas flow rate was controlled by a mass flow controller (Gilson model 803c, maximum pressure 300 bar, flow range 0-100ml.min<sup>-1</sup>) and the liquid flow controlled by an HPLC pump (Gilson model 302).

A “showerhead” distributor was used to ensure a more dispersed fluid distribution over the catalyst. Nitrogen gas and a 2% gas mixture of oxygen in argon were available as gas feed when required.

The temperature of the catalyst bed was measured using a thermocouple located at the outside of the reactor wall. Control of temperature was achieved by a furnace attached to a DMG temperature controller (West 4400, accuracy  $\pm 1^{\circ}\text{C}$ ). The system had a pressure gauge (Doedijns, maximum 4 bar) fitted to monitor pressure and a relief valve for safety in the event of a reactor blockage.

**Figure 4.4: Trickle Bed Reactor**



## **4.5 Experimental procedure**

### **4.5.1 Calcination**

All catalysts were calcined prior to reaction in a muffle furnace. Each catalyst was heated over 5 hours to 550°C under a 1000ml.min<sup>-1</sup> flow of air. The temperature was kept constant for 16 hours and then the sample was allowed to cool to room temperature.

### **4.5.2 Activation**

Following calcination, the catalysts were then activated within the reaction vessel. Activation of a heterogeneous catalyst often refers to a number of different procedures

depending on the nature of the catalyst and its intended purpose. In this study activation of the catalyst involved thermal treatment. The catalyst was heated under a  $20\text{ml}\cdot\text{min}^{-1}$  flow of  $\text{N}_2$  gas to  $500^\circ\text{C}$ . This was to drive off adsorbed molecules, such as water, from the surface of the catalyst.

### 4.5.3 Setup

1.5g of catalyst was loaded into the reactor in four portions, adding inert fine particles between loadings. In this case, silicon carbide ( $180<\mu\text{m}<355$ ) fines were used. The first portion of catalyst was loaded followed by just enough silicon carbide fines to cover the bed of catalyst. The reactor was then tapped to ensure gaps between catalyst particles and the reactor walls were filled. The second loading of catalyst followed and another layer of silicon carbide. This procedure was repeated, (variation of Al-Dahhan and Duduković [82, 83] packing method) tapping the reactor after each loading of silicon carbide, until all four portions of catalyst had been loaded.

The catalyst was then heated over five hours to  $500^\circ\text{C}$  under a  $20\text{ml}\cdot\text{min}^{-1}$  flow of nitrogen. This temperature was maintained for 16 hours. Following activation, the catalyst was allowed to cool to  $50^\circ\text{C}$ .

A 2% reactant feed solution was prepared. Firstly 2ml of allylbenzene was measured out into a 100ml volumetric flask. Next, 1ml of an inert marker, in this case decane, was measured out and added to the flask. The purpose of the inert marker was to aid normalisation of GC results. Peak areas were measured for allylbenzene, both cis- and trans- isomers and indeed decane. The concentration of decane should remain constant throughout the reaction so the peak area recorded for decane can be used to normalise the peak areas recorded for the other species. This reduces the impact of variations caused by error in GC analysis.

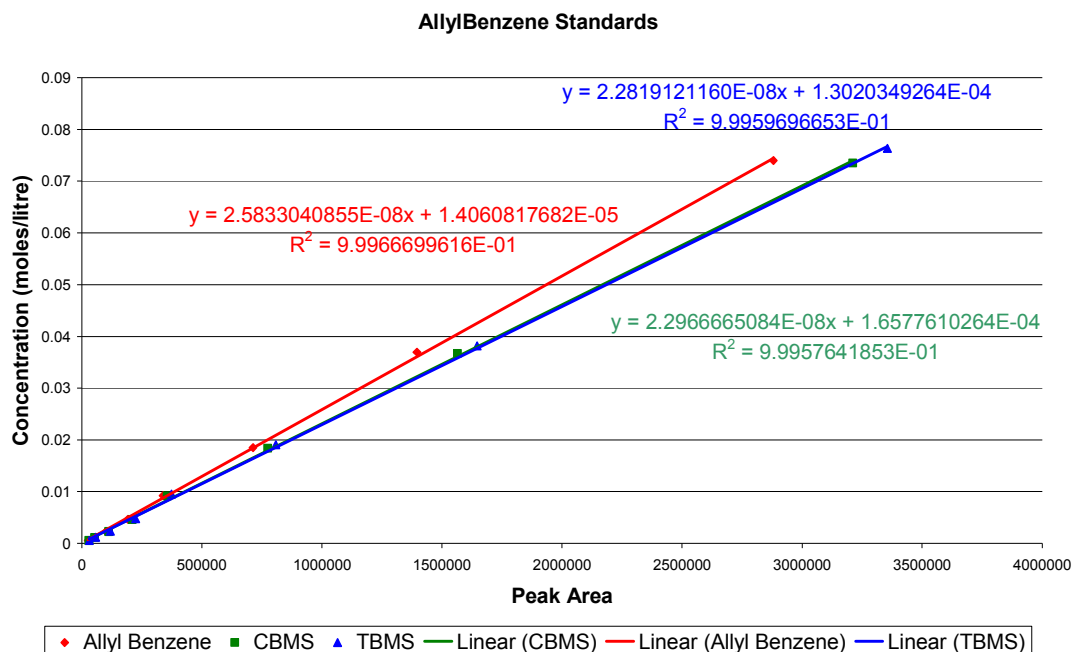
Before introduction of the feed solution, the catalyst bed was wetted for ten minutes using a  $1.5\text{ml}\cdot\text{min}^{-1}$  flow of toluene under nitrogen atmosphere ( $20\text{ml}\cdot\text{min}^{-1}$ ). A liquid hourly space velocity of  $30\text{h}^{-1}$  was maintained. The weight hourly space velocity for allylbenzene was calculated to be  $1.07\text{h}^{-1}$ .

Liquid samples (~2.5ml) were taken every five minutes for half an hour followed by sampling at fifteen minute intervals for a further hour and a half. From each of these samples 2ml was taken and added to a 10ml volumetric flask. Toluene was then added to these flasks to produce 10ml solutions of the product mixture. Initially samples were to be analysed by gas chromatography with a split flow of 500ml.min<sup>-1</sup> and a ratio of 250, however, this flow rate did not allow for reproducible results as it was outside the stable area of the GC. Thus a lower split flow (100ml.min<sup>-1</sup>) and ratio (50) was adopted after manual dilution of samples.

#### **4.5.4 Standard Solutions**

Standard solutions of known concentrations were prepared by the following method. Firstly 1ml of the starting material, allylbenzene, was measured out using a syringe and added to a 100ml volumetric flask. Next, 1ml of each isomer, cis- and trans- $\beta$ -methyl styrene, was measured out using another syringe and added to the same 100ml volumetric flask. Toluene was then added to the flask until the solution was 100ml. From this 100ml solution a 2ml sample was taken and analysed by gas chromatography. A 10ml sample was then taken from the original 100ml solution using a pipette and put into a 20ml volumetric flask. Toluene was added to this flask to make the solution up to a 20ml solution. A 2ml sample was taken from this flask and analysed by gas chromatography. A further 10ml was then taken from the newly diluted 20ml solution and placed into another 20ml volumetric flask using a pipette. This sample was then diluted using toluene and a sample taken for analysis using gas chromatography. This process was repeated, diluting each solution by half and a sample of each solution taken for GC analysis until 8 samples had been taken to be analysed. The peak areas of these solutions were then plotted against their known concentrations to produce calibration graphs. The graph below shows the correlation between peak area and moles giving correlation factors of  $R^2 < 9.99$ .

**Figure 4.5: Calibration for Allylbenzene**



#### 4.5.5 GC Analysis

Gas Chromatography analysis was obtained using a ThermoFinnigan Focus gas chromatograph fitted with a flame ionisation detector and using a 30m HP1701 column. The instrument was operated under an argon flow of 500ml.min<sup>-1</sup> and programmed as follows: An inlet temperature of 290°C, a split flow of 100ml.min<sup>-1</sup> and a split ratio of 50 were used. The auto-sampler used was an AI/AS 3000, the injection size was 1µl and the detector temperature was 250°C.

#### 4.5.6 Regeneration

Regeneration of the catalyst was attempted. Once sampling over 120 minutes was complete the system was flushed using toluene to remove traces of organic materials from the catalyst bed, under a nitrogen atmosphere for two hours. The flow of toluene was then stopped and the temperature set to increase slowly past the boiling point of toluene (110°C). At around 200°C, nitrogen gas feed was switched to a 2% O<sub>2</sub>/Ar mix. As the auto-ignite temperature of toluene is 480°C, the temperature was allowed to climb very slowly towards 500°C and all waste solvent was removed from the reactor chamber as a precaution. The temperature was held at 500°C for 16 hours under 2% O<sub>2</sub>/Ar. Subsequently, the gas feed was switched back to nitrogen for one hour at 500°C. After one hour, the catalyst was allowed to cool to 50°C at which the catalyst was wetted using

toluene, the reactant feed stock introduced and sampling at previously defined intervals occurred.

#### **4.5.7 Deactivation**

To investigate the means by which the catalyst becomes deactivated, alterations were made to the experimental procedure, as described below. Deactivation constants were calculating by plotting  $\ln[(C_0/C_A)-1]$  vs. time on stream.  $C_0$  and  $C_A$  are the initial concentration of allylbenzene and the concentration measured at point  $A$  respectively. The graph obtained shows a linear relationship where gradient  $k$  is equal to the deactivation constant.

##### **4.5.7.1 Guard bed**

To study deactivation of the catalysts, the effect of a guard bed was investigated. To do this an additional amount of support material was added on top of the original catalyst bed. 1.5g of catalyst was weighed out and loaded into the reactor with inert fines as previously described. Then on top of this 1.5g of support material only was loaded into the reactor. 2% allylbenzene feed stock was then introduced and sampling proceeded as normal.

##### **4.5.7.2 Water Addition**

In addition, the effect of water on the deactivation of the catalyst was studied. A volume of de-ionised water (50ml) was added to a 2% feed solution of allylbenzene in a partitioning column. Firstly, a 300ml solution of 2% allylbenzene feed solution was prepared. 50ml of de-ionised water was added to this solution and the mixture transferred into a partitioning column. The column was shaken to try and mix the liquids. Once the layers had separated, the feed solution was saturated with a low-level of water and appeared as an oily layer above the aqueous layer. The aqueous layer was removed and the oily layer placed in a feed solution bottle. The experimental procedure was followed as described previously.

### **4.5.7.3 Effect of Concentration**

A study of the effect of the concentration of reactant on catalyst deactivation was also carried out. Firstly, feed solutions of allylbenzene were prepared to 1%, 4% and 6% in toluene. They were prepared by the method described previously, this time halving, doubling or tripling the volume of allylbenzene used. The catalyst used throughout was catalyst P2015 and samples were taken in the usual fashion.

### **4.5.8 Caesium**

An additional experiment was performed involving caesium carbonate on alumina. The catalyst was prepared by incipient wetness and used in the isomerisation of allylbenzene. Caesium carbonate was used to investigate the effect of the use of a stronger base on the activity of the catalyst for the given isomerisation reaction.

### **4.5.9 Post Mortem analysis**

Catalyst characterisation methods were performed on one catalyst post-reaction to explore any differences in the catalyst samples.

#### **4.5.9.1 XRD**

A sample of catalyst P2023 was removed from the reaction vessel and allowed to dry in air. It was analysed at room temperature under an argon flow using a scanning range of  $5^{\circ} < 2\theta < 80^{\circ}$  with a step range size of  $0.02^{\circ}$  and counting time of 1 second per step.

#### **4.5.9.2 TGA-DSC**

Thermo-gravimetric analysis was performed on catalyst P2023 post reaction. After the reaction, the catalyst was removed from the reaction vessel and portioned. One portion of the catalyst was put into the glove box under an inert atmosphere to dry and await analysis. The second portion was left in air to dry and then analysed. The purpose of analysing two separate portions was to investigate the carbon and water composition of the catalyst taking the effect of the atmosphere into account. A sample of P2023 catalyst (0.005g) was heated from room temperature to  $700^{\circ}\text{C}$  under an  $\text{O}_2/\text{Ar}$  atmosphere with a flow rate of

100ml.min<sup>-1</sup> and at a rate of 10°C.min<sup>-1</sup>. Species monitored with m/e equal to 18, 28, 44, 78, 118 correspond to water, carbon monoxide, carbon dioxide, benzene and allylbenzene.

#### **4.5.9.3 BET**

Surface area, pore volume and pore diameter measurements were obtained for catalyst P2023 post reaction via the method described in section 4.2.1.

## 5. RESULTS

### 5.1 Catalyst Characterisation

#### 5.1.1 Surface area determination

BET analysis was carried out as described in section 4.2.1. The data obtained was tabulated below.

**Table 5.1: Surface Area Measurements**

Catalyst Code	Nominal K <sub>2</sub> CO <sub>3</sub> Loading / % w/w	Surface Area (m <sup>2</sup> g <sup>-1</sup> )	Pore Diameter (nm)	Cumulative Pore Volume (cm <sup>3</sup> g <sup>-1</sup> )
P2008	15	149	10.93	0.40
P2015	15	133	11.02	0.37
P2030	15	134	10.27	0.35
P2026	12	164	9.79	0.41
P2023	15	149	9.16	0.34
P2027	18	167	8.89	0.34
P2019	20	102	9.10	0.23
P2013	15	130	11.60	0.38
P2017	20	104	12.56	0.33
P2014	15	128	6.19	0.23
P2015	15	133	11.02	0.37
P2016	15	188	5.94	0.28

Catalysts with K<sub>2</sub>CO<sub>3</sub> loadings of 15% exhibited surface areas within the range 128-149m<sup>2</sup>g<sup>-1</sup> with the exception of P2016 (K<sub>2</sub>CO<sub>3</sub>/La Roche (55-1)). While catalyst P2026 with a lower loading of K<sub>2</sub>CO<sub>3</sub> (12%) exhibited a larger surface area than those catalysts with 15% loading. Catalysts P2017 and P2019 both had nominal loadings of 20% and exhibited much lower surface areas than those of 15% loading. Finally, catalyst P2027 (18% K<sub>2</sub>CO<sub>3</sub>/Condea M-1206) exhibited an increased surface area compared to that of catalysts with 15% loading.

## 5.1.2 TGA-DSC profiles

### 5.1.2.1 Alumina

TGA-DSC analysis was conducted on alumina to ensure that results observed were due to the catalyst itself not just the support material. The advantage of this was that changes in the support material could be separated from those of the active phase.

Engelhard AL-3992E support material was heated from room temperature to 700°C at a rate of 10°C.min<sup>-1</sup>. TGA-DSC analysis was conducted under an O<sub>2</sub>/Ar flow with a rate of 100ml.min<sup>-1</sup>.

**Figure 5.1: TGA profile of support in O<sub>2</sub>/Ar**

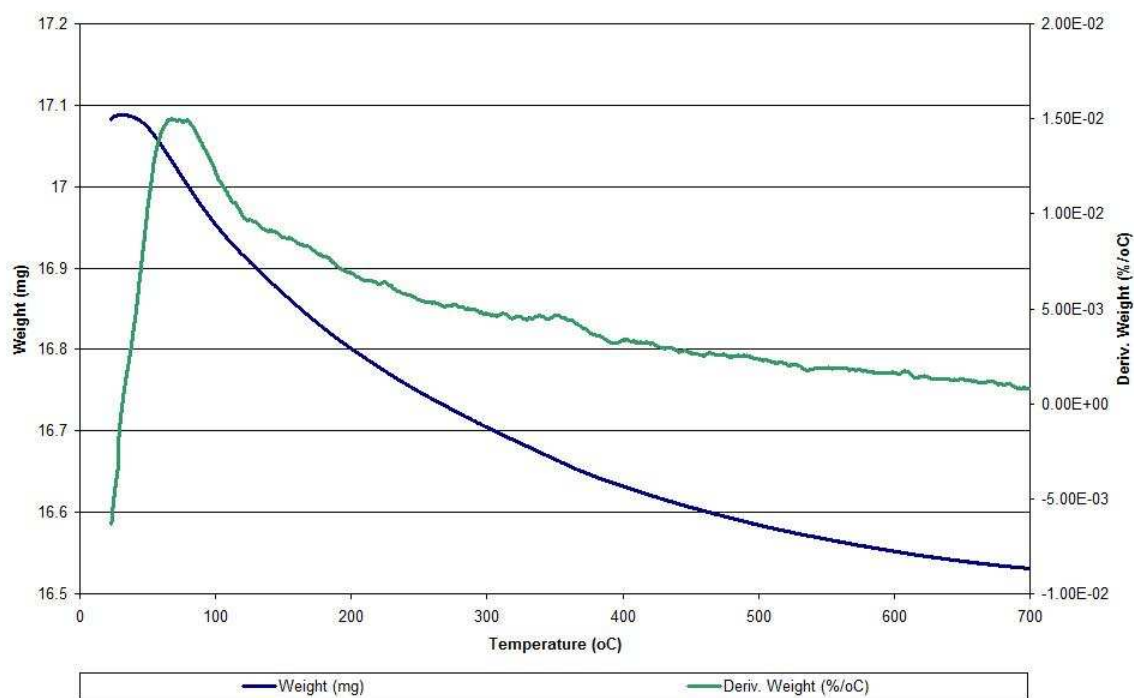


Figure 5.1 shows the weight and derived weight profile for alumina support. There is a continuous weight loss over the whole temperature range which is likely to correspond to the loss of surface OH groups as water. The overall weight loss for the sample was ~3%.

**Figure 5.2: TGA-DSC profiles of support in O<sub>2</sub>/Ar**

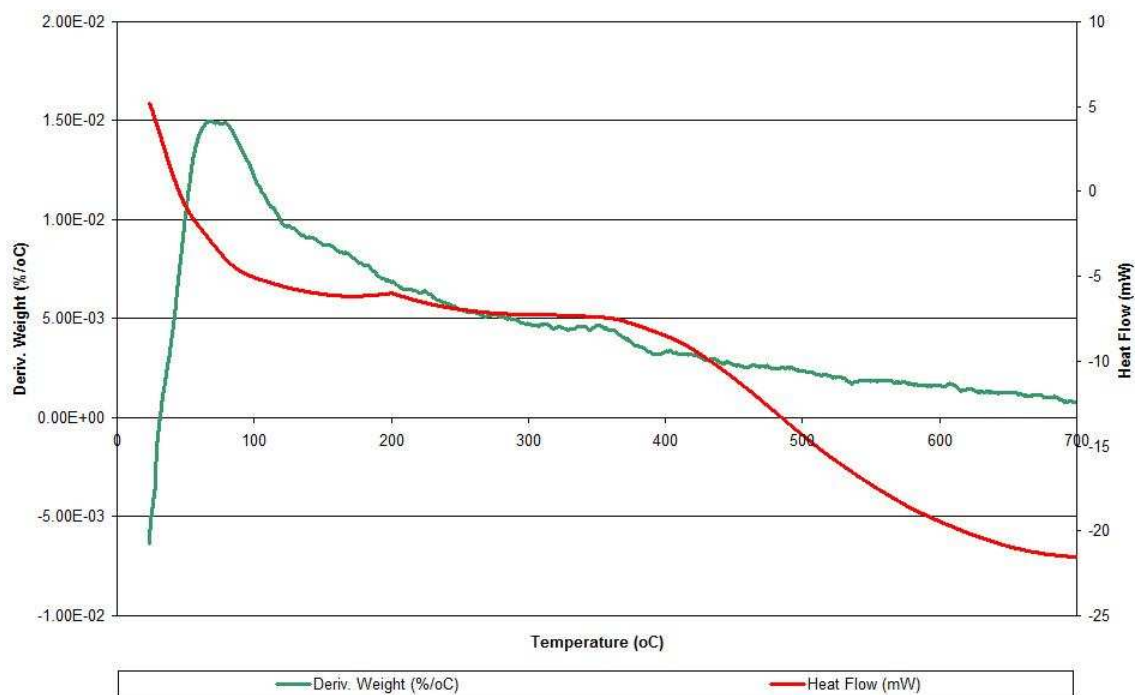
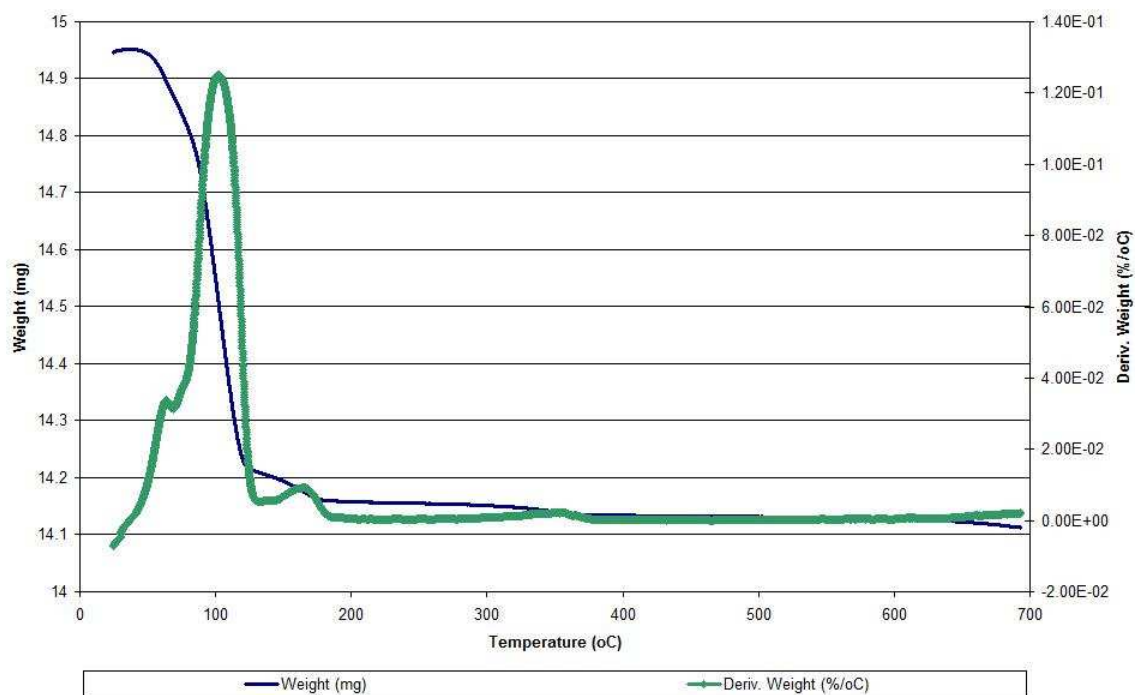


Figure 5.2 shows that the weight loss event before 100°C was endothermic and corresponded to ~1% weight loss.

### 5.1.2.2 Potassium Carbonate

TGA-DSC analysis was conducted on a sample of potassium carbonate. The sample was heated from room temperature to 700°C at 10°C.min<sup>-1</sup> under an O<sub>2</sub>/Ar atmosphere (flow rate of 100ml.min<sup>-1</sup>).

**Figure 5.3: TGA profile of Potassium Carbonate**



In figure 5.3 there is one main weight loss event at around 100°C with two smaller weight loss events at 165°C and 350°C.

**Figure 5.4: TGA-DSC profiles for Potassium Carbonate**

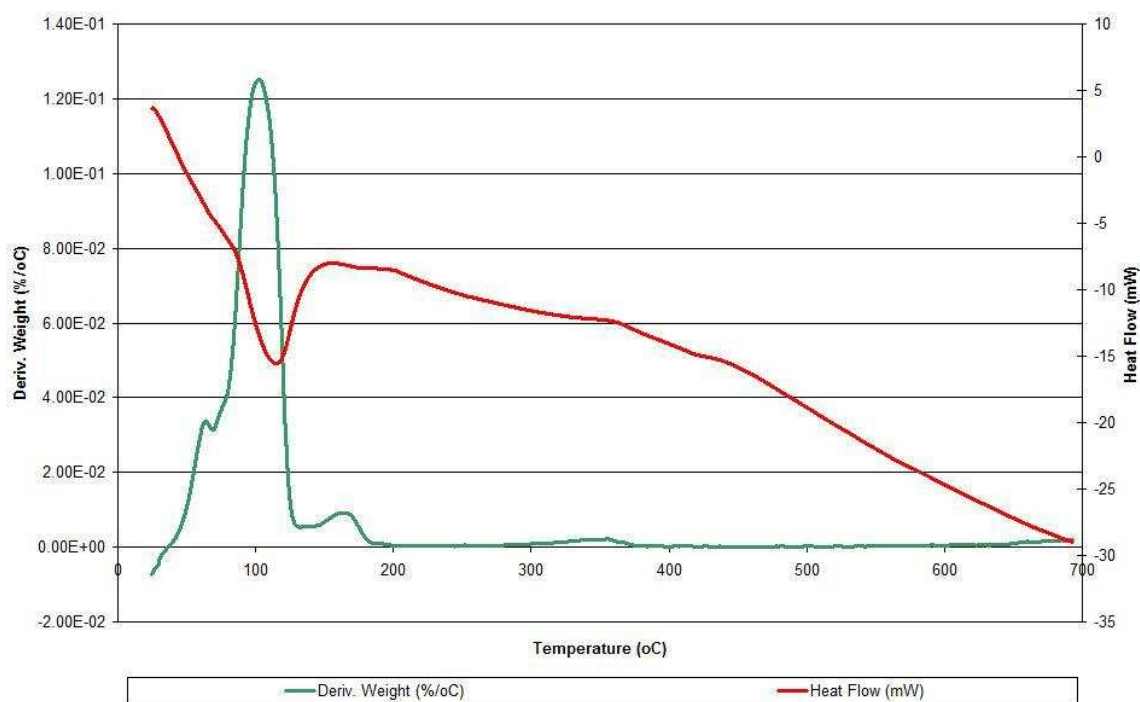


Figure 5.4 shows that the main weight loss event at around 100°C is endothermic and those at 165 and 350°C were exothermic.

**Figure 5.5 Mass Spectrometry data m/e 18**

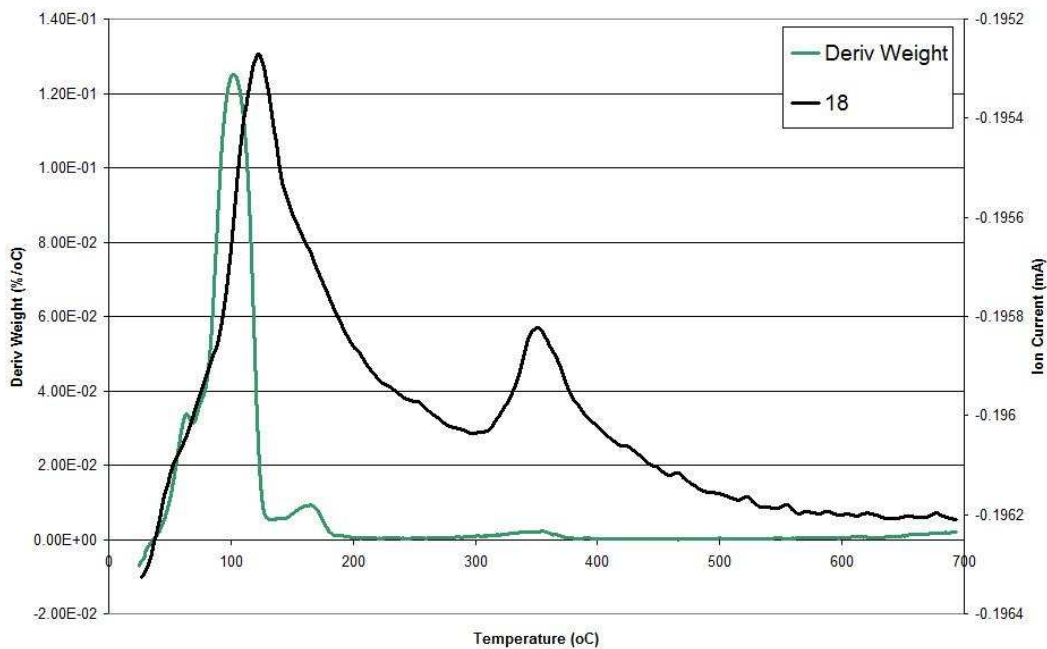
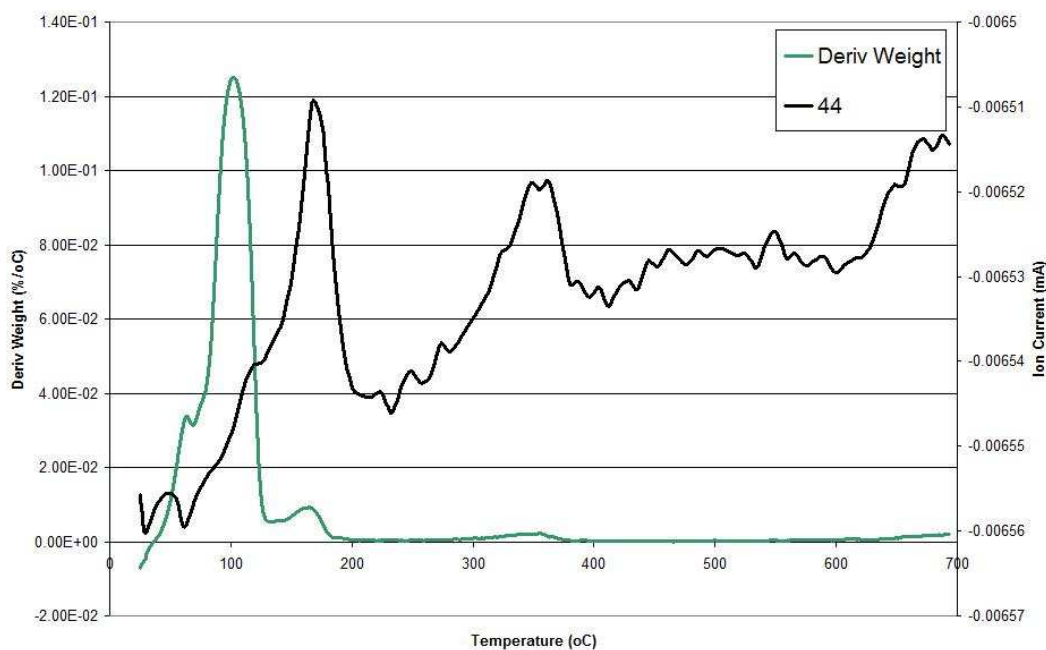


Figure 5.5 shows that both the main weight loss ~100°C and the weight loss at 350°C correspond to water desorption. The sample experiences an overall weight loss of over 5%.

**Figure 5.6: Mass Spectrometry data m/e 44**



The mass spectrometry data for m/e 44 in figure 5.6 shows the evolution of carbon dioxide at 165°C and 350°C.

### 5.1.2.3 Inert Decomposition

Each catalyst was analysed under an inert atmosphere from room temperature up to 700°C. The heating rate used was 10°C.min<sup>-1</sup> under a 100ml.min<sup>-1</sup> flow rate of argon. All catalysts exhibited the same trends, so only data for catalyst P2013 will be reported.

**Figure 5.7: TGA - Inert Decomposition of P2013**

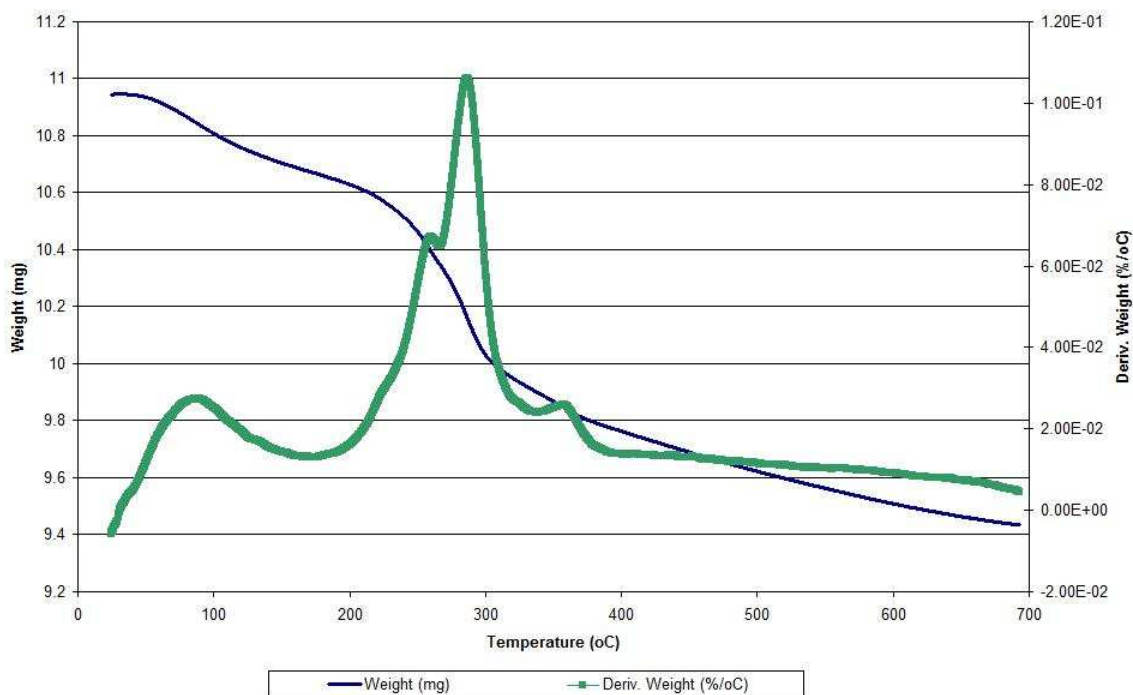


Figure 5.7 shows a clear weight loss event just before 100°C. It also shows a series of weight loss events at 260°C, 287°C, and 360°C.

**Figure 5.8: TGA-DSC Inert Decomposition of P2013**

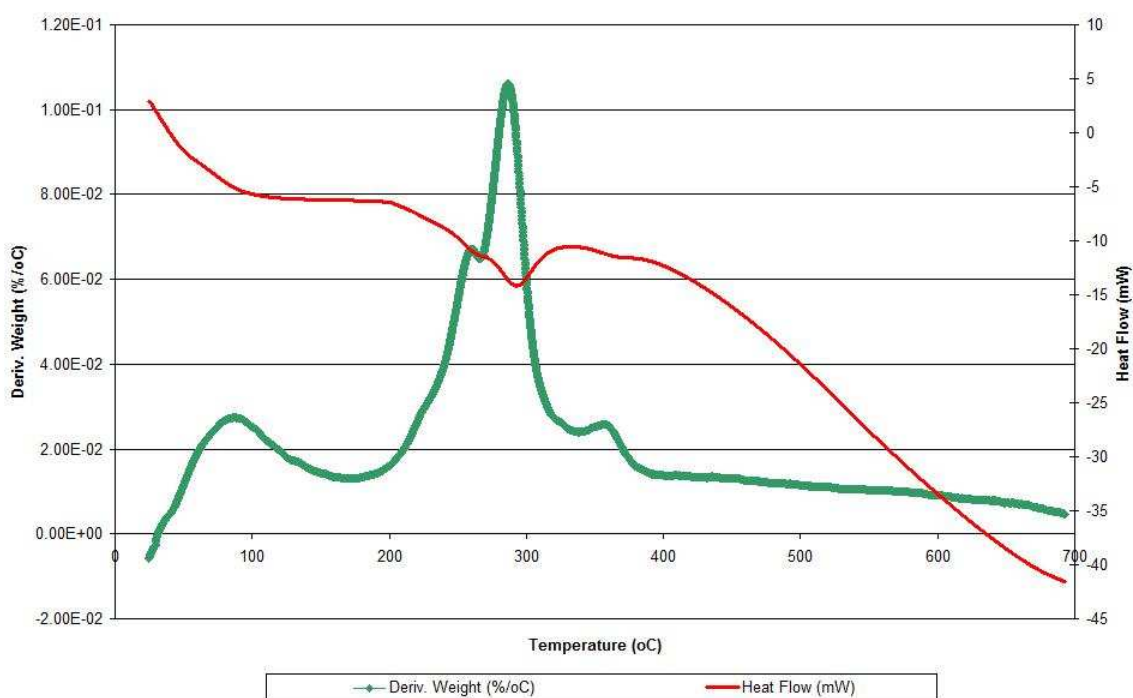
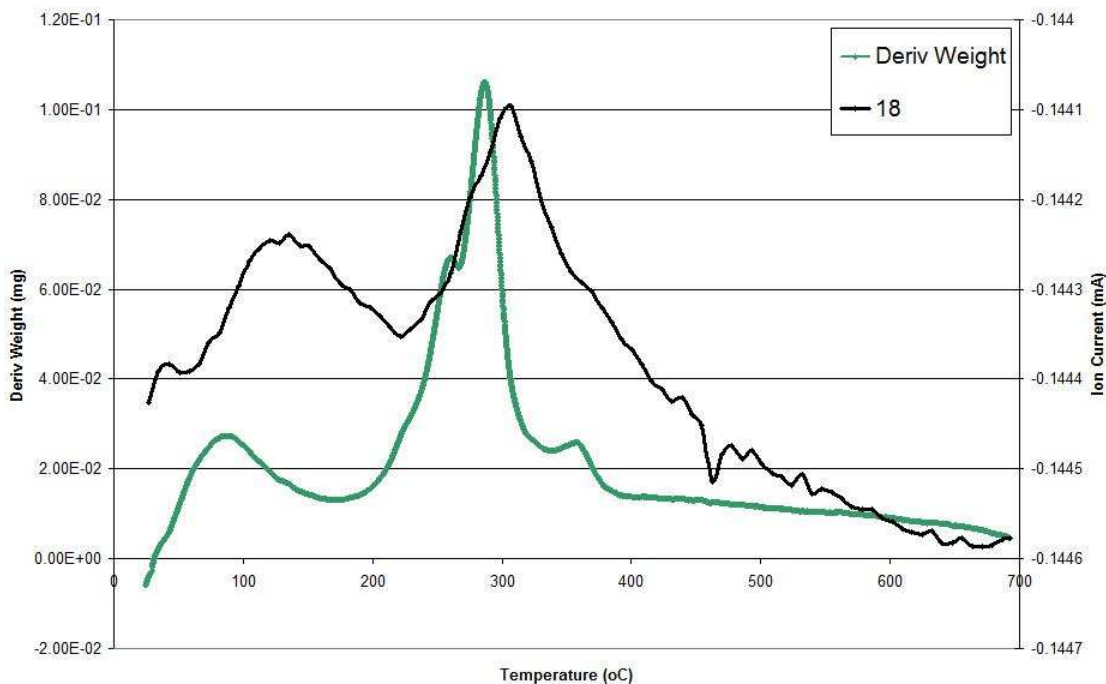


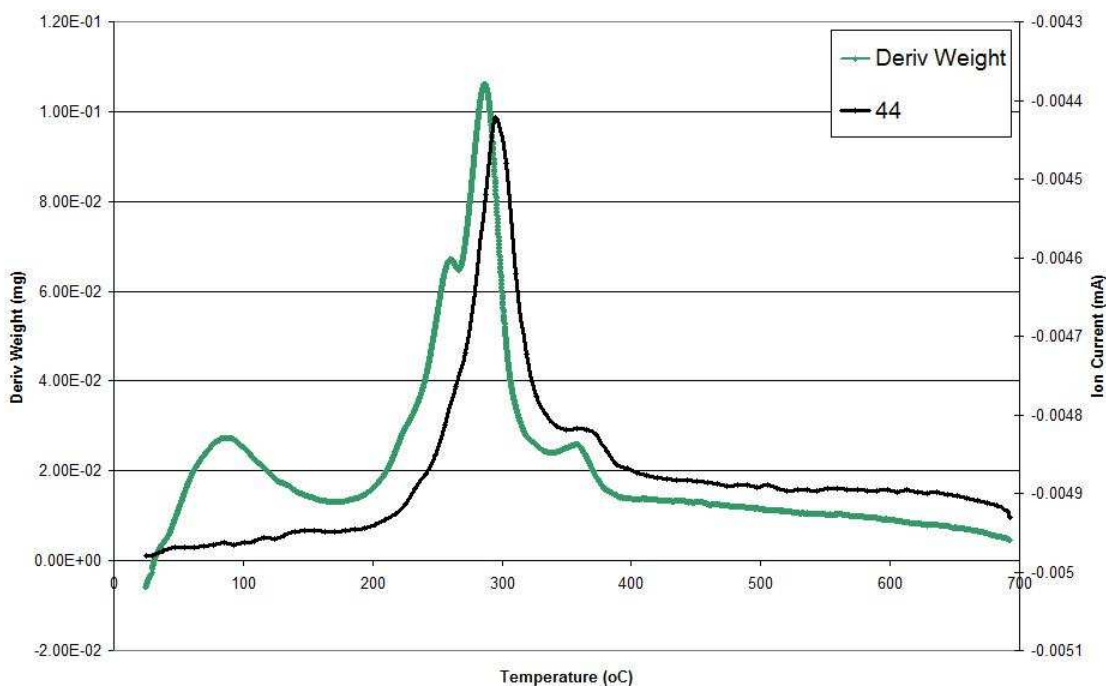
Figure 5.8 shows that all of the weight loss events were endothermic.

**Figure 5.9: Inert Decomposition Mass Spectrometry Data m/e 18**



Mass spectrometry data in figure 5.9 shows that water was evolved at each weight loss event.

**Figure 5.10: Inert Decomposition Mass Spectrometry Data m/e 44**



The mass spectrometry data for m/e 44 in figure 5.10 shows the evolution of carbon dioxide at 290°C and 360°C.

### 5.1.2.4 Calcination

Each catalyst was heated from room temperature to 700°C at 10°C.min<sup>-1</sup> under an O<sub>2</sub>/Ar flow with a rate of 100ml.min<sup>-1</sup>. These conditions were used to mimic calcination and results were as follows. Only the data obtained for catalyst P2030 (15% K<sub>2</sub>CO<sub>3</sub>/Condea M-1206) will be reported as all catalysts showed the same trends.

**Figure 5.11: P2030 TGA weight profile in oxygen**

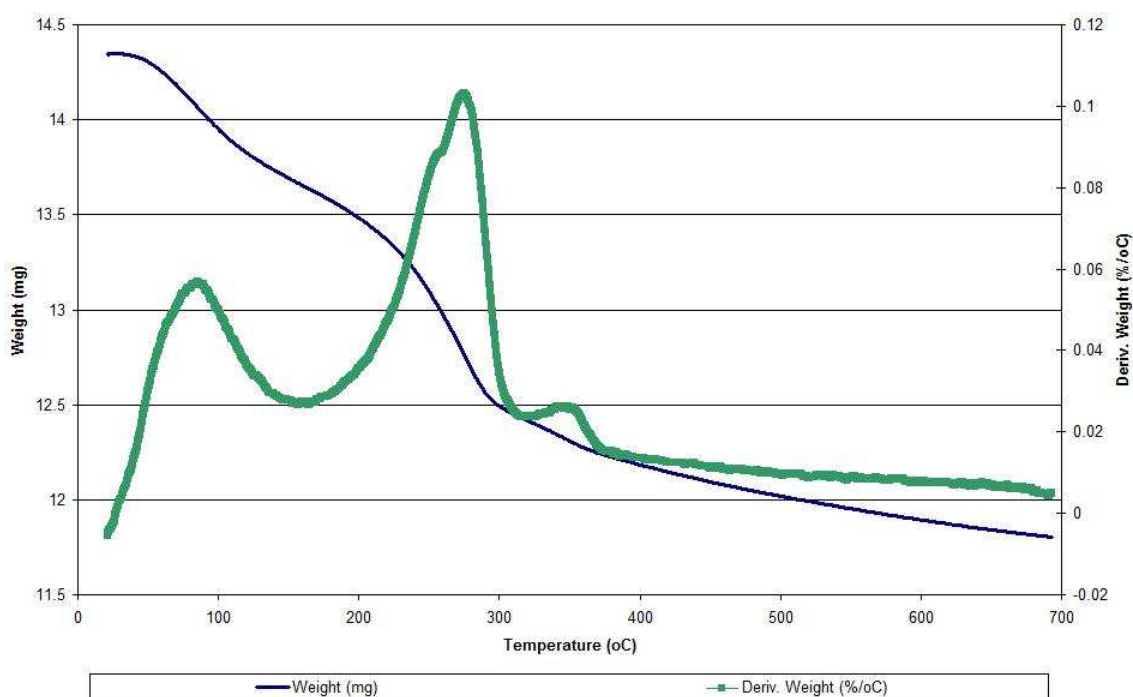


Figure 5.11 shows three main weight loss events at 87°C, 287°C and 350°C. The second weight loss also exhibited a shoulder peak at 257°C. The weight loss event before 100°C corresponded to a ~4% weight loss. Weight loss events between 200-350°C corresponded to a combined weight loss of 7%.

**Figure 5.12: P2030 TGA-DSC profiles in oxygen**

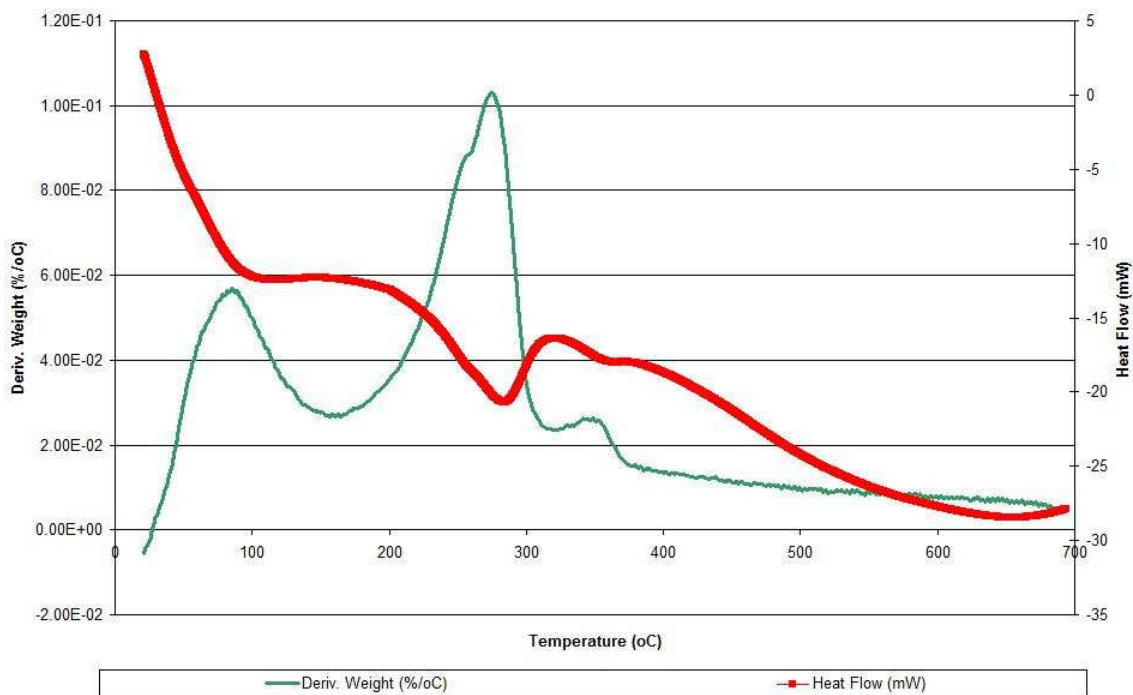
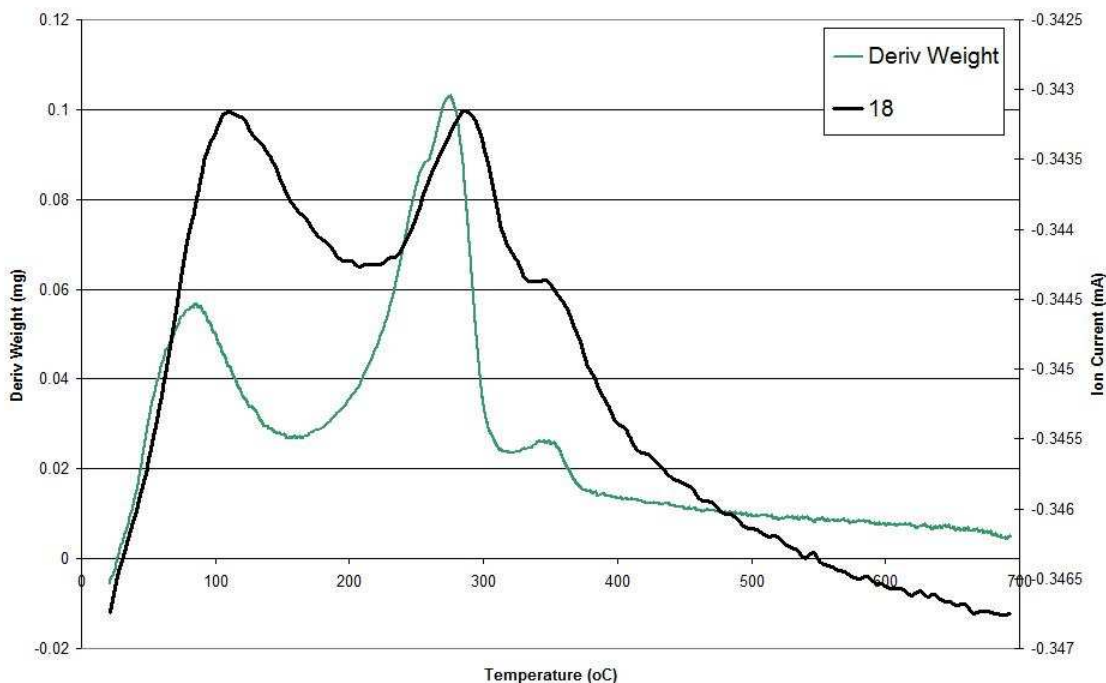


Figure 5.12 shows that all of the weight loss events were endothermic.

**Figure 5.13: P2030 Mass Spectrometry data m/e 18**



Mass spectrometry data for m/e 18 in figure 5.13 confirmed that endothermic weight loss events relate to desorption of water. Water was also liberated during the endothermic weight loss at 350°C.

**Figure 5.14: P2030 Mass Spectrometry data m/e 44**

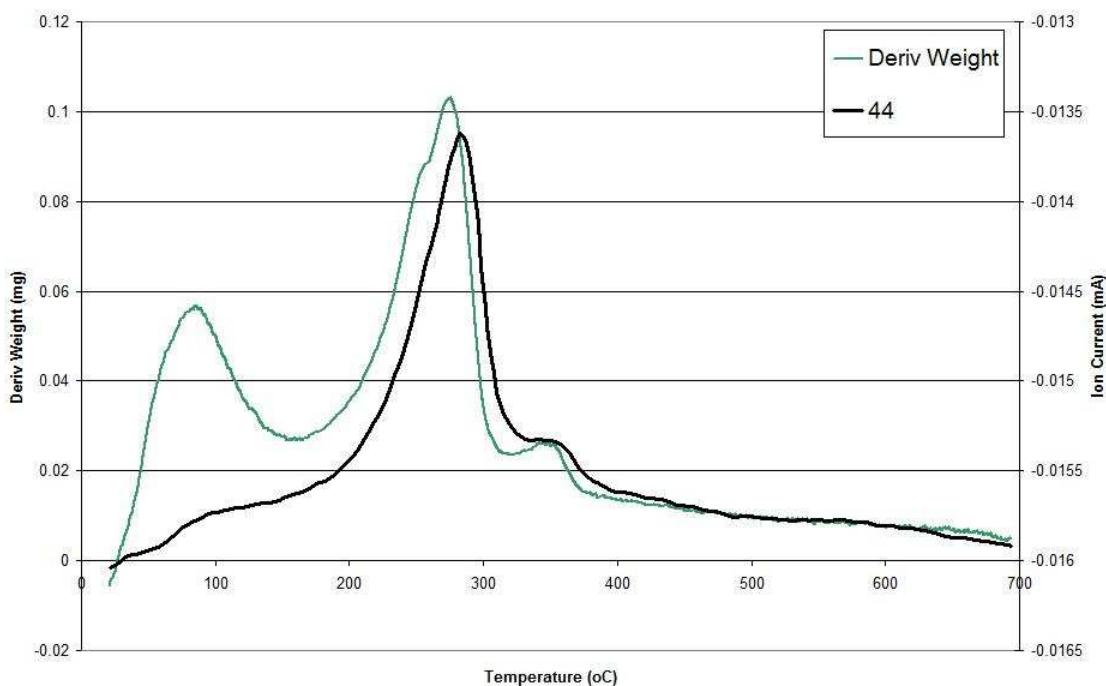


Figure 5.14 shows the evolution of carbon dioxide corresponded to an endothermic weight loss event. This indicated the degradation of the carbonate species on the alumina surface.

### **5.1.2.5 Activation**

Activation of calcined catalysts was performed under argon flow ( $100\text{ml}\cdot\text{min}^{-1}$ ) from room temperature to  $700^{\circ}\text{C}$ . All catalysts showed similar trends and the results obtained for catalyst P2008 are shown below.

**Figure 5.15: TGA profile for activation of calcined P2008**

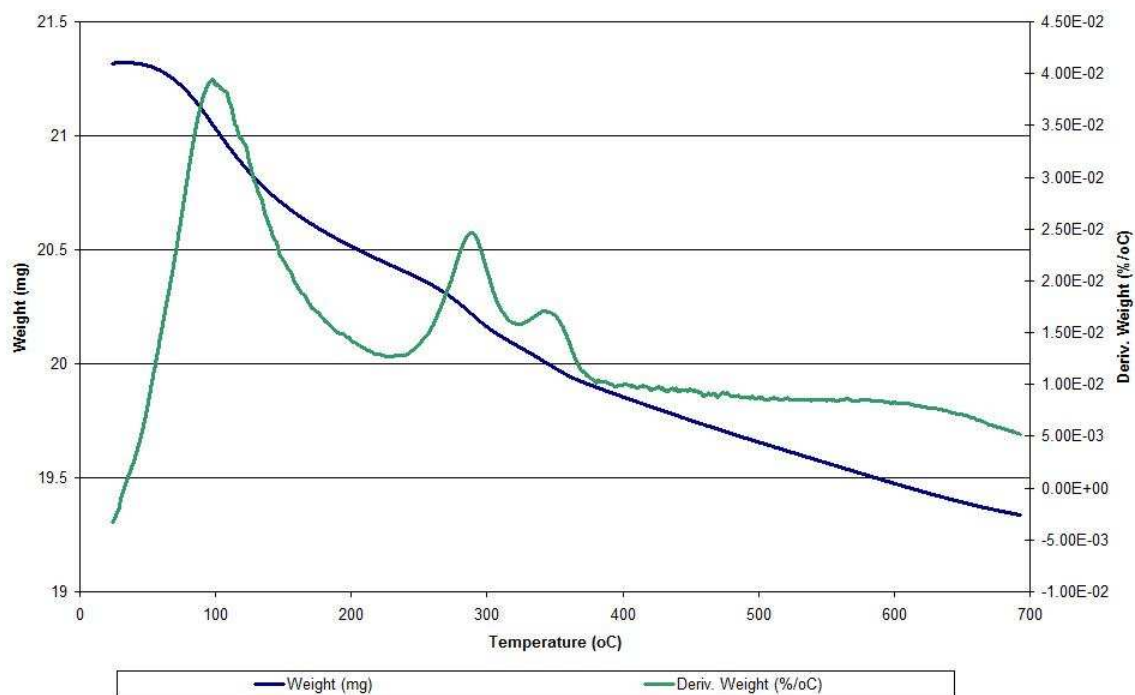


Figure 5.15 shows three clear weight loss events at 99°C, 291°C and 347°C and an overall weight loss of ~9%.

**Figure 5.16: TGA-DSC profile for activation of calcined P2008**

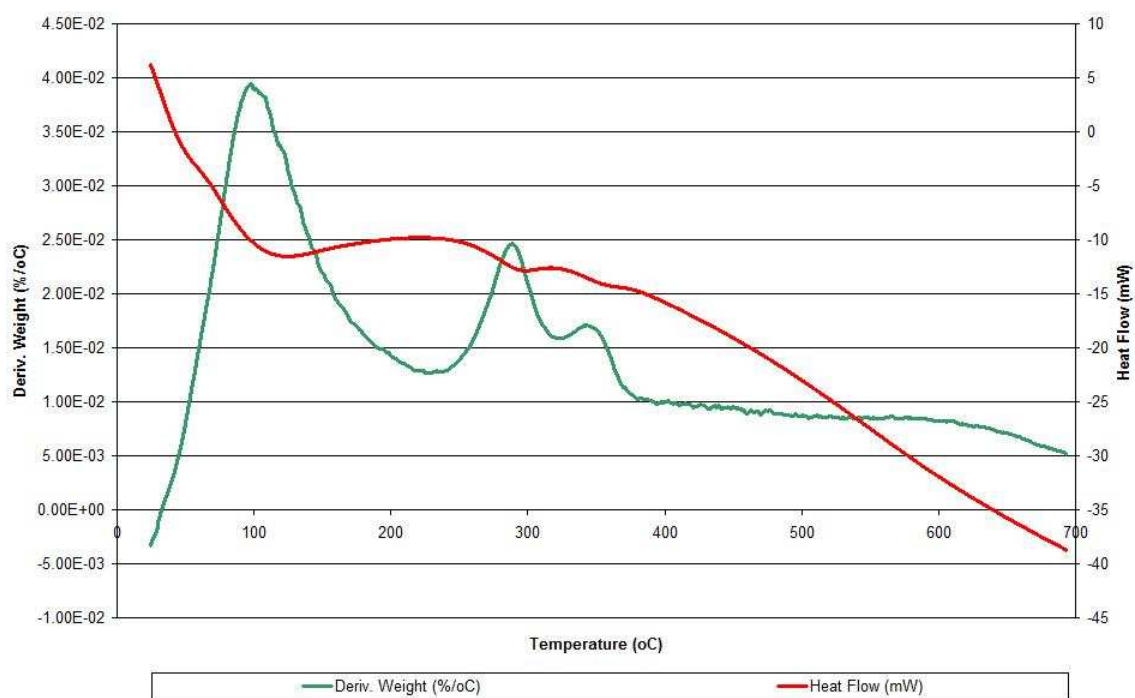
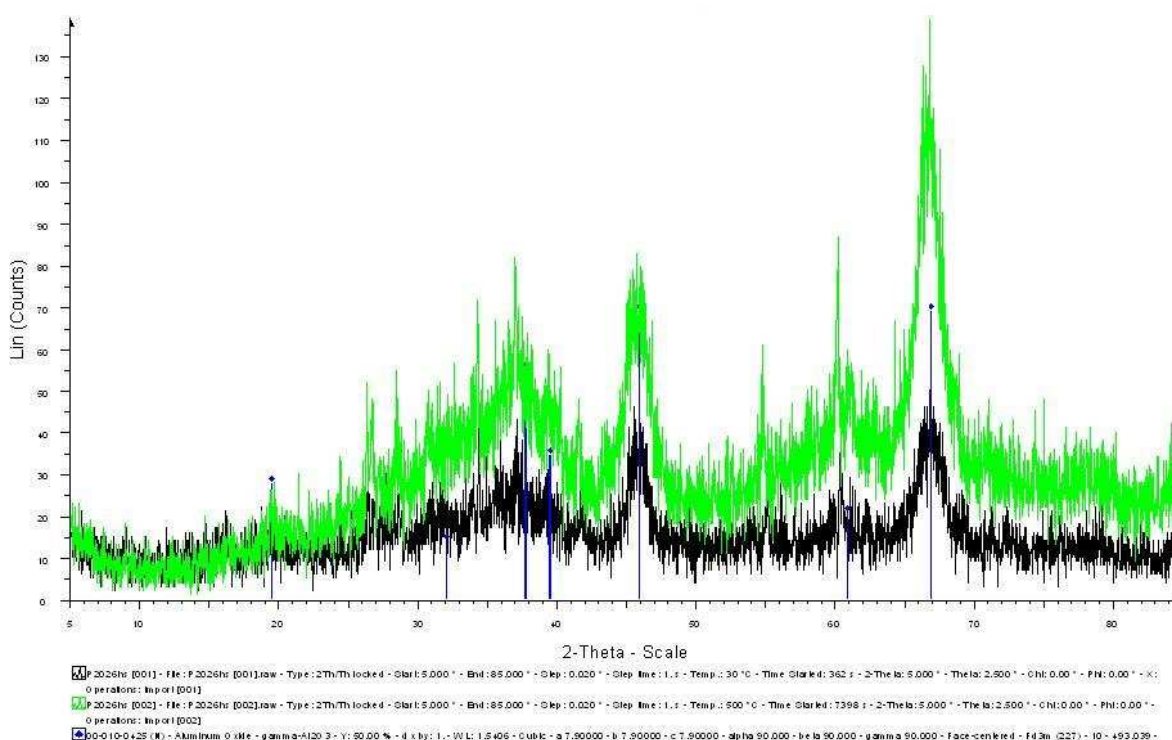


Figure 5.16 shows that all of the weight loss events were endothermic. This relates closely to the weight losses that occurred during calcination. Mass spectrometry data confirmed that the weight loss at 99°C corresponded to desorption of water and weight losses at 291°C and 347°C corresponded to the evolution of carbon dioxide.

### 5.1.3 High Temperature *in-situ* XRD

XRD *in situ* hot stage analysis was performed on all catalysts prior to reaction as described in section 4.2.3. All catalysts showed the same trends and pattern so only catalyst P2026 will be shown.

**Figure 5.17: XRD of Catalyst P2026 at room temperature and 500°C**

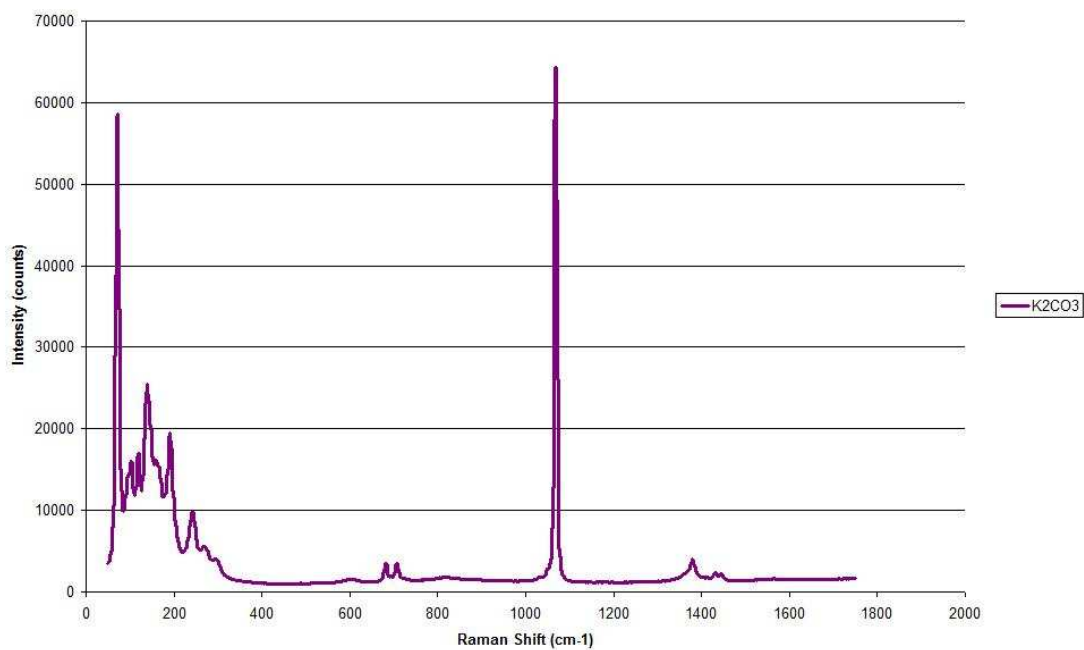


The pattern observed relates to  $\gamma$ -alumina and it does not change after heating to 500°C. No X-ray diffraction pattern was observed for potassium carbonate, which suggested that no crystals of  $K_2CO_3$  were large enough to be detected by X-ray or that  $K_2CO_3$  was amorphous.

## 5.1.4 Raman Spectroscopy

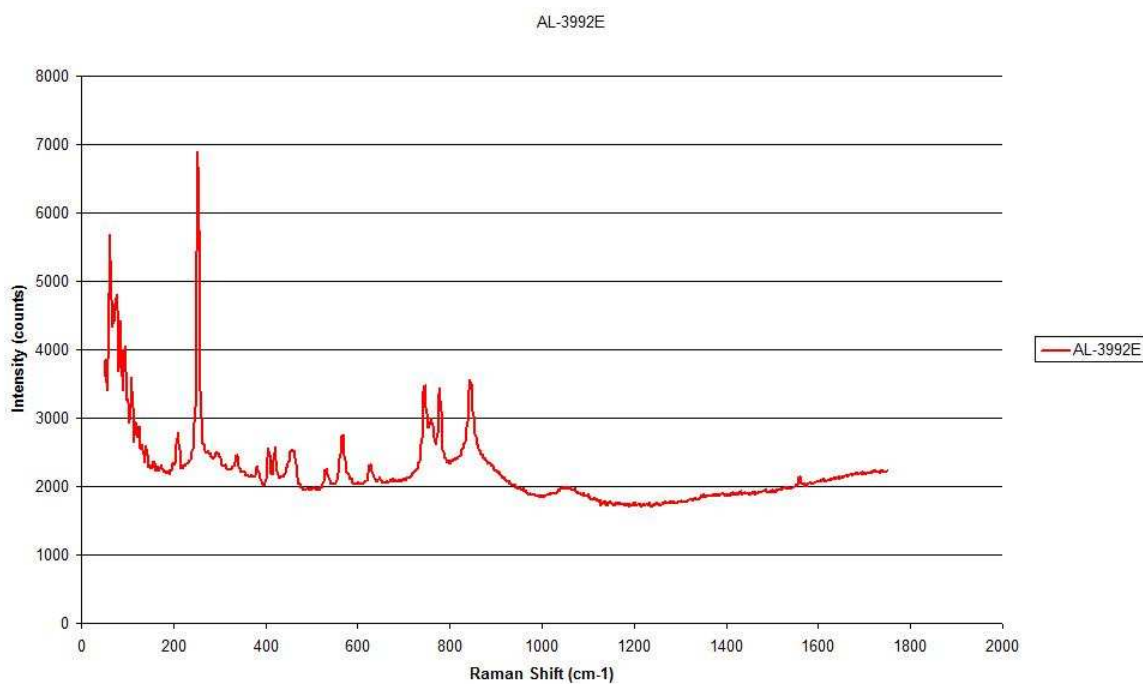
The Raman spectrum of potassium carbonate was recorded and is shown in Figure 5.20.

**Figure 5.18: Raman Spectrum of  $K_2CO_3$**



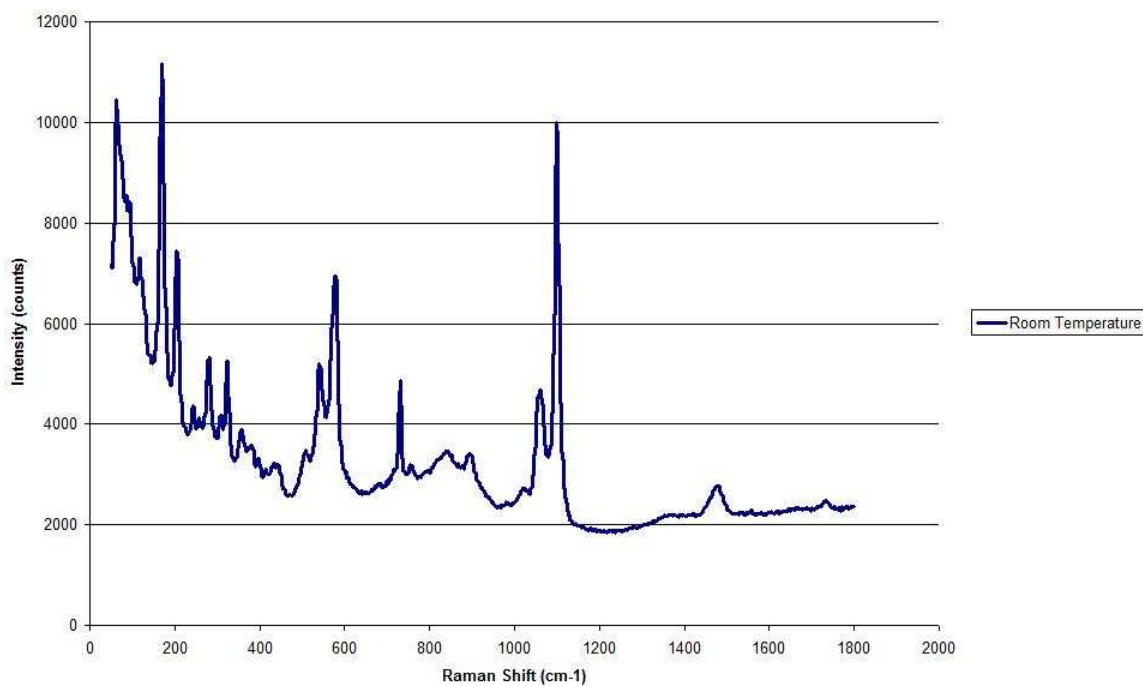
This spectrum shows one main peak at  $1068\text{cm}^{-1}$ , two small peaks at  $684\text{cm}^{-1}$  and  $709\text{cm}^{-1}$ , a slightly larger peak at  $1382\text{cm}^{-1}$  and finally, two small peaks at  $1439\text{cm}^{-1}$  and  $1449\text{cm}^{-1}$ . A cluster of peaks were also observed at  $243\text{cm}^{-1}$ ,  $191\text{cm}^{-1}$ ,  $140\text{cm}^{-1}$  and  $71\text{cm}^{-1}$ .

**Figure 5.19: Raman Spectrum for Engelhard AL-3992E Alumina**



The spectrum for alumina support material, in figure 5.21, shows an intense peak at  $253\text{cm}^{-1}$  and less intense peaks at  $63\text{cm}^{-1}$ ,  $746\text{cm}^{-1}$ ,  $779\text{cm}^{-1}$  and  $846\text{cm}^{-1}$ .

**Figure 5.20: Raman Spectrum of Catalyst P2013 at room temperature**



The spectrum of potassium carbonate on alumina (P2013) was recorded and is shown in figure 5.22. There are two main peaks at  $1060\text{cm}^{-1}$  and  $1099\text{cm}^{-1}$  and a much smaller peak at  $1480\text{cm}^{-1}$ . There is also a series of peaks from  $470\text{--}970\text{cm}^{-1}$ .

The catalyst was heated to  $500^\circ\text{C}$  under an  $\text{O}_2/\text{Ar}$  gas mix to mimic the conditions under which the catalyst would be calcined. Figure 5.23 includes spectra obtained at room temperature and then every  $100^\circ\text{C}$  up to  $500^\circ\text{C}$ .

**Figure 5.21: Raman Spectra for calcination of catalyst P2013**

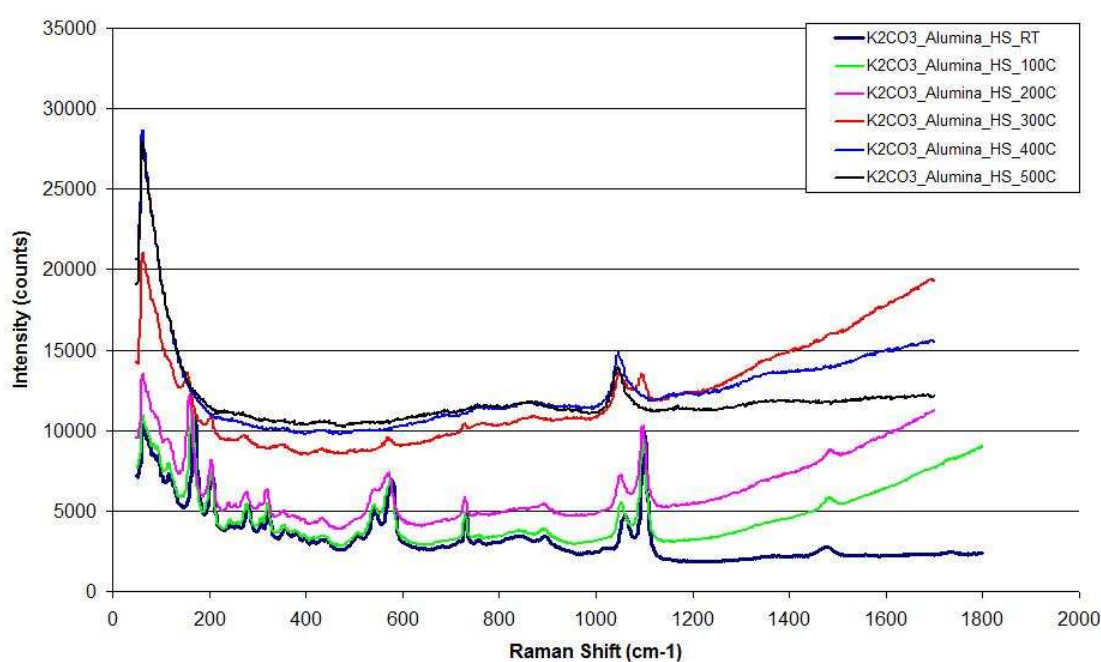


Figure 5.21 shows two clear peaks at  $\sim 1060\text{cm}^{-1}$  and  $1099\text{cm}^{-1}$  present at room temperature. Beyond  $300^\circ\text{C}$  however, there is only one peak present at  $\sim 1060\text{cm}^{-1}$ . It is also apparent that the series of peaks between  $470\text{--}970\text{cm}^{-1}$  and the small peak at  $1480\text{cm}^{-1}$  disappear.

**Figure 5.22: Catalyst P2013 post-calcination Raman Spectrum**

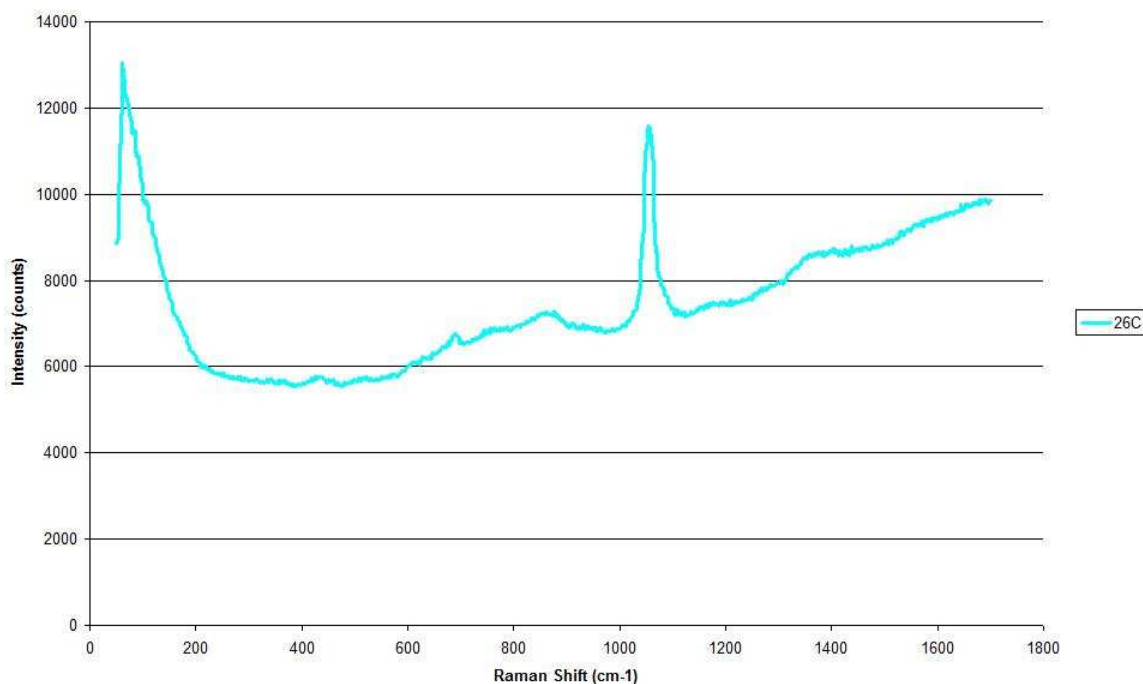
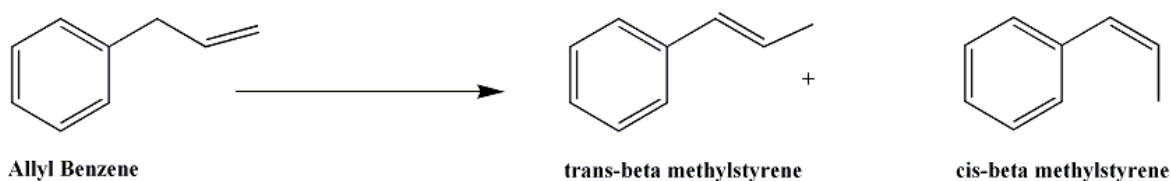


Figure 5.22 shows the spectrum obtained after the catalyst was allowed to cool to room temperature. It shows clearly a significant peak at  $1056\text{cm}^{-1}$  and some other poorly resolved peaks. As the peak at  $61\text{cm}^{-1}$  is present throughout the calcination and indeed at room temperature it is likely to be the result of lattice modes.

## 5.2 Catalyst Testing

The isomerisation of allylbenzene produces a mixture of cis and trans- $\beta$ -methylstyrene as shown in figure 5.23.

**Figure 5.23: Isomerisation of Allylbenzene**



Experiments were conducted to investigate the effect of preparation method,  $\text{K}_2\text{CO}_3$  loading and alumina supplier on the activity and selectivity of the catalyst. The effect of

the concentration of allylbenzene was also used to determine the order of reaction. Experiments were carried out as described in section 4.5.

### 5.2.1 Alumina

A reaction was carried out whereby alumina support material was used instead of the catalyst. The purpose of this was to ensure that the support material exhibited no catalytic activity for the given reaction. Engelhard AL-3992E alumina (1.5g) was measured and loaded into the reaction vessel with silicon carbide fines as described in section 4.5.3. The procedure outlined in the Experimental section was followed and samples analysed by gas chromatography.

It was found that the alumina support material showed no activity for the given reaction.

### 5.2.2 Preparation Methods

Reactions were conducted to investigate the effect of the catalyst preparation method on the nature of the catalyst and the subsequent activity and selectivity. The catalysts used within this study are shown in table 5.2. All catalysts had a loading of 15% and were ground to  $225 < \mu\text{m} < 455$  prior to use in the reaction.

**Table 5.2: Catalysts formed by different Preparation Methods**

Catalyst Code	Supplier Code	Appearance	Preparation Method	Nominal $\text{K}_2\text{CO}_3$ loading (% w.w)	Surface Area ( $\text{m}^2\text{g}^{-1}$ )
P2008	Condea M-1206	0.8mm diameter extrudate pellet	Wet Impregnation	15	149
P2015	Condea M-1206	0.8mm diameter extrudate pellet	Incipient Wetness	15	133
P2030	Condea M-1206	0.8mm diameter extrudate pellet	Spray Impregnation	15	134

All catalysts showed activity for the reaction and the following figures show the conversion of allylbenzene against time on stream.

**Figure 5.24: (P2008) Conversion of allylbenzene against time**

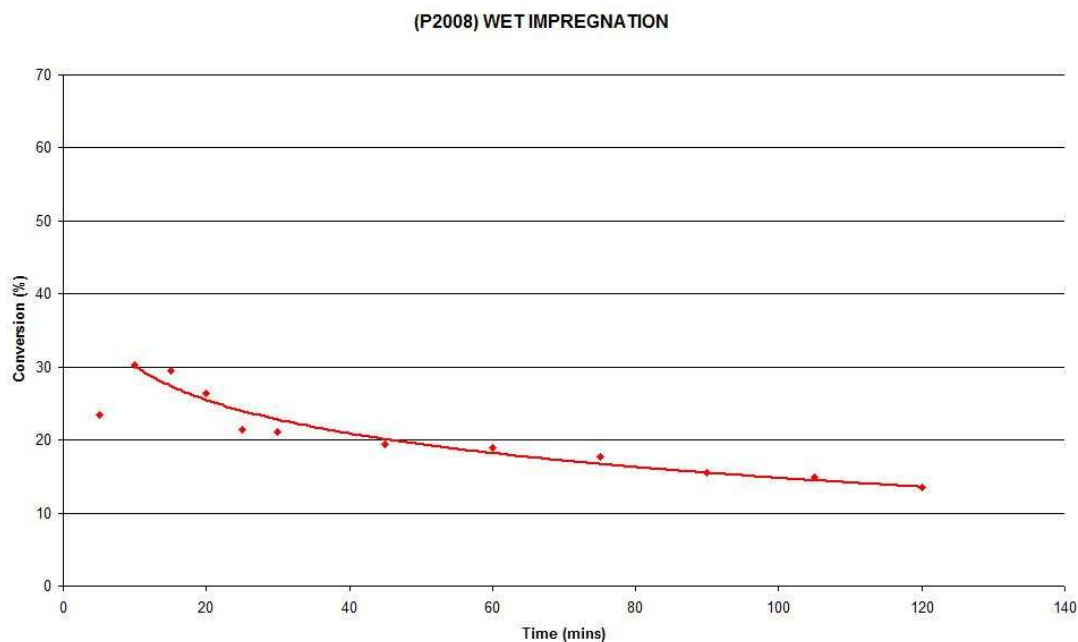
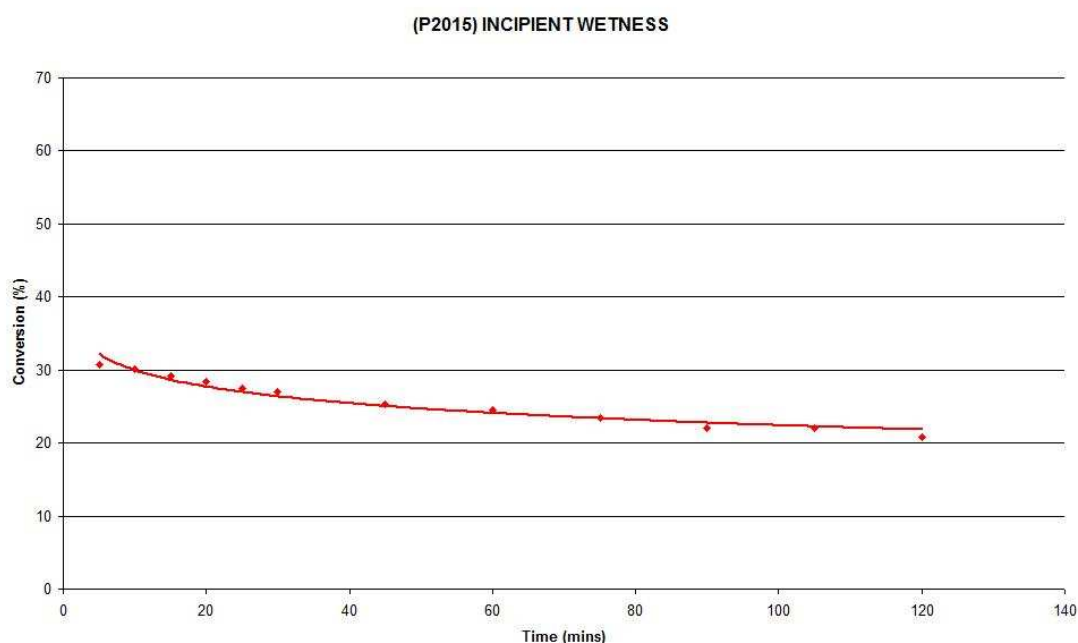


Figure 5.24 shows the conversion of allylbenzene over 120 minutes. Conversion was low at the beginning of the observed period and decreased quickly from around 30% to about 13% after 120 minutes.

Figure 5.25 shows the conversion of allylbenzene for catalyst P2015 which was prepared by incipient wetness.

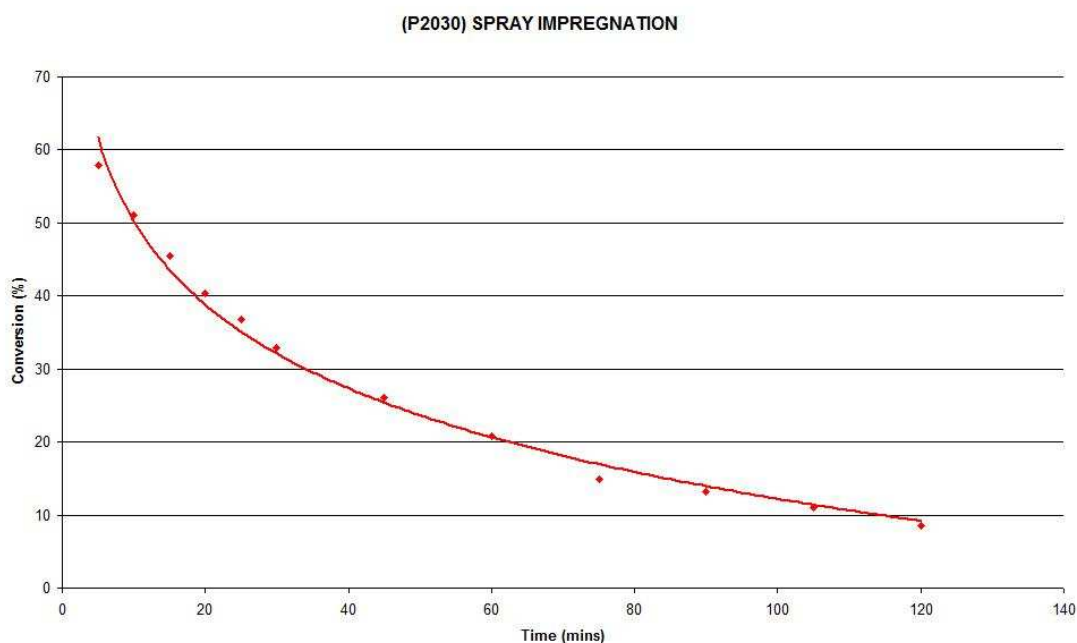
**Figure 5.25: (P2015) Conversion of allylbenzene against time**



The conversion of allylbenzene decreased from around 30% initially to just above 20% after 120 minutes.

Figure 5.26 shows the final catalyst P2030 prepared by spray impregnation.

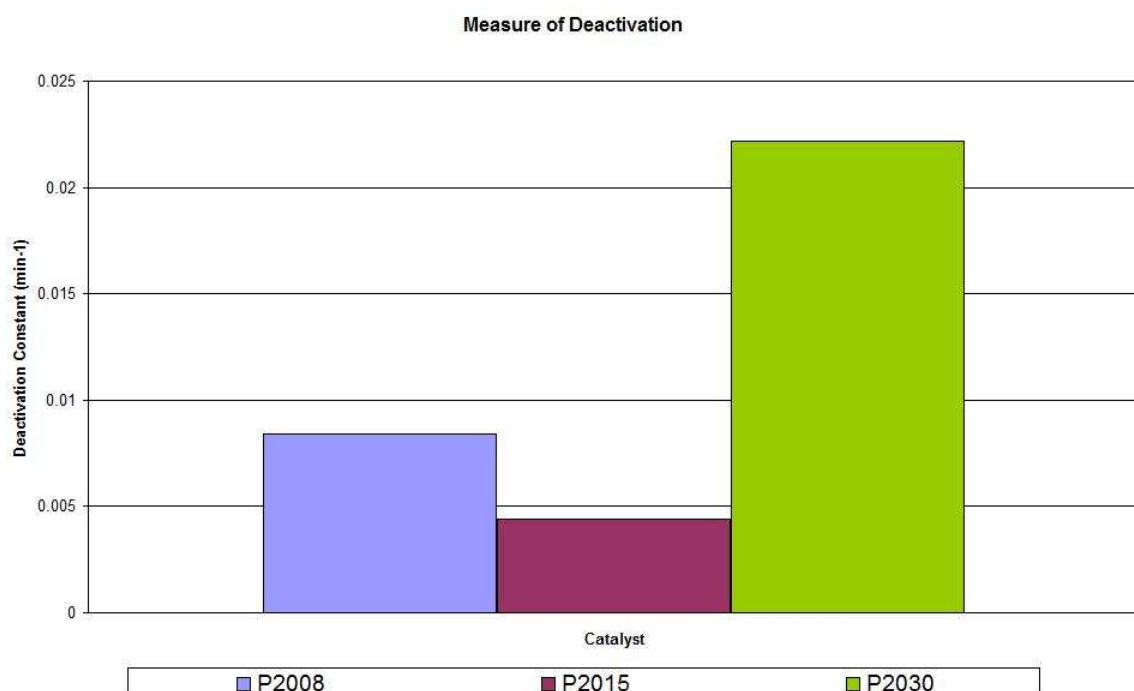
**Figure 5.26: (P2030) Conversion of allylbenzene against time**



Catalyst P2030 deactivated quickly, shown by the steep gradient of the curve. Over 120 minutes the conversion of allylbenzene dropped from around 60% to just below 10%.

To determine the deactivation constant for each catalyst  $\ln [(C_0/C_A)-1]$  was plotted against time to produce a linear relationship as described in section 4.5.7. Figure 5.27 shows the deactivation constants obtained for each of the catalysts.

**Figure 5.27: Deactivation Constants**



From figure 5.27, P2030 catalyst exhibited the fastest deactivation, shown by the highest deactivation constant. P2015 exhibited the lowest deactivation constant and so deactivated relatively slowly.

The product alkenes were analysed and the cis:trans ratio determined. This is displayed in Table 5.3.

**Table 5.3: Selectivity of cis/trans- isomers**

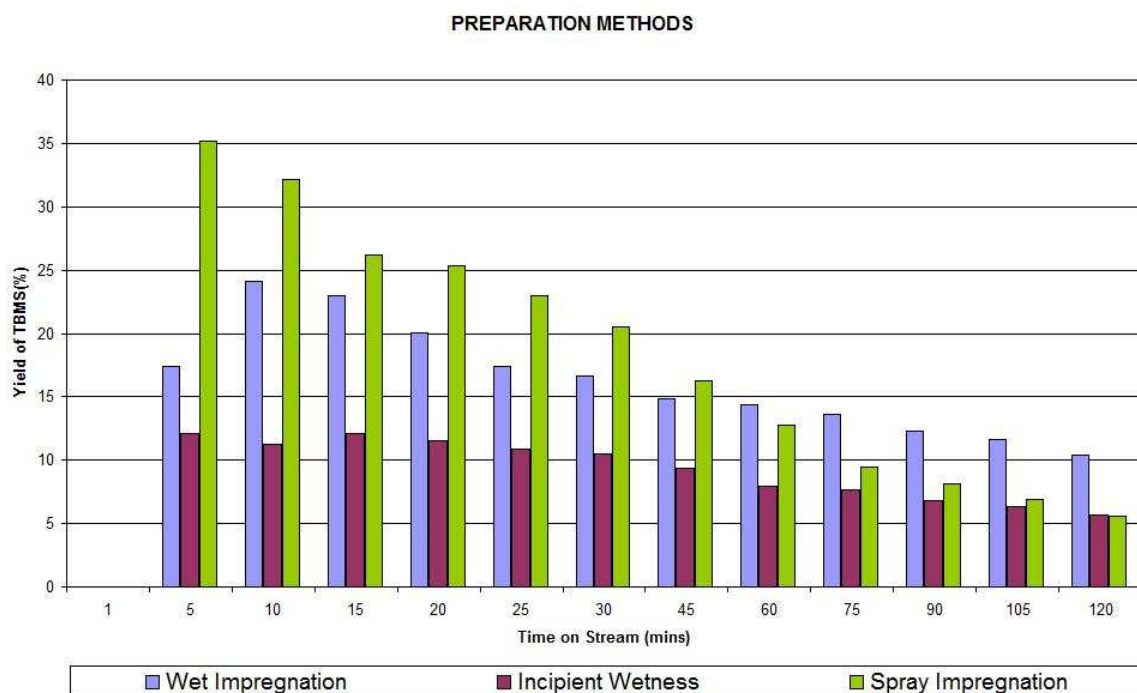
Catalyst Code	Cis-isomer (%)	Trans-isomer (%)	Cis:trans ratio
P2008	7.7 ± 1.0	77.7 ± 2.1	1:10
P2015	3.5 ± 0.4	35.5 ± 4.9	1:10
P2030	8.0 ± 1.1	61.8 ± 2.2	1:8

For all catalysts a cis:trans ratio in favour of the thermodynamic trans- isomer was observed. It can also be seen from these results that the use of catalyst P2015 produces less than 40% product alkenes. Although other products may have been produced there

were no other liquid products detected by GC analysis, however gas phase products would not have been detected.

The yield of trans- $\beta$ -methyl styrene was plotted for each catalyst in figure 5.28.

**Figure 5.28: Yield of trans- $\beta$ -methyl styrene for P2008/P2015/P2030**



Catalyst prepared by spray impregnation (P2030) exhibited the highest yield of trans- $\beta$ -methylstyrene whereas catalyst P2015 exhibited the lowest yield.

### 5.2.3 K<sub>2</sub>CO<sub>3</sub> Loading

The catalysts shown in table 5.4 were used in isomerisation of allylbenzene to determine the effect of K<sub>2</sub>CO<sub>3</sub> loading on the activity and selectivity of the catalyst. All catalysts were prepared by incipient wetness and the K<sub>2</sub>CO<sub>3</sub> loading varied from 12-20%. Two catalysts using Engelhard AL-3992E alumina with different K<sub>2</sub>CO<sub>3</sub> loadings were also prepared and tested.

**Table 5.4: Comparison of catalysts with different nominal K<sub>2</sub>CO<sub>3</sub> loading**

Catalyst Code	Supplier Code	Preparation Method	Nominal K <sub>2</sub> CO <sub>3</sub> loading (% w/w)	Surface Area (m <sup>2</sup> g <sup>-1</sup> )
P2026	Condea M-1206	Incipient Wetness	12	164
P2023	Condea M-1206	Incipient Wetness	15	149
P2027	Condea M-1206	Incipient Wetness	18	167
P2019	Condea M-1206	Incipient Wetness	20	102
P2013	Engelhard AL-3992-E	Incipient Wetness	15	130
P2017	Engelhard AL-3992-E	Incipient Wetness	20	104

All catalysts showed activity for the reaction and the following results are for catalysts prepared using Condea M-1206 alumina support material.

**Figure 5.29: Conversion for loadings 12%, 15%, 18% and 20%**

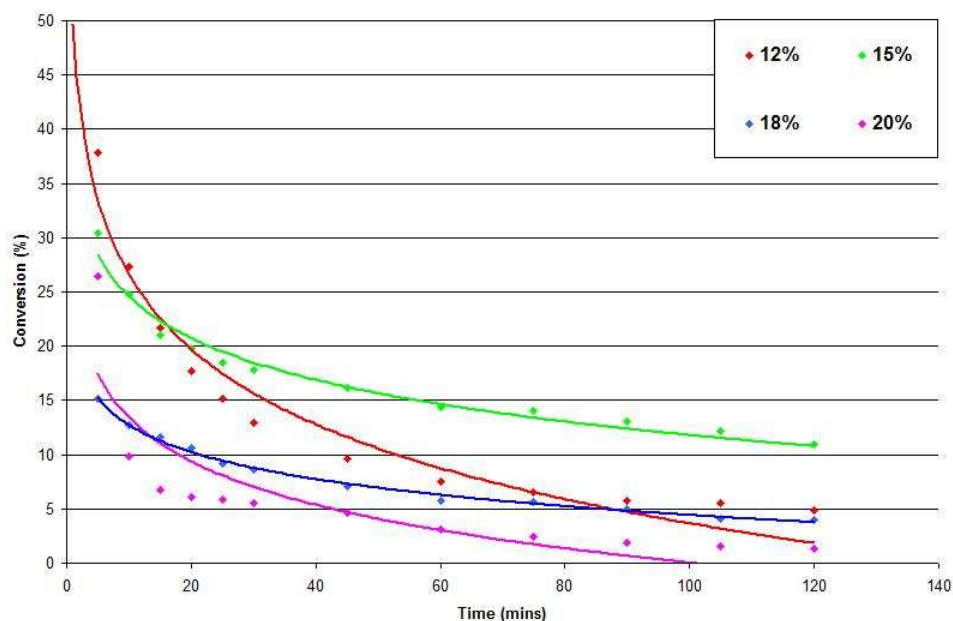


Figure 5.29 shows that initially the highest conversion of allylbenzene was obtained through the use of 12%  $K_2CO_3$  on alumina catalyst. However, for this catalyst the conversion of allylbenzene decreased rapidly during 120 minutes. The highest conversion of allylbenzene at 120 minutes was obtained through use of 15%  $K_2CO_3$  on alumina catalyst. Higher  $K_2CO_3$  loadings, such as 18 and 20%, exhibited low conversions throughout 120 minutes.

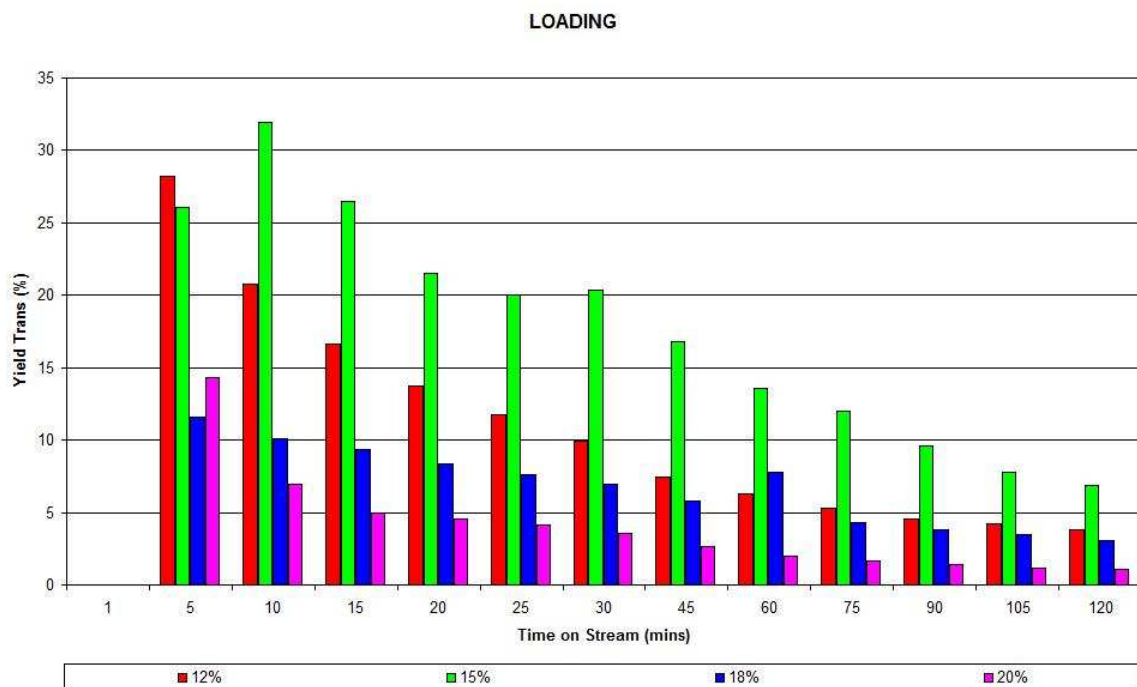
Table 5.5 shows the selectivity of product alkenes obtained through reaction for each catalyst.

**Table 5.5: Selectivity of cis/trans- isomers**

Catalyst Code	Cis-isomer (%)	Trans-isomer (%)	Cis:trans ratio
P2026	10.8 ± 2.0	78.0 ± 2.5	1:7
P2023	6.0 ± 0.4	65.6 ± 4.3	1:10
P2027	11.6 ± 1.3	79.4 ± 3.0	1:7
P2019	12.4 ± 2.6	71.1 ± 7.7	1:6

Table 5.5 shows that product selectivity was high for all catalysts (~70-80%) and although cis:trans ratios varied slightly the predominant product was the trans- isomer.

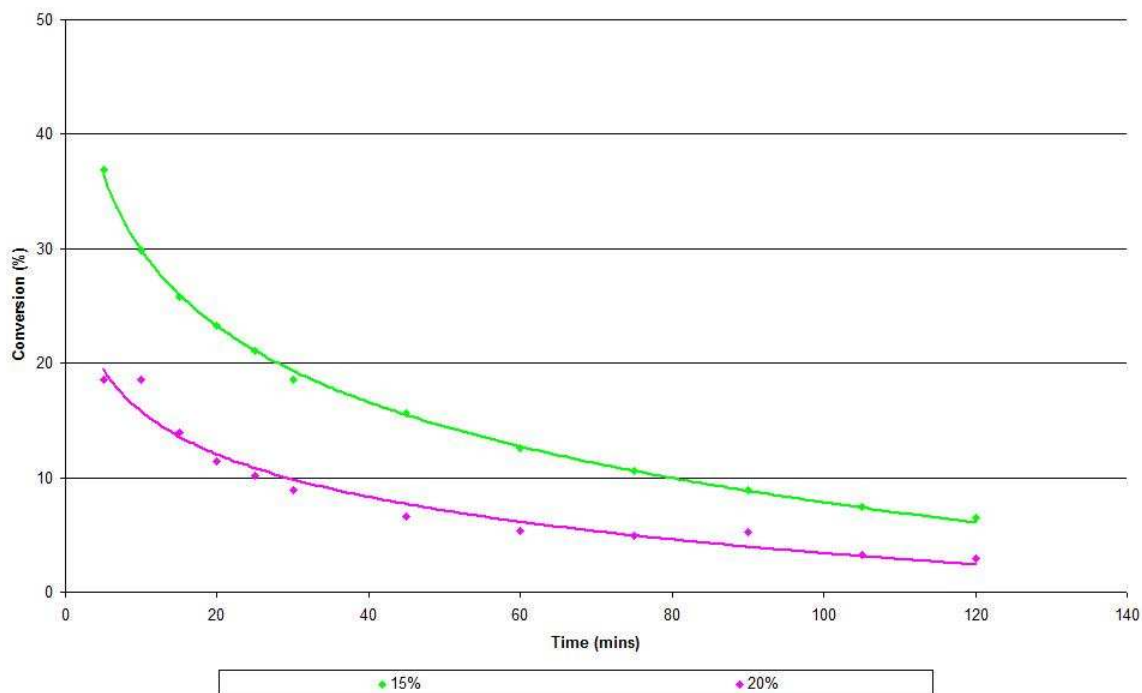
**Figure 5.30: Yield of trans- isomer for loading catalysts**



The highest yield of trans- isomer was obtained through use of 15%  $K_2CO_3$  loading. Although at 5 minutes on stream it appeared that 12%  $K_2CO_3$  loading gave a higher yield, the yield for 15%  $K_2CO_3$  loading was higher at every other stage throughout 120 minutes. The optimum  $K_2CO_3$  loading for this catalyst appeared to be 15% as it provided a moderate yield of trans- $\beta$ -methylstyrene and deactivated relatively slowly compared to the other catalysts.

Additionally, catalysts P2013 and P2017 were investigated in a similar way. Both catalysts consisted of Engelhard AL-3992E support material and had  $K_2CO_3$  loadings of 15 and 20% respectively.

**Figure 5.31: 15%/20% Engelhard Alumina Catalysts**



From figure 5.31 it can be clearly seen that conversion is almost halved with the use of a 20% metal loading catalyst.

The selectivity for product alkenes was analysed and the results are shown in table 5.6.

**Table 5.6: Selectivity of cis/trans- isomers**

Catalyst Code	Cis-isomer (%)	Trans-isomer (%)	Cis:trans ratio
P2013	9.5 ± 1.0	78.9 ± 2.2	1:8
P2017	8.5 ± 1.1	74.3 ± 5.8	1:8

From this it was noted that the cis:trans ratio remained in the favour of the thermodynamically stable trans- isomer. Product selectivity of 80-90% product alkenes was obtained through the use of catalysts P2013 and P2017.

## 5.2.4 Alumina Supplier

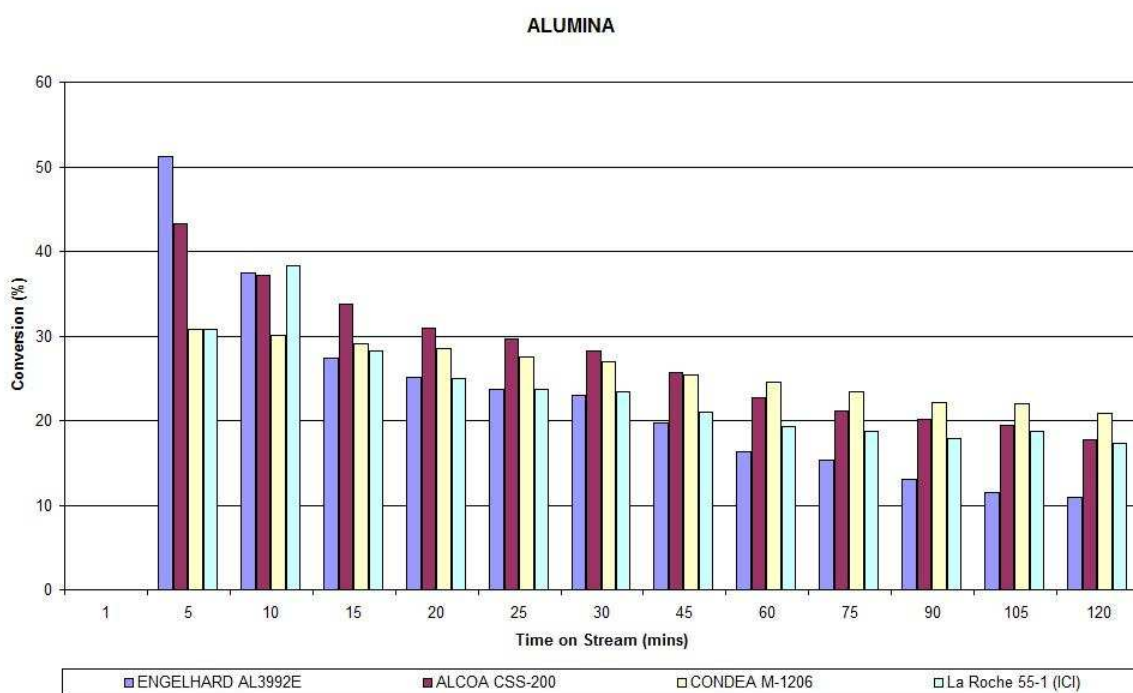
Alumina support material provided by Condea, Engelhard, Alcoa and La Roche were used in the preparation of the catalysts shown in table 5.7.

**Table 5.7: Catalysts prepared using alumina support material provided by different suppliers**

Catalyst Code	Supplier Code	Appearance	Preparation Method	Nominal K <sub>2</sub> CO <sub>3</sub> loading (% w.w)
P2013	Engelhard AL-3992-E	3.2mm diameter extrudate pellet	Incipient Wetness	15
P2014	Alcoa CSS-200	3.2mm diameter sphere	Incipient Wetness	15
P2015	Condea M-1206	0.8mm diameter extrudate pellet	Incipient Wetness	15
P2016	La Roche 55-1 (ICI)	3.2mm diameter sphere	Incipient Wetness	15

Each catalyst was ground to 225<μm<455 and used in a reaction of allylbenzene to investigate the effect of alumina supplier on the activity of the catalyst. Figure 5.32 shows the conversion for each catalyst.

**Figure 5.32: % Conversion against time for each alumina supplier**



The reduction in conversion against time shows deactivation for each catalyst. It was observed that the Condea M-1206 support material produced a catalyst that deactivated very slowly over 120 minutes. The catalyst that exhibited the highest initial conversion of allylbenzene consisted of Engelhard AL-3992E alumina.

**Figure 5.33: % Yield of TBMS for each alumina supplier**

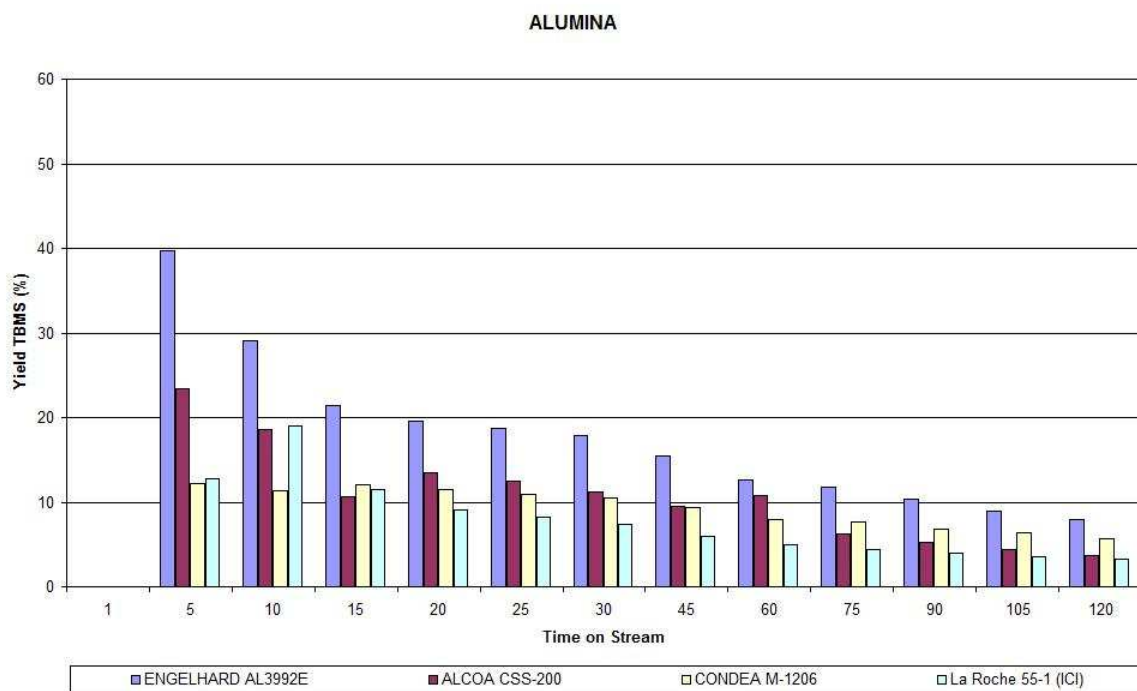


Figure 5.33 shows the yield of trans- $\beta$ -methylstyrene for each catalyst against time on stream. Engelhard AL-3392E alumina catalyst produced the highest yield of trans- $\beta$ -methylstyrene.

The product alkenes were analysed and the selectivity is shown in table 5.8.

**Table 5.8: Selectivity of cis/trans- isomers**

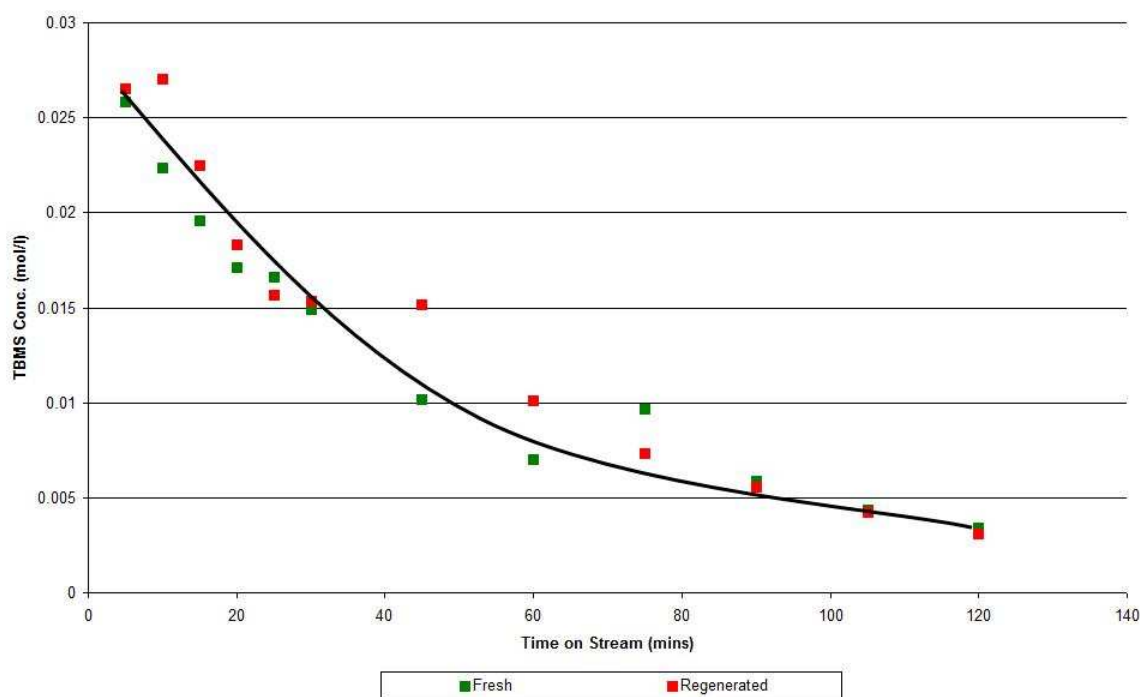
Catalyst Code	Cis-isomer (%)	Trans-isomer (%)	Cis:trans ratio
P2013	8.2 $\pm$ 1.2	77.1 $\pm$ 2.1	1:9
P2014	4.2 $\pm$ 0.8	37.1 $\pm$ 10.9	1:8
P2015	3.5 $\pm$ 0.4	35.5 $\pm$ 4.9	1:10
P2016	4.0 $\pm$ 1.0	31.1 $\pm$ 9.8	1:7

Catalyst P2013 showed the highest product alkene selectivity (~85%). The remaining catalysts produced poor selectivity (35-40%) however no other liquid phase products were detected.

### 5.3 Regeneration

Regeneration of catalyst P2030 was attempted following the procedure described in section 3.5.6. It was possible to regenerate the catalyst at high temperatures in air. Figure 5.34 shows the concentration of trans-beta-methyl-styrene against time on stream.

**Figure 5.34: Concentration of trans- $\beta$ -methyl styrene**



The concentration of trans-beta-methyl styrene produced by the catalyst after regeneration was similar to that found during the first use of the catalyst.

## 5.4 Deactivation

Two separate reactions were conducted to investigate the deactivation of potassium carbonate supported on alumina through the isomerisation of allylbenzene.

### 5.4.1 Water Addition

Water was added to a feed solution prior to reaction to investigate its effect on the reaction. Catalyst P2013 (15%  $K_2CO_3$ /Engelhard AL-3992E alumina) was used.

**Figure 5.35: Conversion of allylbenzene plus water over P2013**

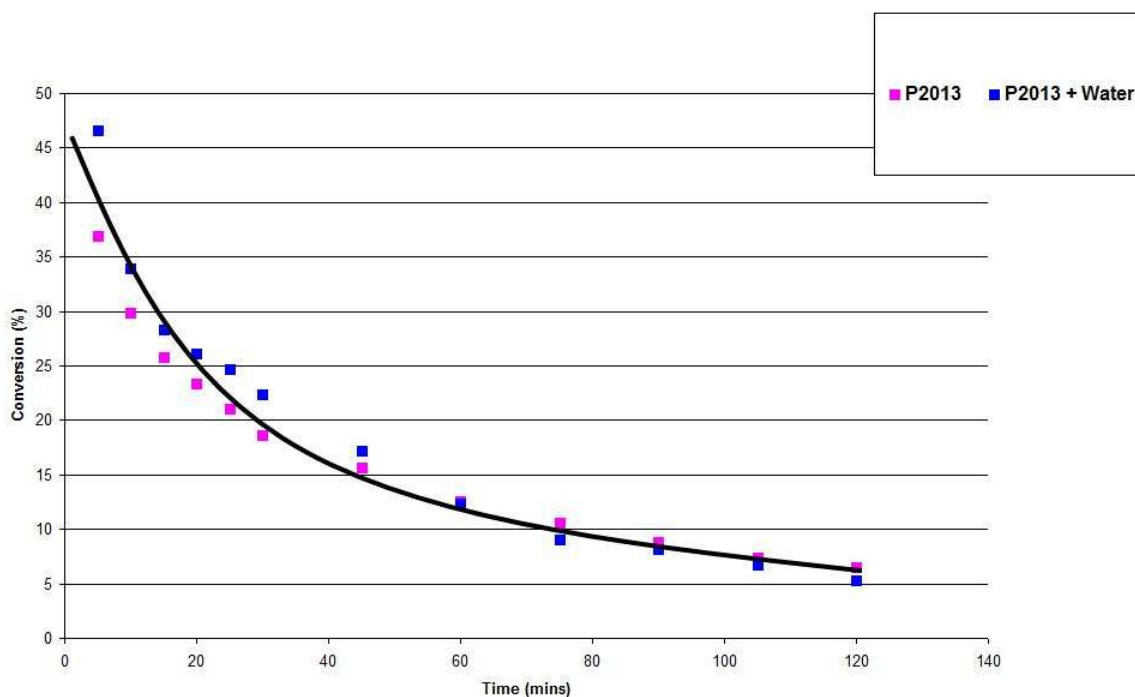


Figure 5.35 show that the addition of water had little effect on the conversion of allylbenzene. However, there was a slight variation in deactivation constants as shown in table 5.9.

**Table 5.9: Deactivation constants**

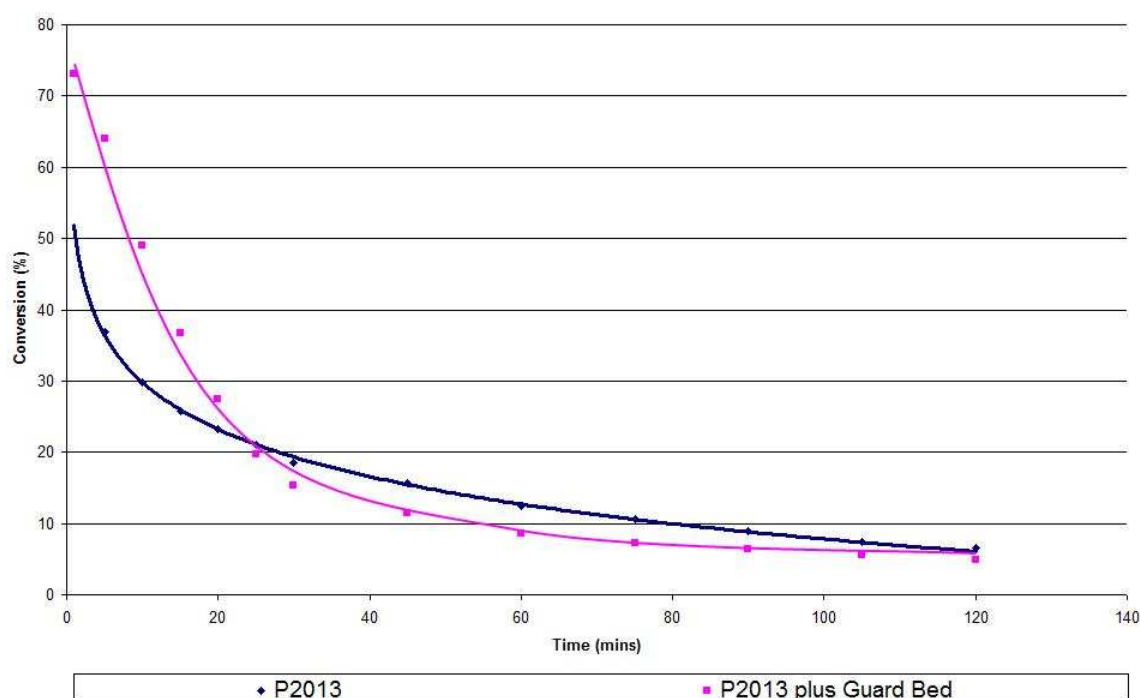
Catalyst	Deactivation Constant ( $\text{min}^{-1}$ )
P2013	$0.0190 \pm 0.0012$
P2013 plus water	$0.0213 \pm 0.0015$

Although the reaction involving the addition of water exhibited a higher deactivation constant the errors in this measurement mean that there is no significant difference between the two constants. Therefore the addition of water to the feed solution has no significant effect on the deactivation of the catalyst.

### 5.4.2 Guard Bed

The introduction of a guard bed was used to investigate the means by which the catalyst was deactivating. The guard bed consisted of 1.5g of alumina support material layered on top of the catalyst bed including fines. For this reaction, catalyst P2013 was used with the corresponding Engelhard AL-3992E alumina support.

**Figure 5.36: Conversion of allylbenzene over P2013 plus guard bed**



The influence of the guard bed was to increase catalyst efficiency at the beginning of the reaction, producing a greater conversion of allylbenzene (~75%). However, conversion rapidly decreased throughout the 120 minutes observed time to a level similar to that found in the absence of the guard bed (~6%).

Table 5.10 shows that the cis:trans ratio for all reactions was 1:7. It also shows that the product alkene selectivity for these reactions was ~90% or higher.

**Table 5.10: Selectivity of cis-/trans- isomers**

Catalyst Code	Cis-isomer (%)	Trans-isomer (%)	Cis:trans ratio
P2013	9.5 ± 1.0	78.9 ± 2.2	1:7
P2013 plus water	9.2 ± 1.6	81.1 ± 6.5	1:7
P2013 plus guard bed	10.1 ± 1.0	79.9 ± 3.4	1:7

## 5.5 Caesium

A reaction was conducted involving a caesium carbonate catalyst prepared by incipient wetness. The catalyst was found to show activity for the isomerisation of allylbenzene, however it deactivated rapidly.

**Figure 5.37: Conversion of allylbenzene against time on stream (Cs)**

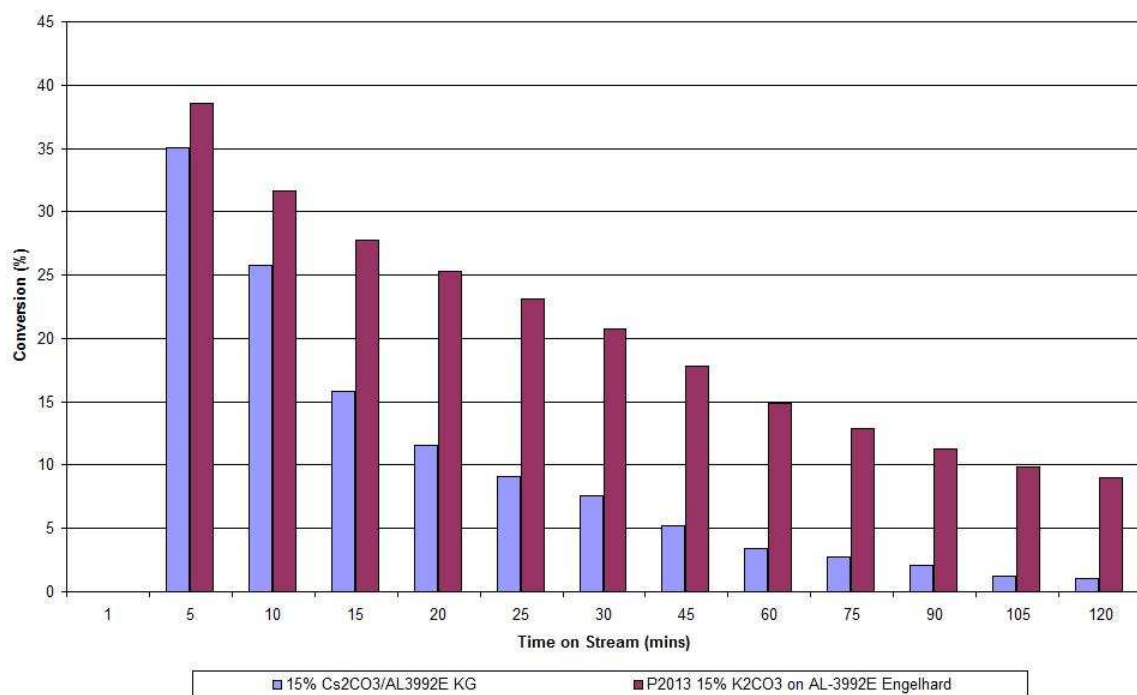


Figure 5.37 shows the conversion of allylbenzene for 15% Cs<sub>2</sub>CO<sub>3</sub>/Al<sub>2</sub>O<sub>3</sub> catalyst and the corresponding K<sub>2</sub>CO<sub>3</sub>/Al<sub>2</sub>O<sub>3</sub> catalyst. It shows that the caesium catalyst exhibited a lower conversion throughout time on stream.

In terms of deactivation constant, the caesium catalyst exhibited a deactivation rate constant double that found for 15% K<sub>2</sub>CO<sub>3</sub> on Engelhard AL-3992E (P2013).

**Table 5.11: Product selectivity for Cs<sub>2</sub>CO<sub>3</sub>/AL-3992E and K<sub>2</sub>CO<sub>3</sub>/AL-3992E**

Catalyst	Cis-isomer (%)	Trans-isomer (%)	Cis:trans ratio
Cs <sub>2</sub> CO <sub>3</sub> /AL-3992E	7.9 ± 3.6	81.5 ± 3.8	1:10
K <sub>2</sub> CO <sub>3</sub> /AL-3992E	7.7 ± 0.1	66.1 ± 4.9	1:8

Table 5.11 shows that both catalysts exhibited high product alkene selectivity (~70-85%); however the caesium catalyst had a slightly higher trans- ratio than that of the potassium catalyst.

## 5.6 Effect of Concentration

A series of experiments were conducted to investigate the effect of the concentration of allylbenzene on the activity of the catalyst. Feed solutions of 1%, 4% and 6% allylbenzene were prepared and catalyst P2015 was used in each reaction.

**Figure 5.38: Conversion against Concentration at 90 minutes on stream**

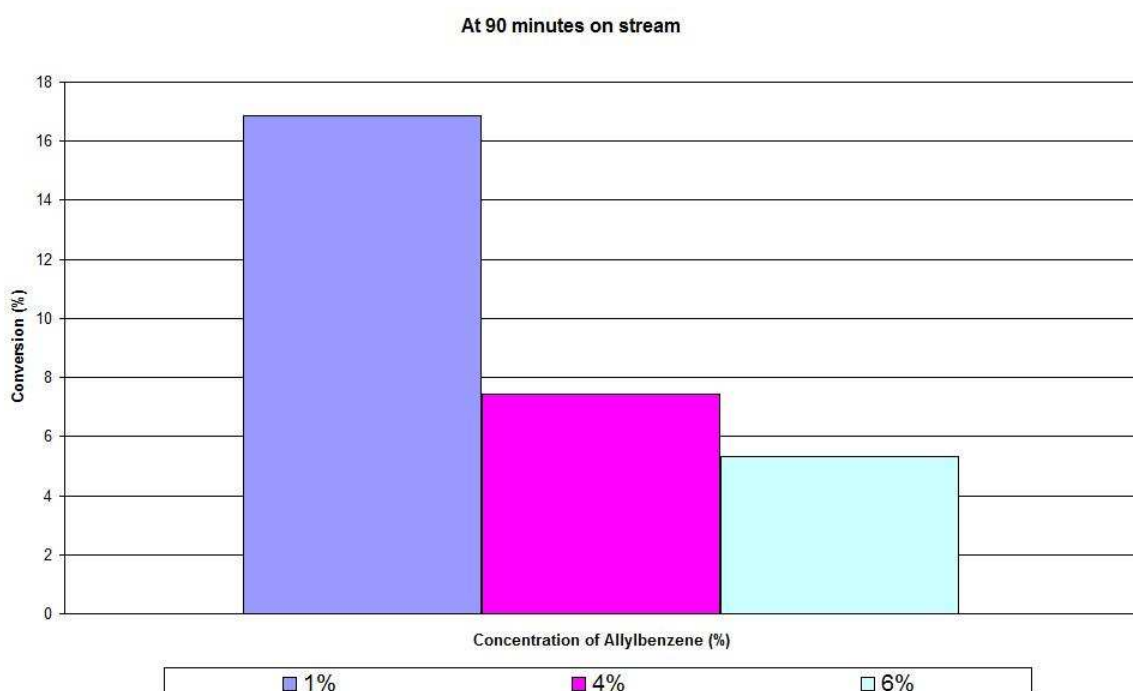


Figure 5.38 shows that conversion decreased with increasing concentration of allylbenzene. Table 5.12 shows the concentration of allylbenzene and the rate of conversion at 90 minutes on stream. These results were then used to calculate the kinetic order with respect to concentration of allylbenzene.

**Table 5.12: Determination of kinetic order with respect to concentration of allylbenzene at 90 minutes on stream**

Concentration	[AB]	ln[AB]	Rate	ln(rate)
1%	0.1	-2.30	17	2.83
4%	0.4	-0.92	7	1.95
6%	0.6	-0.51	5	1.61

Assuming pseudo-first-order kinetics then:

$$\text{rate} = k[\text{AB}]^x$$

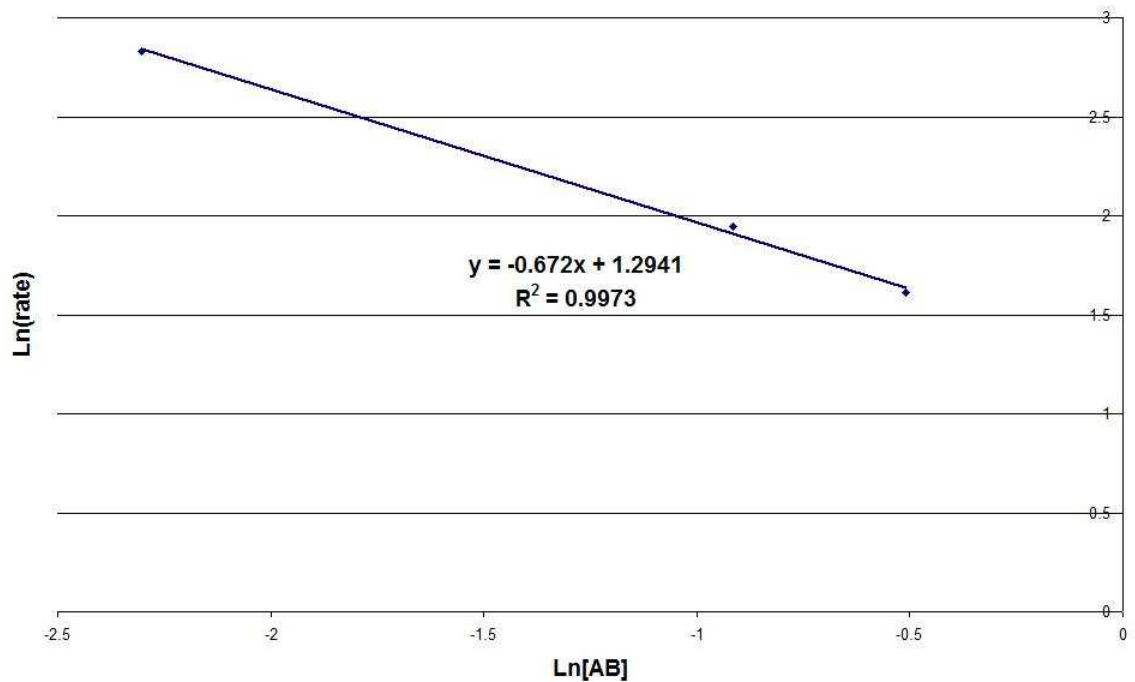
then  $\ln(\text{rate}) = x \cdot \ln[\text{AB}] + \ln k$

where  $[\text{AB}] =$  Concentration of allylbenzene

and rate is a measure of the conversion of allylbenzene.

A graph of  $\ln(\text{rate})$  against  $\ln[\text{AB}]$  was plotted to produce a linear relationship with gradient equal to the order of reaction with respect to the concentration of allylbenzene.

**Figure 5.39: Determination of kinetic order with respect to concentration of feed solution (-0.672) at 90 minutes on stream**



The gradient of the slope was -0.672 which indicated a negative reaction order with respect to concentration of feed solution.

## **5.7 Post Reaction Analysis**

Post reaction analysis is reported for only one catalyst, P2023 (15% K<sub>2</sub>CO<sub>3</sub>/Condea M-1206 alumina). Other catalysts analysed gave similar results.

### **5.7.1 TGA-DSC**

Treatment in O<sub>2</sub>/Ar was performed on two separate samples of catalyst P2023. One sample was taken post reaction and allowed to dry in air. The second sample was taken post reaction and allowed to dry within an inert environment using a glove box. Both samples were analysed using TGA-DSC analysis and species with m/e 17, 18, 28, 32, 44, 78 and 118 were monitored. These correspond to water, oxygen, carbon monoxide, carbon dioxide, benzene and allylbenzene/methylstyrene products respectively.

#### **5.7.1.1 Glove Box**

A sample of catalyst post reaction was housed in a glove box prior to analysis to investigate the effect of the atmosphere on the catalyst. This ensured that the species observed to be present on the surface of the catalyst were a result of the isomerisation reaction and not an effect of the atmosphere. The results obtained for the portion of catalyst dried in an inert atmosphere in the glove box are shown in figure 5.40.

**Figure 5.40: TGA profile P2023 in Oxygen**

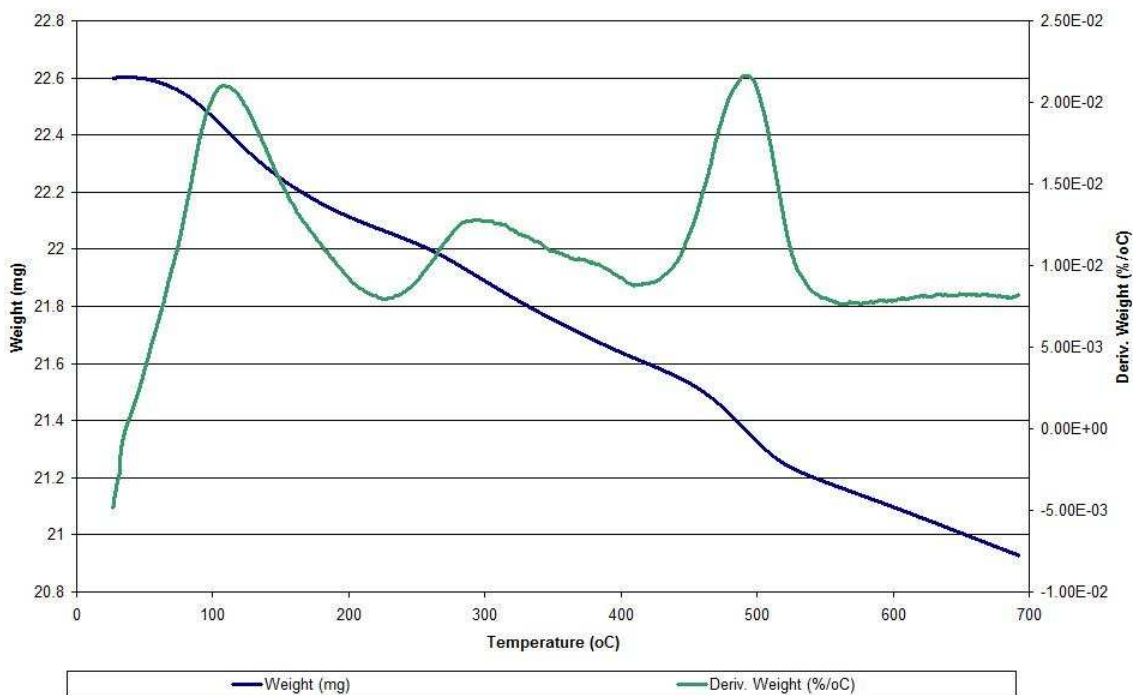


Figure 5.40 shows three main weight loss events at 110°C, 295°C and 495°C and the overall weight loss of the sample is ~7%.

**Figure 5.41: TGA-DSC Profile P2023 in Oxygen**

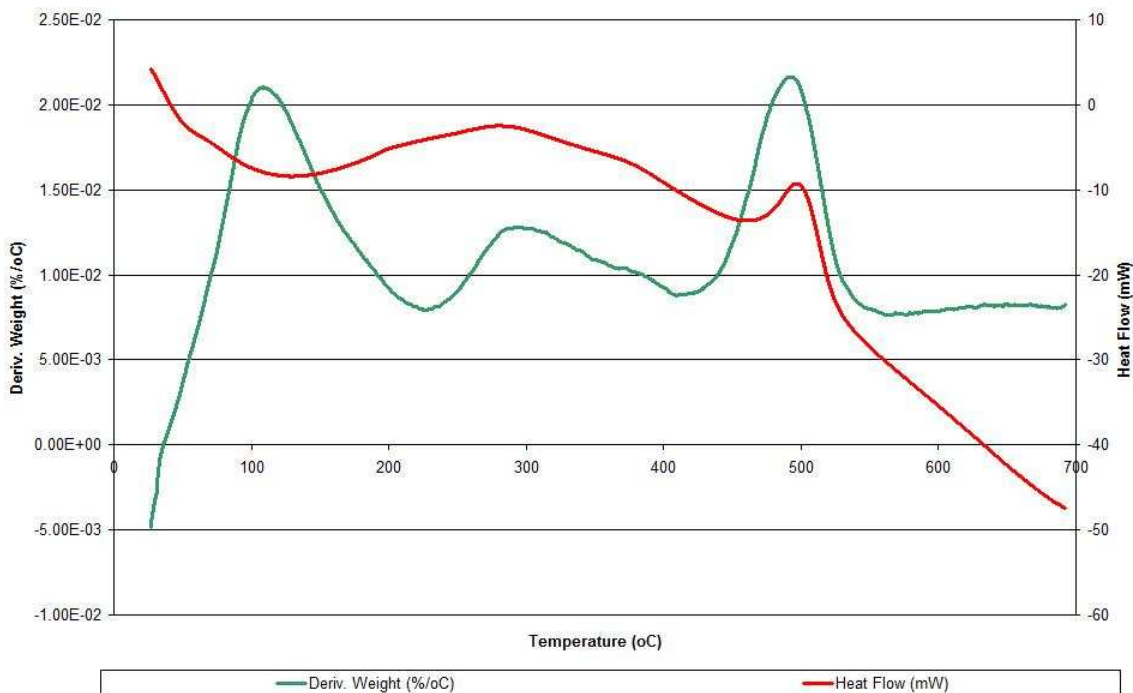
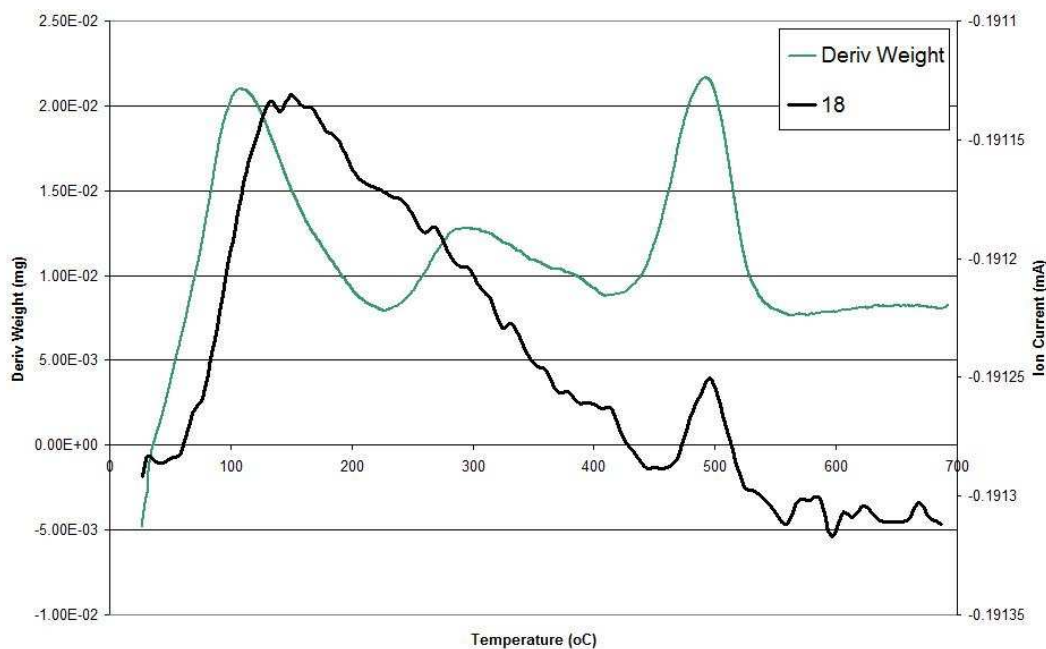


Figure 5.41 shows that the first weight loss event ( $\sim 110^{\circ}\text{C}$ ) is endothermic. The second and third weight loss events were exothermic.

**Figure 5.42: Mass Spectrometry Data P2023 in Oxygen m/e 18**



Mass spectrometry data for m/e 18 in figure 5.42 indicated that the weight loss event occurring around  $100^{\circ}\text{C}$  corresponded to the endothermic desorption of water. It also shows the exothermic evolution of water at  $480^{\circ}\text{C}$  possibly as a result of the combustion a combustion event.

**Figure 5.43: Mass Spectrometry Data P2023 in Oxygen m/e 44**

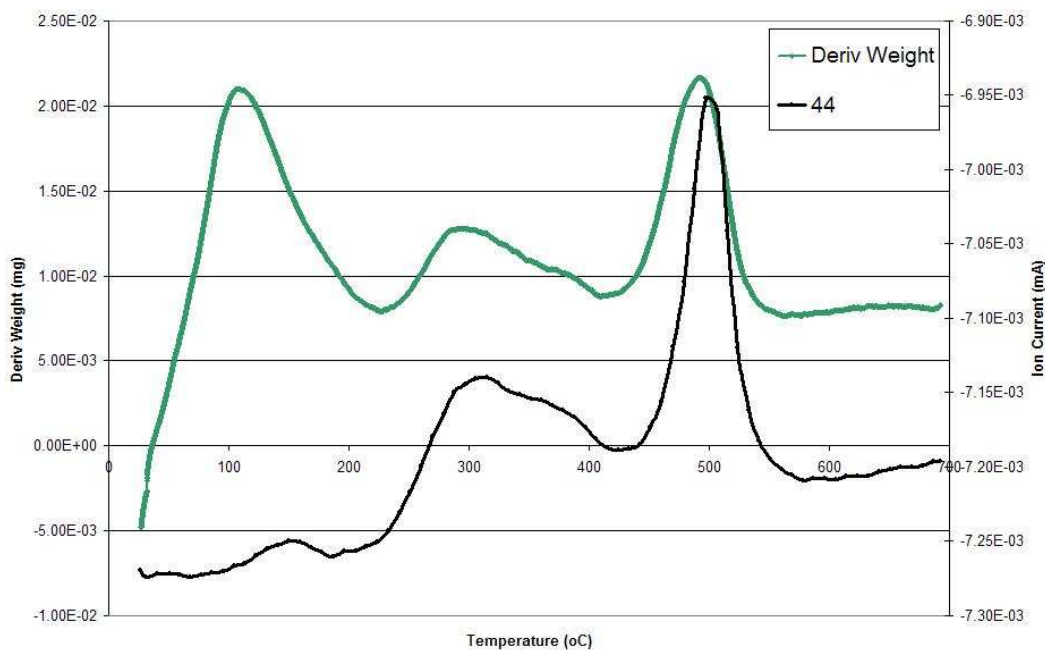


Figure 5.43 shows the evolution of carbon dioxide at 295°C and 495°C. At 495°C both water and carbon dioxide were evolved suggesting that the combustion of a hydrocarbon occurs at this temperature.

**Figure 5.44: Mass Spectrometry Data P2023 in Oxygen m/e 78**

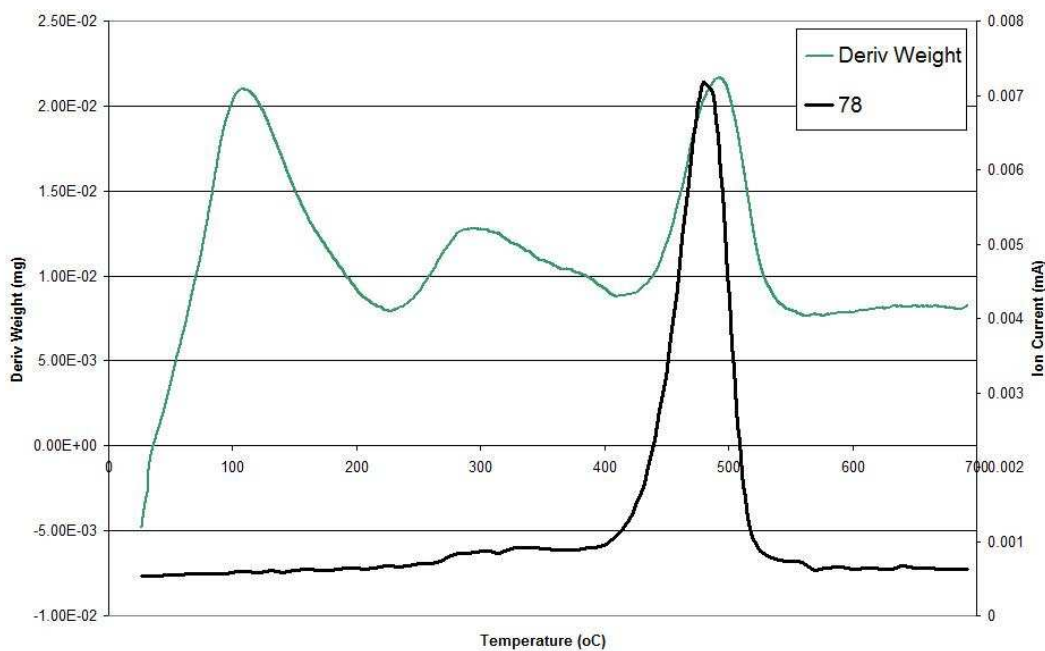
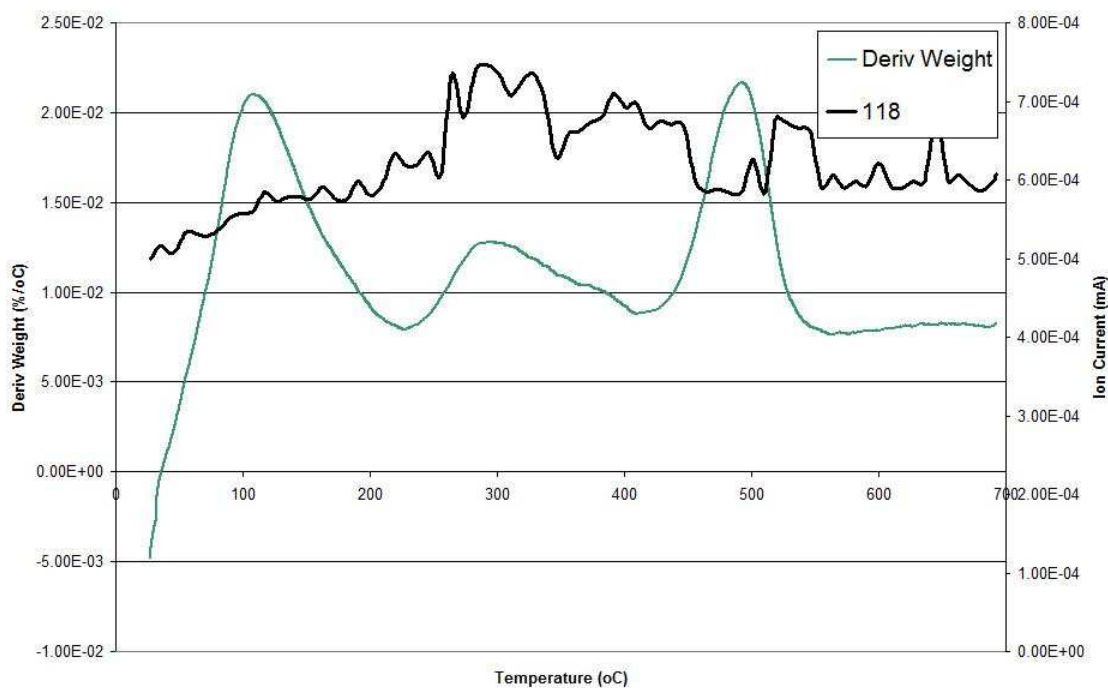


Figure 5.44 shows a weight loss at 495°C corresponding to the evolution of benzene.

**Figure 5.45: Mass Spectrometry Data for P2023 in Oxygen m/e 118**

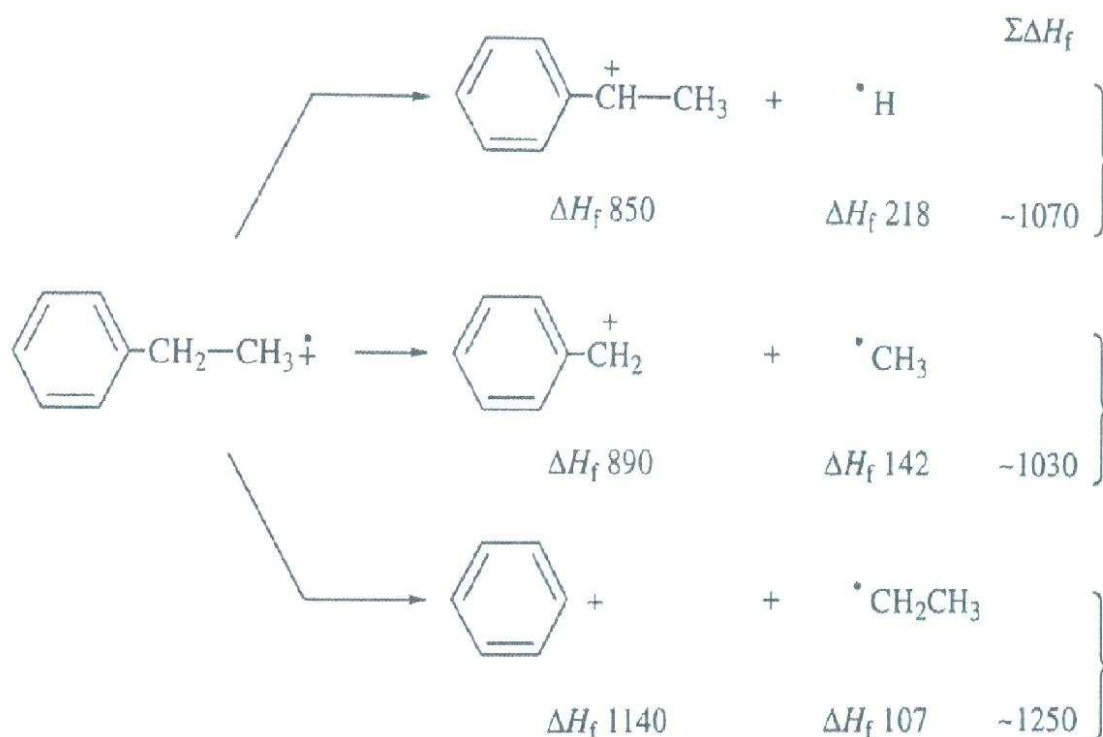


The mass spectrometry data for m/e 118, shown in figure 5.45, may suggest two desorption events at 300 and 410°C, however from the limited response it is unlikely that significant weight loss corresponded to desorption of allylbenzene or methylstyrene products.

Although mass spectrometry data suggested that neither reactant nor product material was present on the surface of the catalyst post-reaction to any significant extent, it is possible that fragmentation has occurred producing benzene fragments. To investigate the fragmentation of allylbenzene/methylstyrene the cracking patterns for the following aromatic alkenyls are discussed.

The fragmentation of ethylbenzene illustrates clearly that the bonds involved in the benzene ring will be stronger than those involved in the side chain. It is therefore energetically favourable that cleavage of bonds occurs at the side chain. Figure 5.51 shows the possible fragmentation that may occur for ethylbenzene.

**Figure 5.46: Possible fragmentation of ethylbenzene**



The enthalpy of formation of  $sp^2$  hybridised carbonium ions, such as  $\text{C}_6\text{H}_5^+$  cation, is very high and therefore these fragments are energetically unfavourable. The secondary benzylic carbonium ion has a lower enthalpy of formation ( $\Delta H_f = 850\text{kJ mol}^{-1}$ ) than that of the primary benzyl cation ( $\Delta H_f = 890\text{kJ mol}^{-1}$ ). However, the stability of the methyl radical is far greater in relation to the hydrogen radical. Therefore, the most favoured pathway for fragmentation would involve the generation of the benzyl cation and methyl radical. This means that species  $m/z$  91 would be the primary species in abundance and the molecular ion would be of moderate abundance [85].

In a study of the mechanism of thermal degradation of alkylbenzenes, it was reported that aromatic compounds with simple chain substituents predominantly produced styrene components. Whereas, compounds such as iso-propylbenzene which contain a tertiary carbon atom tend to produce benzene as a fragment due to the lower strength of the C-C bond between the tertiary atom and the phenyl group [86].

As allylbenzene consists of an aromatic ring with a simple chain substituent the predominant fragment produced is likely to be styrene. The electron ionisation mass spectrum for methylstyrene shows benzene as a fragment but at a relatively low abundance [87]. Therefore, benzene is likely to be present on the surface of the catalyst as result of

the isomerisation reaction and not as a result of fragmentation of adsorbed allylbenzene/methylstyrene compounds in the mass spectrometer.

### 5.7.1.2 Air

The following results were obtained for the portion of catalyst P2023 dried in an ambient atmosphere.

**Figure 5.47: TGA profile for P2023 in Oxygen**

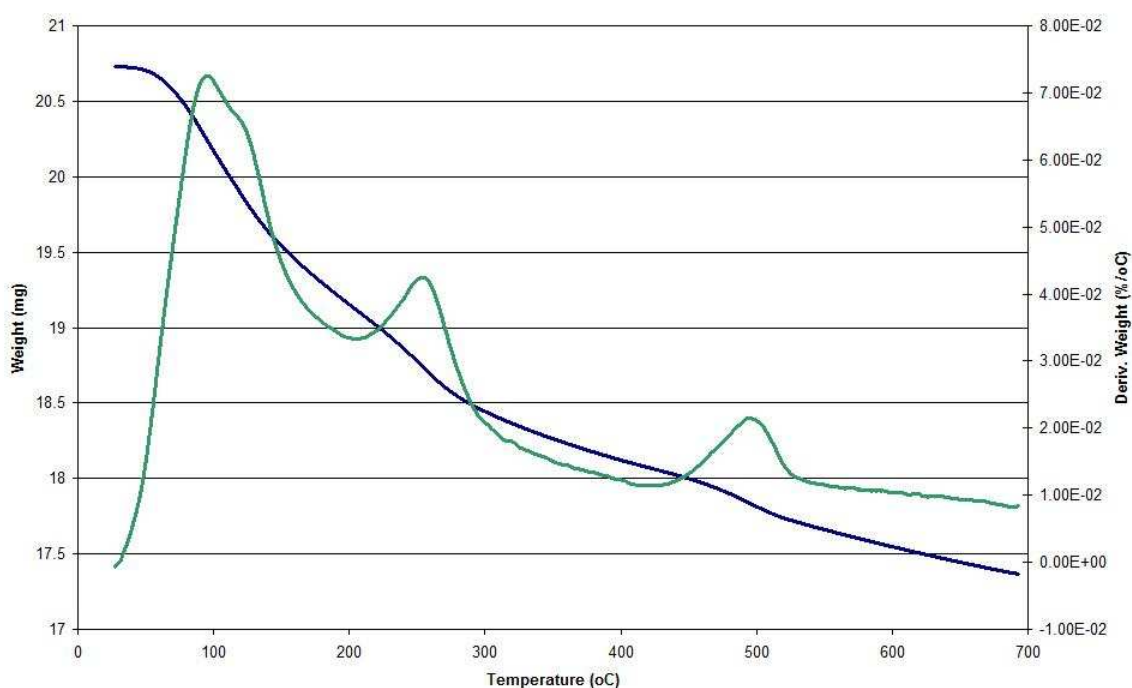


Figure 5.47 shows three weight loss events from the sample of catalyst allowed to dry in air. They occurred at 98°C, 255°C and 498°C and the overall weight loss of the sample was ~16%.

**Figure 5.48: TGA-DSC profile for P2023 in Oxygen**

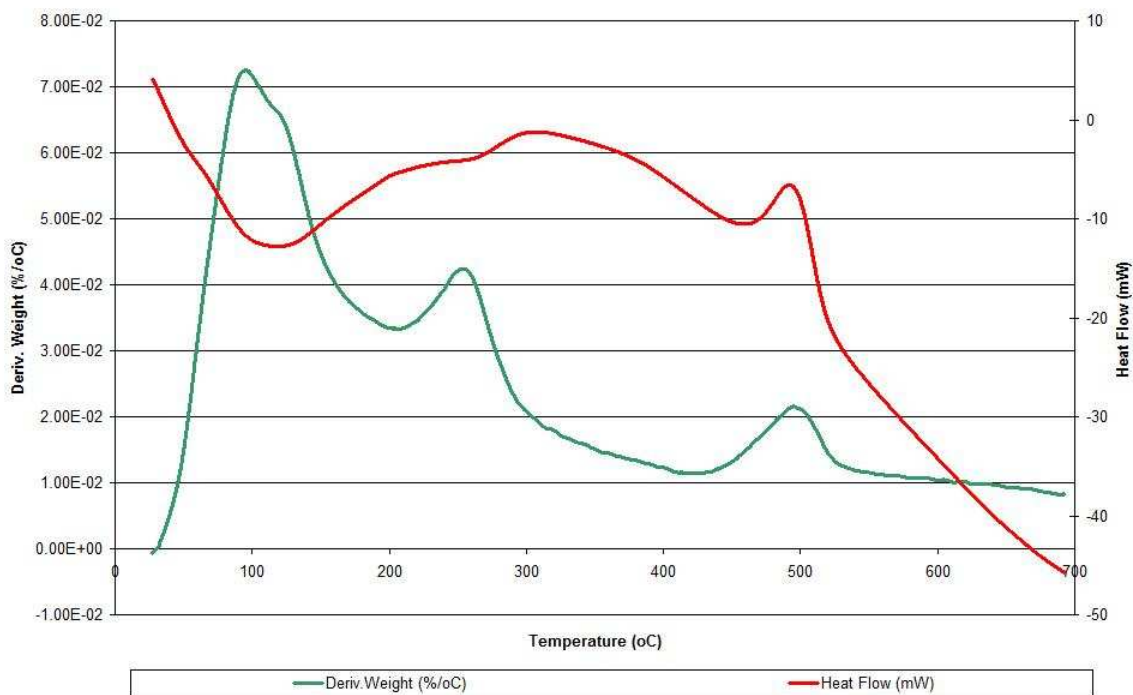
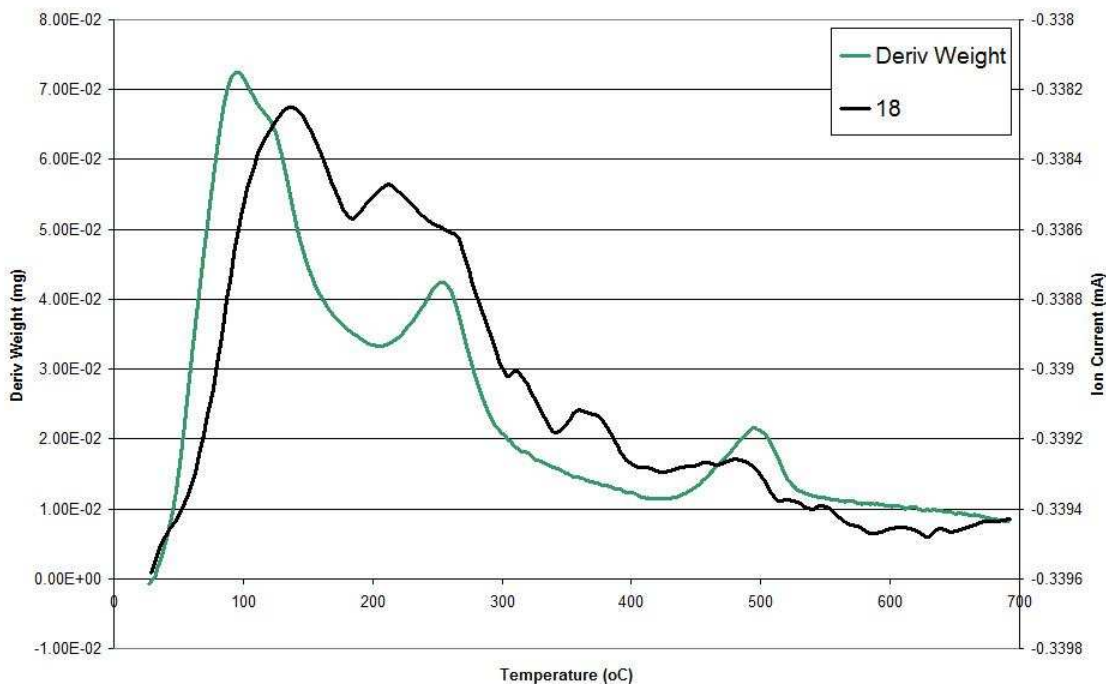


Figure 5.48 shows the first weight loss event was endothermic and the other two weight loss events were exothermic.

**Figure 5.49: Mass Spectrometry data m/e 18**



Mass spectrometry data for species corresponding with m/e 18 in figure 5.49 shows that water was desorbed throughout the observed temperature range with the main weight events occurring at ~150 and between 200-300°C.

**Figure 5.50: Mass Spectrometry data m/e 44**

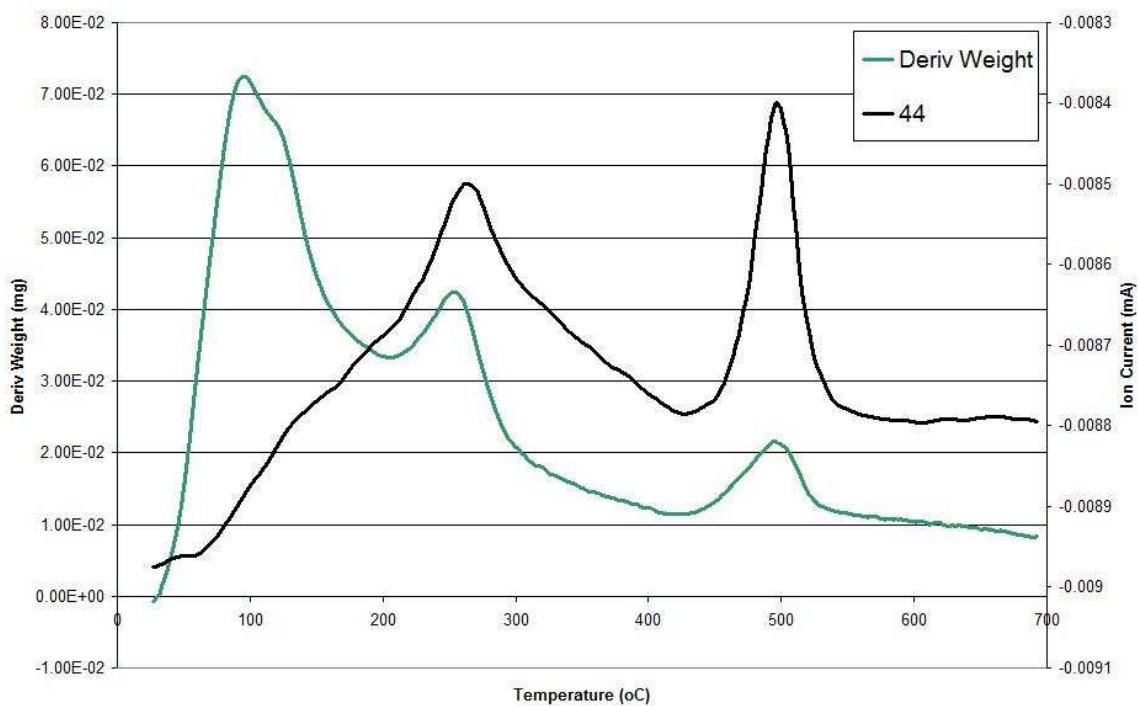


Figure 5.50 shows that carbon dioxide is evolved at 260°C and at 500°C.

**Figure 5.51: Mass Spectrometry data m/e 78**

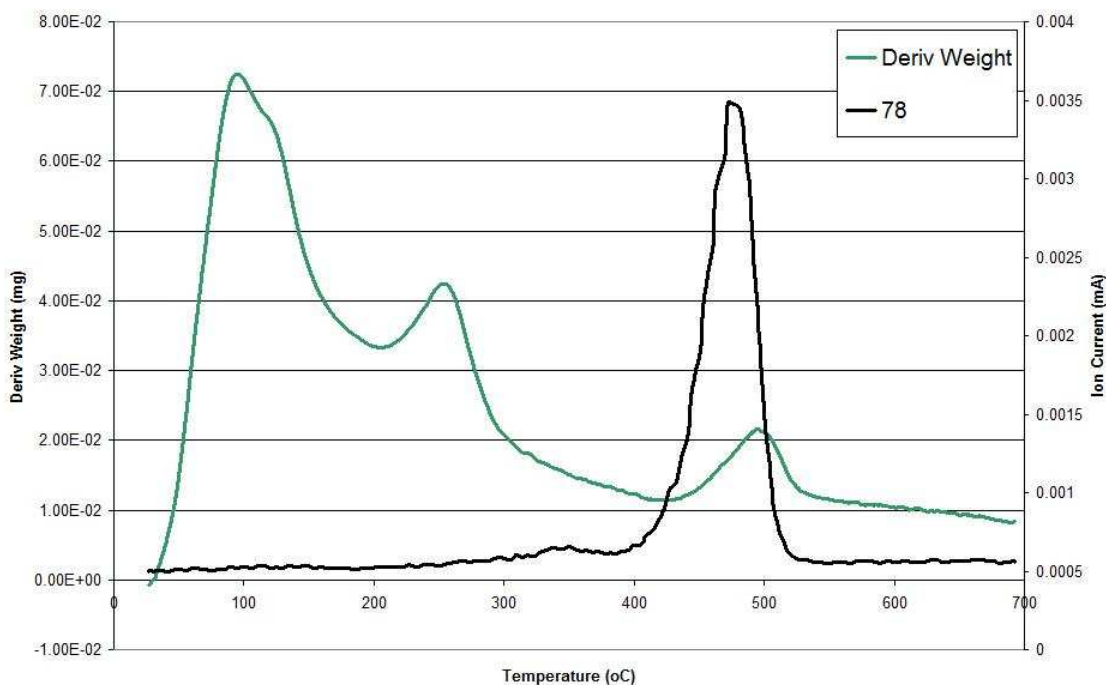


Figure 5.51 shows mass spectrometry data for m/e 78 which corresponded to benzene. Desorption of benzene was observed at 480°C.

**Figure 5.52: Mass Spectrometry data m/e 118**

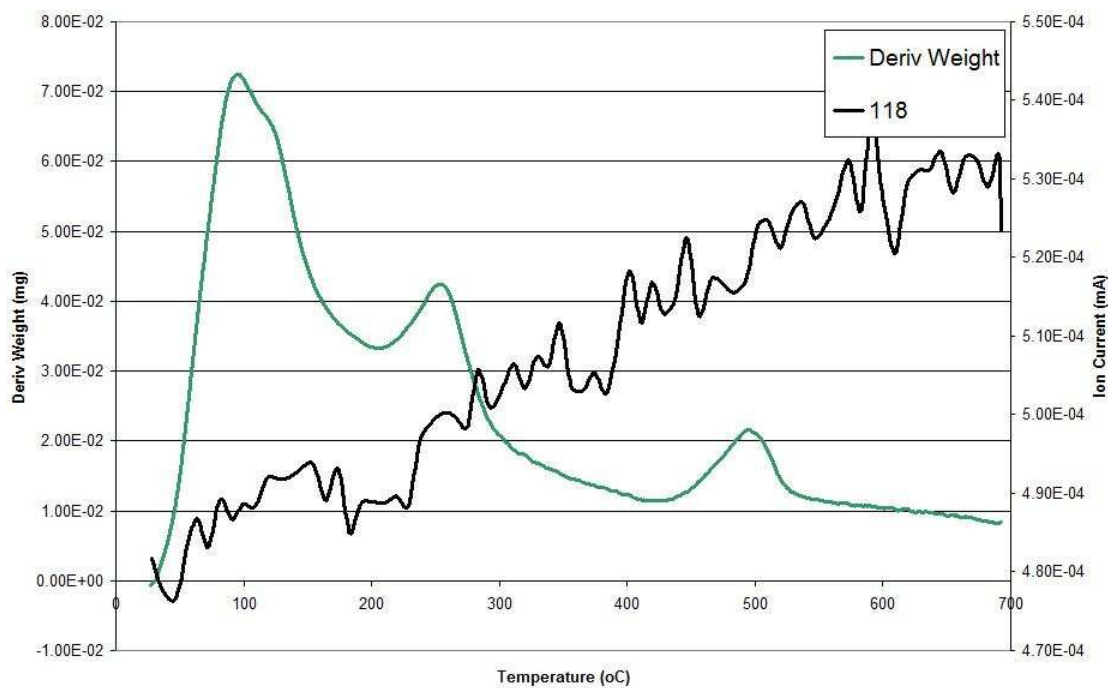
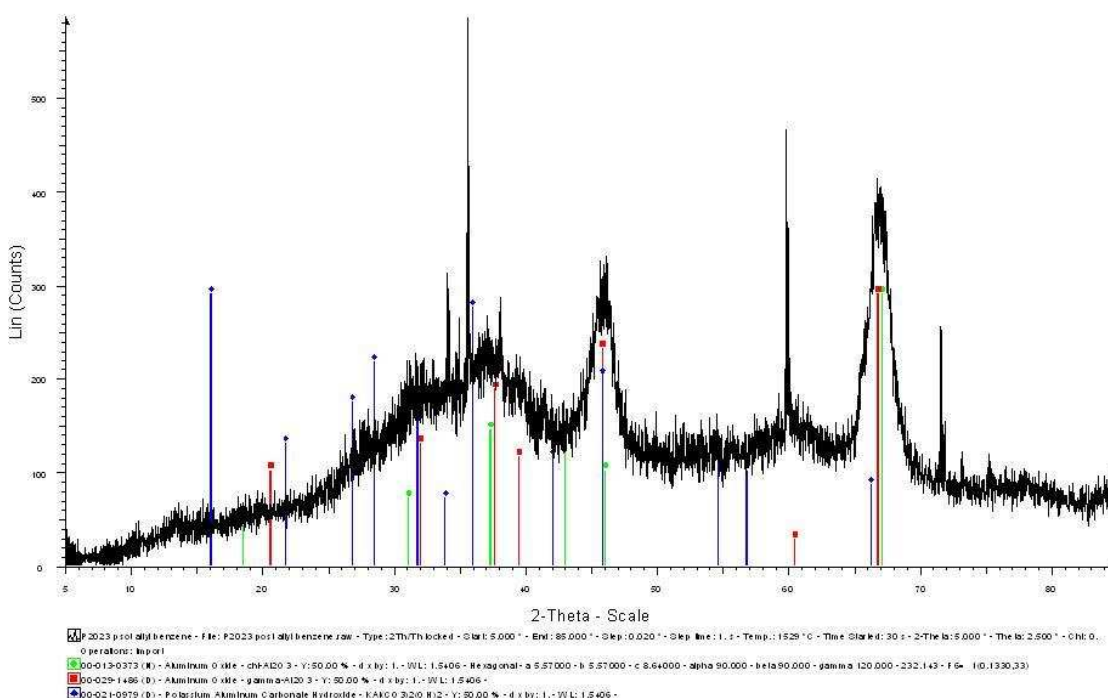


Figure 5.52 shows that weight losses did not correspond to desorption of allylbenzene or methylstyrene products from the surface of the catalyst.

### 5.7.3 XRD

X-ray diffraction analysis was conducted on catalyst P2023 post-reaction at ambient temperature only.

**Figure 5.53: XRD for Catalyst P2023 post-reaction**



The x-ray diffraction pattern for  $\gamma$ -alumina was observed. Additional peaks were observed post-reaction and were identified tentatively as a potassium aluminium carbonate hydroxide compound. Further identification was not possible.

#### 5.7.4 BET

A significant change was noted in the surface area determination results post-reaction in relation to those pre-reaction.

**Table 5.13: Comparison of surface area determination analysis pre/post reaction P2023**

Catalyst P2023	Surface Area (m <sup>2</sup> g <sup>-1</sup> )	Pore Diameter (nm)	Pore Volume (cm <sup>3</sup> g <sup>-1</sup> )
pre-reaction	149	9.16	0.34
post-reaction	112	11.70	0.33

Post reaction the catalyst exhibited a decreased surface area; approximately 25% surface area was lost through reaction.

## 6. DISCUSSION

### 6.1 Pre-reaction Catalyst Characterisation

#### 6.1.1 Surface Area Determination

BET analysis of all catalysts prior to reaction was used to determine surface area, pore diameter and pore volume measurements. The results obtained are shown in table 5.1.

**Table 6.1: Surface Area Measurements**

Catalyst Code	Nominal K <sub>2</sub> CO <sub>3</sub> Loading / % w/w	Surface Area (m <sup>2</sup> g <sup>-1</sup> )	Pore Diameter (nm)	Cumulative Pore Volume (cm <sup>3</sup> g <sup>-1</sup> )
P2026	12	164	9.79	0.41
P2008	15	149	10.93	0.40
P2013	15	130	11.60	0.38
P2014	15	128	6.19	0.23
P2015	15	133	11.02	0.37
P2016	15	188	5.94	0.28
P2023	15	149	9.16	0.34
P2030	15	134	10.27	0.35
P2027	18	167	8.89	0.34
P2017	20	104	12.56	0.33
P2019	20	102	9.10	0.23

Although there were no clear trends in surface area, catalysts P2017 and P2019 were observed to have slightly lower surface areas relative to the other catalysts. The catalysts with a 20% nominal loading of potassium, exhibited significantly lower surface areas than those with a 15% loading suggesting that the increased loading of active phase has resulted in pore blockage, thus reducing the available surface area.

## 6.1.2 TGA-DSC Analysis

### 6.1.2.1 Support

Results obtained from the treatment of the Engelhard AL-3992E alumina support material under an O<sub>2</sub>/Ar gas mix heated from room temperature to 700°C showed continuous weight loss throughout the whole temperature range. The overall weight loss of the sample was ~3% and corresponded to desorption of water. This behaviour is typical of a γ-alumina and represents the removal of adsorbed H<sub>2</sub>O at low temperature before loss of hydroxyls over the rest of the temperature range.

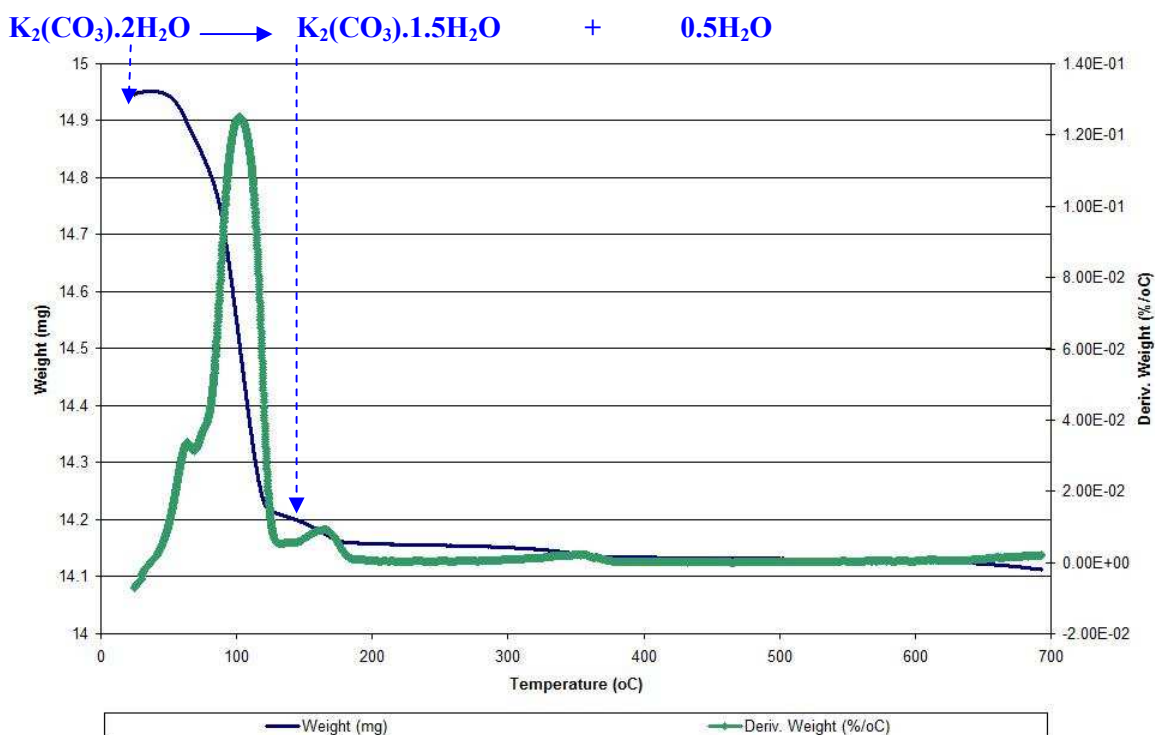
### 6.1.2.2 Potassium Carbonate

Calcination of potassium carbonate showed four main weight loss events at 65°C, 102°C, 167°C and 355°C. The weight losses at 65°C and 102°C were attributed to desorption of water. At 167°C and 355°C, carbon dioxide was evolved, however this contributed very little to the overall weight loss of the sample. The overall weight loss of the sample was 5.5% and as most of the weight lost could be attributed to desorption of water, the following equation was derived.



In Figure 6.1 the weight loss event, indicated by the arrows, corresponds to the loss of half a mole of water from the sample.

**Figure 6.1: Weight loss profile for Potassium Carbonate**



The weight loss which corresponded to the loss of water suggested that potassium carbonate existed in the di-hydrate. The endothermic evolution of carbon dioxide at 167°C and 355°C only contributed ~1% weight loss and did not therefore correspond to any significant decomposition of potassium carbonate.

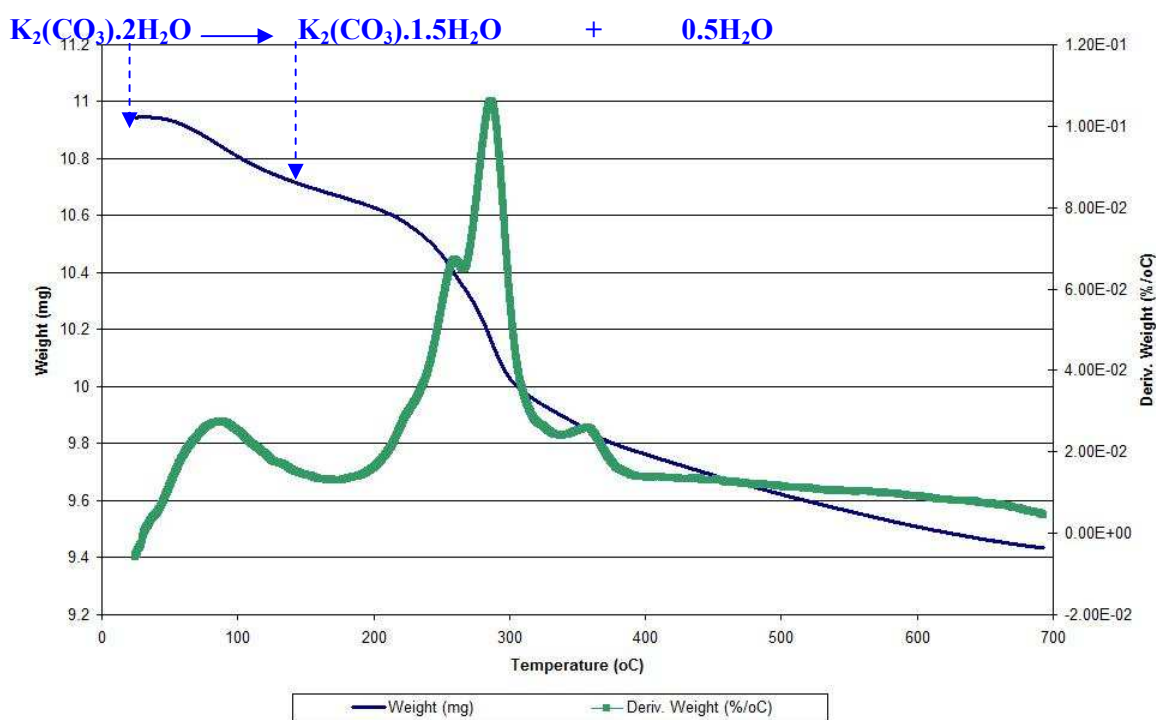
In a previous study involving the thermal decomposition of potassium carbonate, Knacke *et al.* [88] stated that the decomposition of potassium carbonate to form potassium oxide is negligible before its melting point of 900°C (in N<sub>2</sub>). The results for the calcination of potassium carbonate were in agreement with the literature, as potassium carbonate did not decompose over the temperature range (below the melting point of K<sub>2</sub>CO<sub>3</sub>).

### 6.1.2.3 Inert Atmosphere

Catalysts were heated from room temperature to 700°C at 10°C.min<sup>-1</sup> under an inert atmosphere. Four main weight loss events were observed at ~100°C, 253°C, 285°C and 384°C. Mass spectrometry data indicated that water was desorbed at ~100°C and at 384°C

carbon dioxide was evolved. At 253 and 285°C however, there was an overlap of desorption of water and evolution of carbon dioxide. Investigation of the actual weight lost at each of these temperatures suggests that potassium carbonate existed in the dihydrate state. Half a mole of water of hydration was lost at ~100°C as shown in figure 6.2.

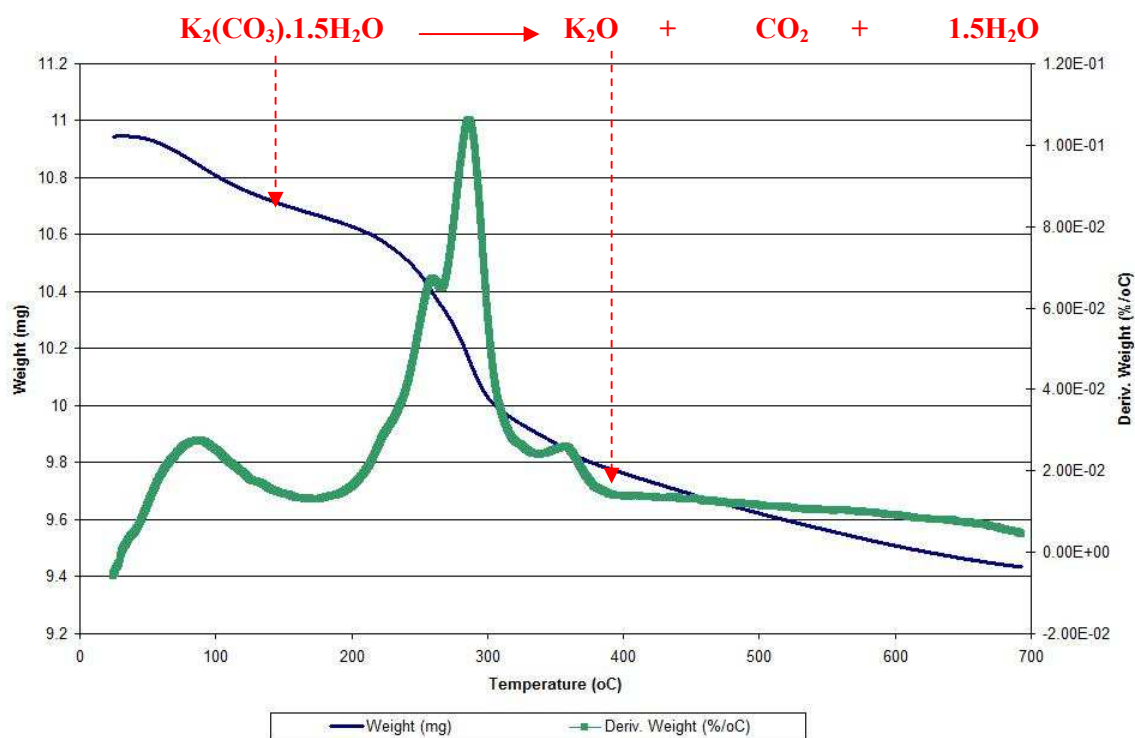
**Figure 6.2: Weight loss profile of P2013 in Argon (~100°C)**



It is assumed that the rest of the water of hydration associated with potassium carbonate was lost around 285°C however due to the evolution of carbon dioxide at this temperature the weight of water could not be quantified.

Heat flow data (figure 5.8) showed that all weight loss events were endothermic and mass spectrometry data confirmed that carbon dioxide was evolved between 200-400°C. This suggests that carbon dioxide was liberated from the active phase at these temperatures. If it is assumed that all of the weight lost between 200-400°C can be attributed to the evolution of carbon dioxide, i.e. neglecting to consider desorption of water around these temperature the following equation shown in figure 6.3 could be derived

**Figure 6.3: Weight loss profile of P2013 in Argon (200-400°C)**

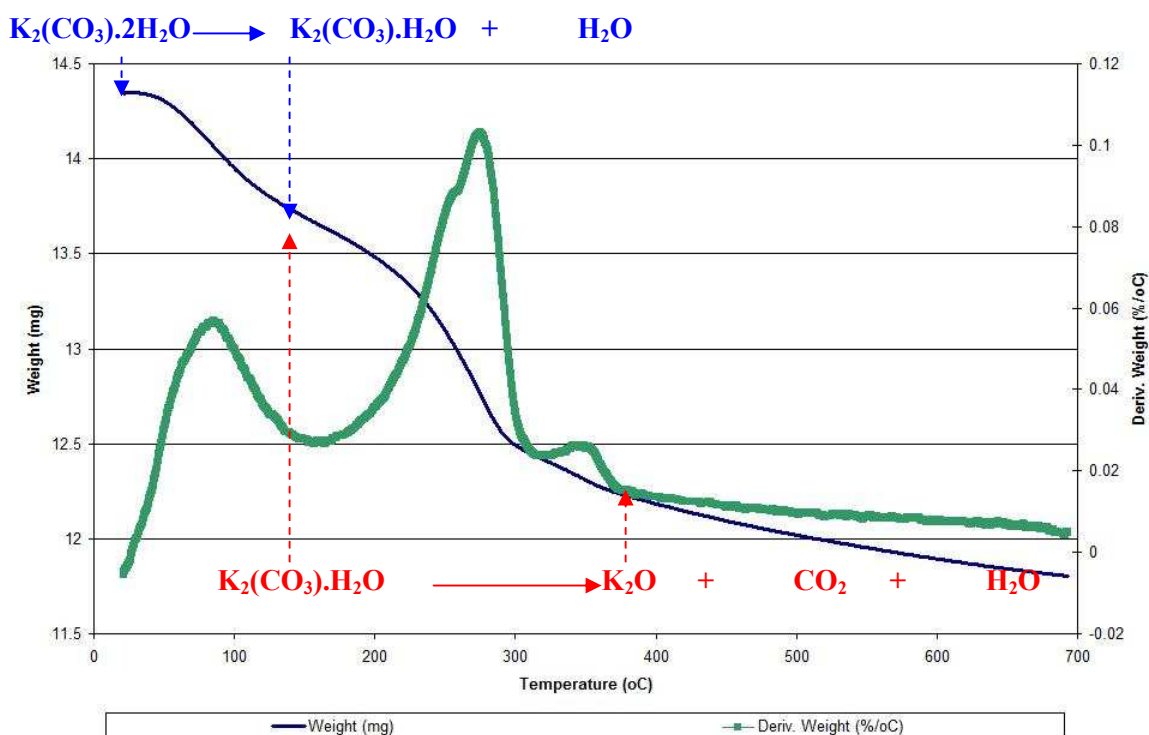


Therefore although water is also evolved that data does indicate that there is significant decomposition of  $\text{K}_2\text{CO}_3$ . The thermal instability of potassium carbonate on alumina is in agreement with previous literature [89, 90]. Stork and Pott [91] reported an endothermic decomposition with the evolution of carbon dioxide around 270°C. However, it is unlikely that there is free potassium oxide present on the surface of the catalyst. Previous studies also suggest a strong interaction between potassium carbonate and the alumina surface resulting in Al-O-K bonding [74, 91]. Dotzel et al. reported the interaction of potassium with hydroxyl groups present on  $\gamma$ -alumina producing Al-O-K groups through the loss of water and carbon dioxide [75].

#### 6.1.2.4 Calcination

The calcination data showed three main weight loss events; the second of which exhibited a shoulder peak at 257°C. Catalyst P2030 experienced an 18% overall weight loss. The first weight loss event occurred around 100°C and corresponded to the loss of water from the dihydrate potassium carbonate active phase. This accounted for 5% weight loss.

**Figure 6.4: Weight loss profile of P2030 in Oxygen (~100°C)**



The further 12% was lost between 200-375°C. The weight loss events at 257°C, 287°C and 360°C were endothermic. Mass spectrometry data showed an overlap of the evolution of carbon dioxide and further desorption of water molecules at these temperatures. The evolution of carbon dioxide at these temperatures shown as endothermic weight loss suggests the degradation of the carbonate active phase.

Indeed, the weight lost between 200-375°C corresponds to the loss of one mole of water and to the decomposition of potassium carbonate to potassium oxide and carbon dioxide. Similar decomposition occurred under an inert atmosphere and agrees with previous studies [74].

Results obtained through this study agree with literature reports of the interaction between potassium carbonate and alumina support. It is thought that potassium penetrates the lattice and thermal treatment causes the decomposition of most of the carbonate producing a potassium oxide species that is strongly interacting with the support.

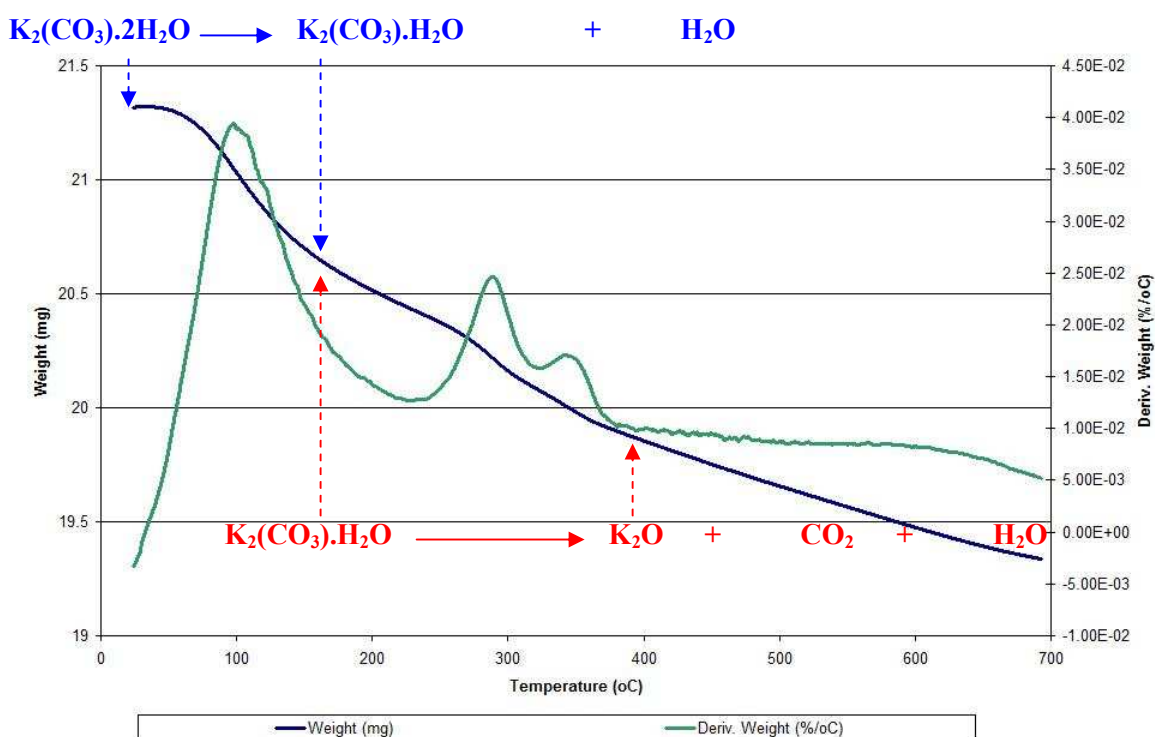
Previous studies show thermal instability of potassium carbonate under an inert atmosphere, this study has shown that similar results can be obtained in air. Therefore the calcination process results in the breakage of the metal carbonate bonds.

Had calcination been performed *in situ* the catalyst would be active but calcination was not performed *in situ*. Catalysts were calcined and then stored allowing for atmospheric water to become adsorbed to the surface. Therefore, further pre-treatment was required before reaction.

#### **6.1.2.5      Activation**

Activation of catalyst P2008 was conducted after calcination. Activation removes water molecules adsorbed to the surface to expose Brønsted basic sites capable of catalysing the reaction. Figure 6.5 shows the reactions that corresponded to the weight losses at given temperatures.

**Figure 6.5: Weight loss profile for calcined P2008**



The first weight loss  $\sim 100^\circ\text{C}$  corresponded to loss of water and weight losses at  $165^\circ\text{C}$  and  $350^\circ\text{C}$  correspond to the evolution carbon dioxide. All weight losses were found to be endothermic therefore indicating decomposition of the active phase. Post-calcined, catalysts had adsorbed water and carbon dioxide and reformed a species that was similar to  $K_2(CO_3) \cdot 2H_2O$  on the surface. Hence the species broke down in a manner similar to that found with the activation directly from a non-calcined catalyst. The water and carbon dioxide losses occur at the same temperatures.

Similar thermal instability of potassium carbonate was observed during the calcination procedure and is in agreement with previous studies [74, 75, 89, 90, 91].

A limiting factor for the use of heterogeneous base catalysts is the rapid deactivation caused through being exposed to the atmosphere [18]. This can be seen clearly from these results. It is therefore important that catalysts do undergo *in situ* high temperature pre-treatment prior to use for the reaction.

### 6.1.3 XRD analysis

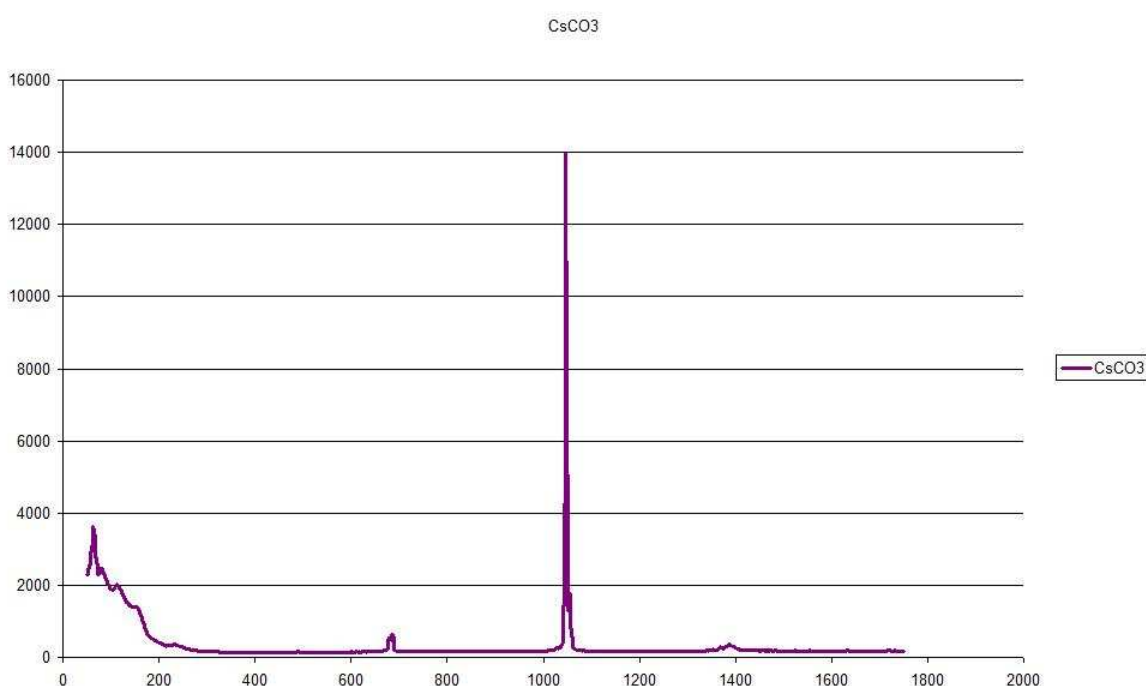
Powder X-ray diffraction analysis of all catalysts prior to reaction identified alumina support material to be  $\gamma$ -alumina. This type of alumina is not expected to change phase ( $\delta$ -alumina) until above  $750^{\circ}\text{C}$  [77]. Samples of catalysts were heated to  $500^{\circ}\text{C}$  under an  $\text{O}_2/\text{Ar}$  atmosphere. The pattern remained constant therefore alumina did not experience a phase change.

A pattern for potassium carbonate could not be identified at room temperature or at elevated temperature ( $500^{\circ}\text{C}$ ). It was concluded that the active phase was amorphous in character and could not be detected by x-ray diffraction.

### 6.1.4 Raman Spectroscopy

The Raman spectra for potassium carbonate and caesium carbonate are similar in that the main peak  $\sim 1068\text{cm}^{-1}$  exists in both traces. Figure 6.6 shows the Raman spectrum of caesium carbonate.

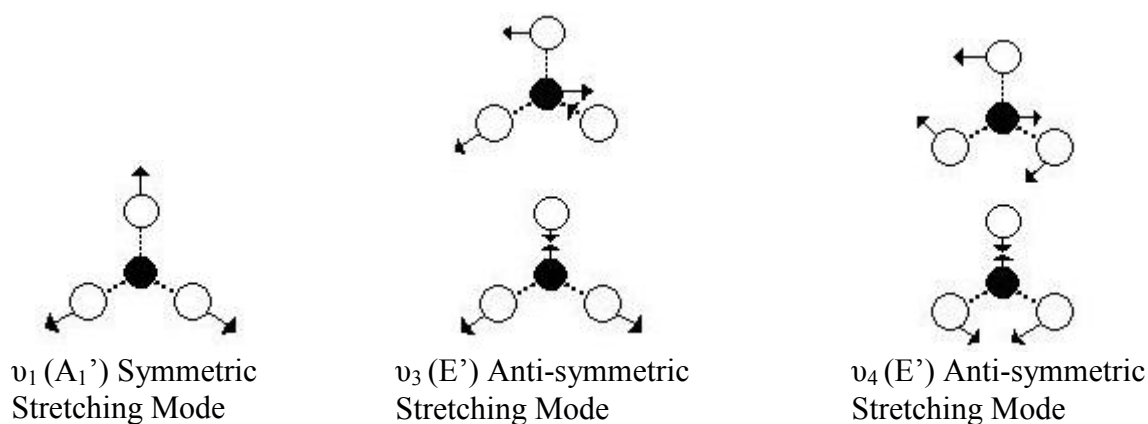
**Figure 6.6: Raman Spectrum of Caesium Carbonate**



In addition, the Raman spectrum of sodium carbonate is reported to show peaks at 1081, 1071 and 701 $\text{cm}^{-1}$  [92]. This suggests that the presence of the carbonate ion gives rise to the main peaks in the spectrum.

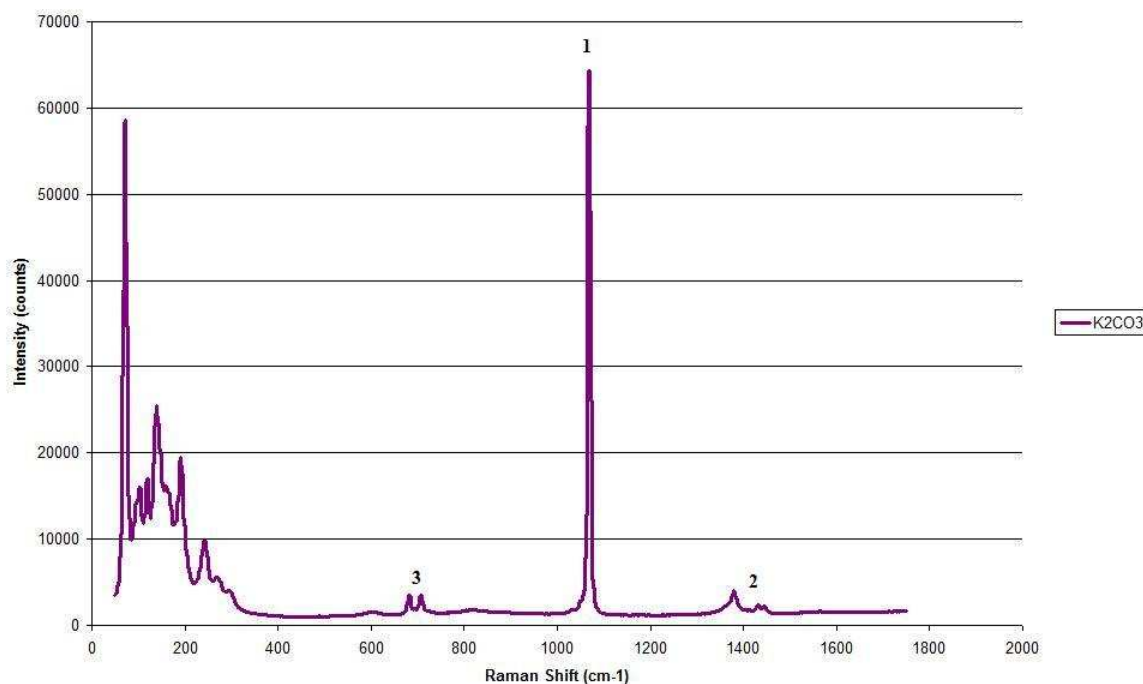
The carbonate ion has  $D_{3h}$  symmetry and exhibits four fundamental modes of vibration [93]. The expected vibrations are  $\nu_1 (A_1')$  R $\sim 1065\text{cm}^{-1}$ ;  $\nu_2 (A_2'')$  i.r.  $\sim 880\text{cm}^{-1}$ ;  $\nu_3 (E')$  R $\sim 1400\text{cm}^{-1}$  and  $\nu_4 (E')$  i.r., R $\sim 685\text{cm}^{-1}$  [94]. Of these, only three are Raman active and are shown in figure 6.7.

**Figure 6.7: Raman Active Vibrations**



Previous studies suggest a breakdown in the selection rules for  $D_{3h}$  symmetry in the carbonate ion with the observation of the Raman inactive  $\nu_2 (A_2'')$  [95]. This band was not observed for this sample. Figure 6.8 shows the bands observed in the Raman spectrum of potassium carbonate.

**Figure 6.8: Bands Observed in Raman Spectrum of K<sub>2</sub>CO<sub>3</sub>**



In the Raman spectra of K<sub>2</sub>CO<sub>3</sub> at room temperature, the principal symmetric stretching mode ( $\nu_1$  (A<sub>1</sub>')) is prominent at 1068cm<sup>-1</sup>. Anti-symmetric stretching ( $\nu_3$  (E')) is seen by three clear peaks at 1382, 1441 and 1449cm<sup>-1</sup>. Equally, anti-symmetric stretching ( $\nu_4$  (E')) is observed at 682 and 709cm<sup>-1</sup>.

The splitting of  $\nu_3$  (E') and  $\nu_4$  (E') bands could be due to the presence of ion-pairs. Lee et al. observed that in dilute solutions of potassium carbonate the band corresponding to  $\nu_3$  (E') was degenerate but in more concentrated solutions there was not degeneracy, shown by the presence of band splitting [96]. This can be used to explain the presence of two bands at 682 and 709cm<sup>-1</sup> however it is unclear why there are three bands for the anti-symmetric stretching mode ( $\nu_4$  (E')).

The following table shows the band present during thermal treatment of K<sub>2</sub>CO<sub>3</sub>/Al<sub>2</sub>O<sub>3</sub> under O<sub>2</sub>/Ar gas mix. Post-treatment, the sample was allowed to cool to ambient temperature (in this case, 26°C) and a measurement taken.

**Table 6.2: Bands Observed (cm<sup>-1</sup>) in Raman Spectra of K<sub>2</sub>CO<sub>3</sub>/Al<sub>2</sub>O<sub>3</sub>**

R.T	100°C	200°C	300°C	400°C	500°C	26°C	Assignment
63	63	63	63	63	63	61	
169	164	160	157				
206	204	205	205				$\nu_L$
281	279	277					
324	321	319					
	354	354					
	437	436					
542	544	545					
578	577	572	574				
730	730	730	731				
	841						
	896	894					
1063	1054	1051	1050	1048	1050	1056	$\nu_1(A_1')$
1099	1098	1098	1096				
1482	1484	1487					$\nu_3(E')$
1740							

From these results it is clear that after thermal treatment the band corresponding to symmetric stretching is still apparent. However, the anti-symmetric modes are not observed. It is suggested that bands 63-280cm<sup>-1</sup> are lattice modes ( $\nu_L$ ) and also that metal-ion-oxygen vibrational frequencies exist within the range 100-350cm<sup>-1</sup> [97].

The presence of two peaks at 1063cm<sup>-1</sup> and 1099cm<sup>-1</sup> must be accounted for. Post-calcination there is only one peak at 1056cm<sup>-1</sup>. The presence of residual carbonate species post-calcination compliments the results obtained through TGA-DSC analysis which indicated that not all of the carbonate ion was decomposed.

It is suggested that the second peak (1099cm<sup>-1</sup>) arises from the presence of bicarbonate ion on the catalyst. During thermal treatment this species is decomposed and post-treatment only the carbonate ion remains. The second peak therefore relates to the C-OH stretching mode ( $\nu_5(A')$ ) [98].

## 6.2 Post Reaction Analysis

Post reaction analysis of the catalyst showed similar trends so results for only one catalyst (P2023) were reported. All catalysts post-reaction were observed to be pale yellow in colour this is in agreement with studies performed by R. Dotzel [84] involving  $K_2CO_3/\gamma$ -alumina.

### 6.2.1 XRD

The post reaction XRD pattern corresponded to that of  $\gamma$ -alumina only, indicating that no phase change occurred. Potassium carbonate was not observed however a species identified tentatively as a potassium aluminium carbonate hydroxide compound was observed. It is thought that this compound is the result of a reaction between the active phase and the alumina. There is a general agreement that potassium carbonate interacts with the alumina support surface, [91, 98, 99] producing Al-O-K systems. Stork and Pott [91] concluded that the carbonate reacts with surface hydroxyl groups to form O-K groups and that no further reaction with the gamma alumina lattice occurs. Hence, the formation of potassium aluminium carbonate hydroxide is in agreement with supporting literature.

### 6.2.2 TGA-DSC

Post-reaction TGA-DSC analysis exhibited three weight loss events at  $\sim 100^\circ\text{C}$ ,  $260\text{-}300^\circ\text{C}$  and  $\sim 500^\circ\text{C}$  corresponding to desorption of water, exothermic evolution of carbon dioxide and desorption of benzene.

The presence of water desorbed from the surface of the catalyst around  $100^\circ\text{C}$  is unlikely to be the result of the isomerisation reaction. The sample of catalyst dried in air showed a 5% weight loss corresponding to desorption of water however, the sample dried under an inert atmosphere showed a lower (2%) relative weight loss. Therefore the water lost at this temperature was due to moisture adsorbed from the atmosphere.

As hydrogen combustion does not contribute greatly to the weight loss it can be assumed that all of the weight lost between  $220\text{-}560^\circ\text{C}$  corresponded to loss of carbon from the surface. From this it can be calculated that 1/3 of the carbon introduced to the surface

through feed stream becomes strongly adsorbed and acts as a poison. It was also calculated that this equates to 1-2 aromatic compounds per potassium atom present on the surface. The product selectivity for catalysts shown in table 6.3 is 60-80% which is in agreement with the amount of carbon deposited on the surface of the catalyst throughout the reaction.

**Table 6.3: Product Selectivity for Loading Catalysts**

Catalyst Code	Cis-isomer (%)	Trans-isomer (%)	Cis:trans ratio
P2026	10.8 ± 2.0	78.0 ± 2.5	1:7
P2023	6.0 ± 0.4	65.6 ± 4.3	1:10
P2027	11.6 ± 1.3	79.4 ± 3.0	1:7
P2019	12.4 ± 2.6	71.1 ± 7.7	1:6

Heat flow data for the sample of catalyst P2023 dried in the glove box is shown in figure 6.9.

**Figure 6.9: TGA-DSC analysis of Catalyst P2023 from Glove box**

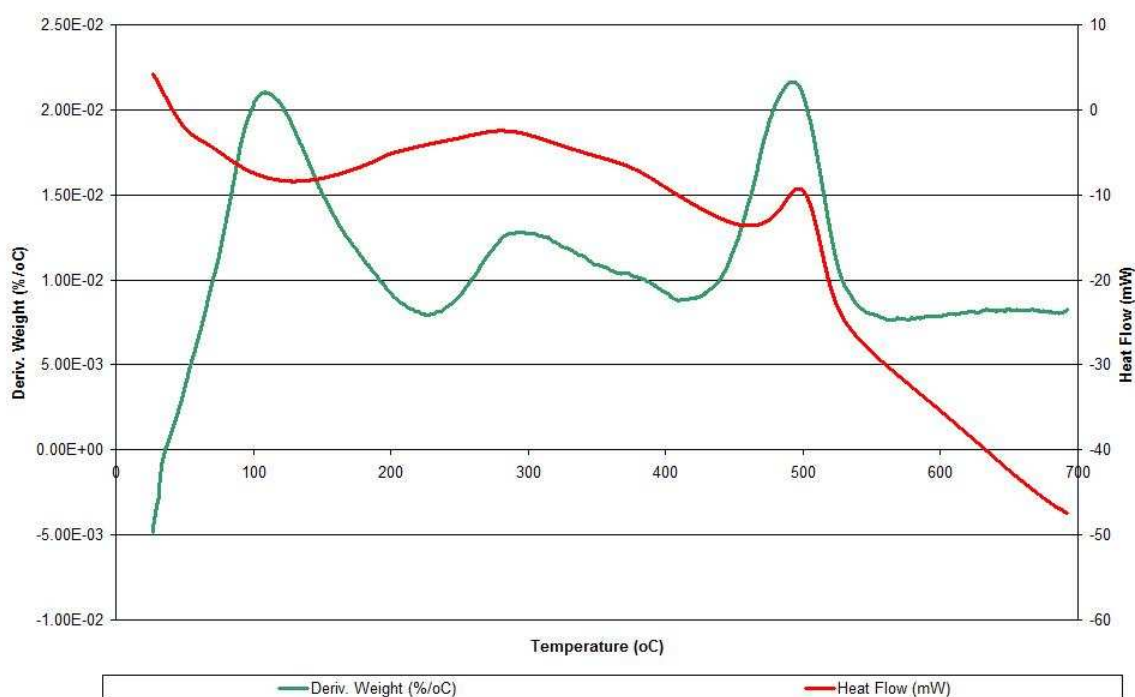


Figure 6.9 shows two exothermic weight loss events at 280 and 495°C. At both of these temperatures there is an overlap in the evolution of carbon dioxide and desorption of water. Aliphatic fragments, such as propane, were not observed in mass spectrometry but as carbon dioxide was evolved at both a low temperature (280°C) and a high temperature (495°C) it is likely that the lower temperature evolution corresponded to the combustion of aliphatic fragments and the high temperature the combustion of aromatic fragments.

For the sample of catalyst P2023 analysed post-reaction after being dried in air, the only significant difference was the increased weight loss corresponding to water desorption. It follows that the main contributing factor for the presence of water on the surface of the catalyst is water adsorbed from the atmosphere.

## **6.3 Deactivation**

### **6.3.1 Poisoning**

Desorption of benzene, detected by mass spectroscopy, was evidence of chemisorbed aromatic reactant/product present on the catalytic surface. Previous studies of cracking patterns for various alkylbenzenes [85, 86] showed that benzene was not a predominant fragment. It is therefore unlikely that benzene was observed in mass spectrometry data was a result of fragmentation of either allylbenzene or methylstyrene products. Instead it is likely that benzene was present on the surface of the catalyst as a result of the isomerisation reaction. It was also found that the higher the concentration of allylbenzene the more the catalyst's activity was inhibited. The rate of reaction was found to be inversely proportional to the concentration of the reactant and a negative order of reaction in allylbenzene was determined. However, the exact identity of the poison was not identified through this study.

The introduction of a guard bed to the system improved the catalyst efficiency in the early time on stream. However, the catalyst still displayed a rapid deactivation over the 120 minutes. It is suggested that the guard bed served to trap contaminants present in the reactant itself [100]. Common contaminants in hydrocarbons include chlorides and sulphides [100]. By removing these contaminant molecules with the guard bed the initial

conversion rate for allylbenzene was high. As the reaction proceeded however the aromatic reactant/products poisoned the surface. Resulting in a similar deactivation.

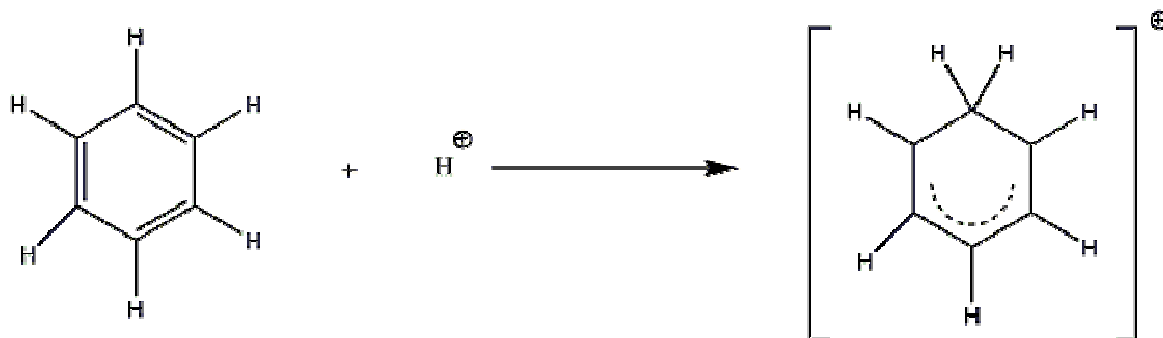
### 6.3.2 Coke Formation

Aromatic molecules are known for their coke forming tendencies [101] and a study conducted by Voge et al. [102] reported a direct relationship between the aromatic content of the feed solution and the amount of coke deposited on a silica-alumina catalyst.

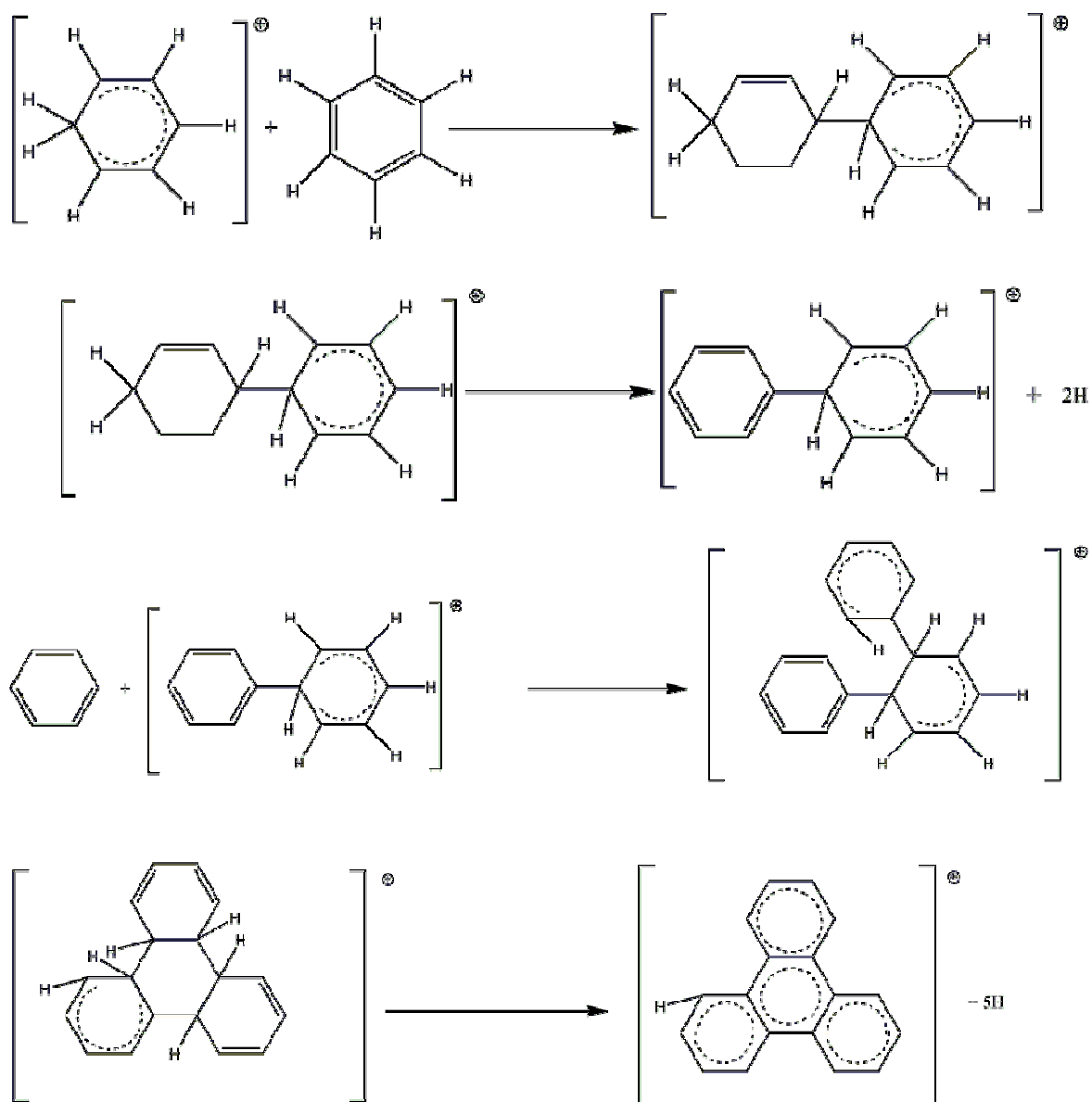
Gates et al. [103] devised a mechanism for coke formation, which consisted of the reaction of benzene to higher hydrocarbons. The mechanism was similar to addition polymerisation and is shown below. It consists of an initiation step, propagation and termination steps via carbonium ions.

**Figure 6.10: Proposed mechanism for coke formation**

Initiation:

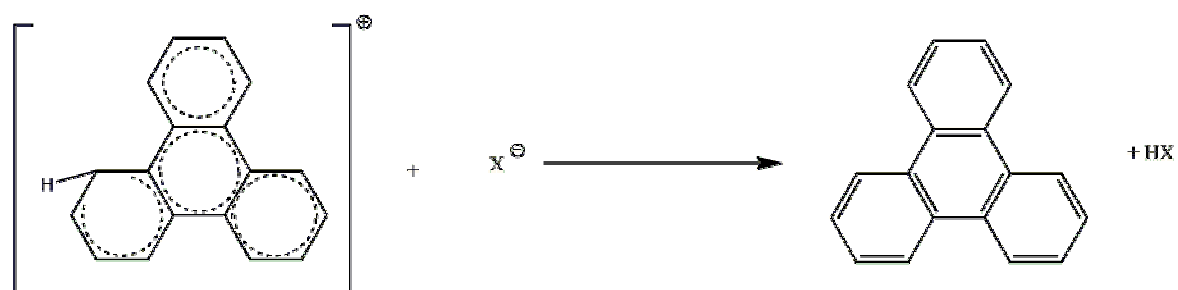


Propagation:



And so forth.

Termination:



A mechanism like this suggests that coke precursors are molecules present in the feed solution. Through a process of polymerisation or dehydrogenation reactions, larger

polynuclear aromatic intermediates are formed. These intermediates are characteristic of structures determined by x-ray examination of coke [104].

It is unlikely that a process such as this could occur as it requires the use of an acid and the generation of a carbonium intermediate. However base catalysed isomerisation of aromatic alkenes has been reported to proceed via anionic intermediates [1, 9, 10, 11, 17, 70]. Hence it is feasible that a similar mechanism, involving a base and the generation of carbanions could occur.

BET analysis showed that there was a significant decrease in the total surface area of the catalyst through the reaction. Table 6.4 shows the surface area measurements for catalyst P2023 prior to reaction and post reaction.

**Table 6.4: Surface area measurements for Catalyst P2023**

Catalyst P2023	Surface Area ( $\text{m}^2\text{g}^{-1}$ )	Pore Diameter (nm)	Pore Volume ( $\text{cm}^3\text{g}^{-1}$ )
pre-reaction	149	9.16	0.34
Post-reaction	112	11.70	0.33

Coke formation is a process that often reduces the surface area of a catalyst. Polymerisation of aromatic intermediates can cause rapid pore blockage and loss of surface area [105] which is in agreement with the results obtained through BET analysis. It is likely that coke formation is the reason for a reduction in surface area post reaction. TGA-DSC data showed three evolutions which corresponded to aliphatic combustion ( $280^\circ\text{C}$ ), desorption of benzene ( $\sim 500^\circ\text{C}$ ) and combustion of an aromatic species at high temperature ( $\sim 500^\circ\text{C}$ ). This data supports the formation of coke on the surface of the catalyst.

## 6.4 Regeneration

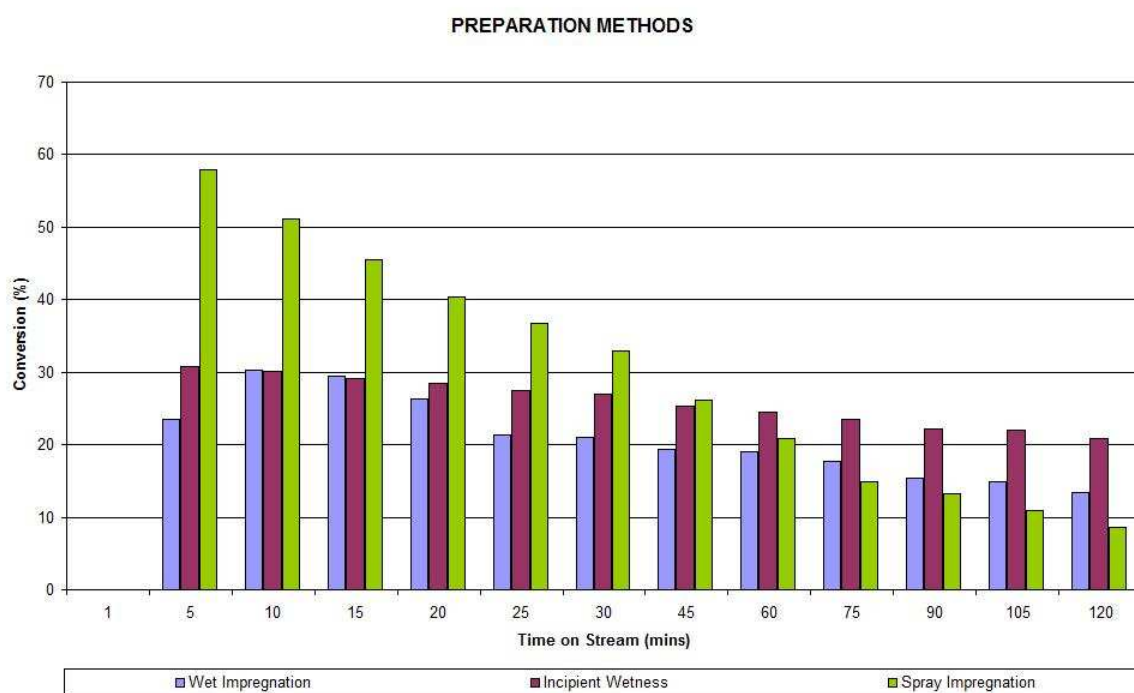
To investigate regeneration of the catalyst, firstly the system was flushed with toluene to remove any excess reactant molecules and subsequently heated to  $500^\circ\text{C}$  under an  $\text{O}_2/\text{Ar}$  gas mixture. This process served to regenerate the catalyst to an activity similar to that of

the first use. Analysis of the TGA data showed two exothermic weight loss events (280, ~500°C) thought to be the combustion of aliphatic and aromatic hydrocarbons respectively. These results reinforce the belief that carbon lay-down is a significant cause of catalyst deactivation.

## 6.5 Preparation Methods

The method by which the catalyst was prepared was found to have a significant effect on the catalyst activity. Figure 6.11 shows the conversion of allylbenzene against time on stream for each of the catalysts.

**Figure 6.11: Conversion of Allylbenzene against time on stream for P2008, P2015 and P2030**



Catalyst P2030 was prepared by spray impregnation and was found to provide the highest conversion of allylbenzene. However, this catalyst also exhibited the fastest deactivation. This can be interpreted as follows. Spray impregnation should produce a highly dispersed surface coating of active phase. This would allow for high conversion in the early stages of the reaction due to a high available catalytic surface. However, the catalyst will rapidly become deactivated as the easily accessible catalytic surface becomes poisoned by strongly adsorbed aromatic species.

Catalyst P2008 exhibited a much slower deactivation than that of catalyst P2030. Wet impregnation allowed for deposition of potassium carbonate active phase within the pores of the support material. This means that the rate at which the catalytic area became poisoned was much slower as it is less accessible than that of catalyst P2030. This is also reflected in the surface area measurements for the catalysts shown in table 6.5.

**Table 6.5: Surface Area Measurements**

Catalyst Code	Supplier Code	Appearance	Preparation Method	Nominal K <sub>2</sub> CO <sub>3</sub> loading (% w.w)	Surface Area (m <sup>2</sup> g <sup>-1</sup> )
P2008	Condea M-1206	0.8mm diameter extrudate pellet	Wet Impregnation	15	149
P2015	Condea M-1206	0.8mm diameter extrudate pellet	Incipient Wetness	15	133
P2030	Condea M-1206	0.8mm diameter extrudate pellet	Spray Impregnation	15	134

Catalysts P2008 and P2015 exhibited a similar rate of deactivation however P2015 was a poorer catalyst producing low conversion of allylbenzene and low product selectivity as shown in table 6.6.

**Table 6.6: Product Alkene Selectivity**

Catalyst Code	Cis-isomer (%)	Trans-isomer (%)	Cis:trans ratio
P2008	7.7 ± 1.0	77.7 ± 2.1	1:10
P2015	3.5 ± 0.4	35.5 ± 4.9	1:10
P2030	8.0 ± 1.1	61.8 ± 2.2	1:8

There was significant mass loss during the reaction involving P2015 however no other liquid products were detected by gc analysis. Poor dispersion may be the cause of the low conversion and carbon transfer to support material may be the cause of low product selectivity. The rate of deactivation of this catalyst was steady and the slowest of the three catalysts. The distribution of potassium carbonate through the support material pellets can vary due to several factors [59]. These include the impregnation method, strength of

adsorption and the reactions that occur upon heating and drying. Wicking, or the movement of a liquid through porous material, can cause deposition of active phase within the pores of the support material. Thus, producing a catalyst that would exhibit low conversion due to diffusion limitations and a slow deactivation as the surface of the catalytic surface is less accessible than that of an immediate outer coating (like that of catalyst P2030).

In conclusion, the preparation method used has a significant effect on both the activity and selectivity of the catalyst. Spray impregnation produced a catalyst that allowed for high conversion in the early stages but rapidly deactivated. Although catalysts prepared by means of wet impregnation exhibited a lower conversion, they deactivated much slower than the catalyst prepared by spray impregnation.

## 6.6 K<sub>2</sub>CO<sub>3</sub> Loading

The optimum K<sub>2</sub>CO<sub>3</sub> loading appeared to be 15%. This allowed for reasonable surface area, moderate conversion and high product selectivity. Lower loadings did not allow for a large enough surface area and higher loadings caused pore blockage leading to low conversions and high rates of deactivation. Table 6.7 shows the surface area measurements obtained for the catalysts involved in this comparison.

**Table 6.7: Surface area measurements for % K<sub>2</sub>CO<sub>3</sub> catalysts**

Catalyst Code	Supplier Code	Preparation Method	Nominal K <sub>2</sub> CO <sub>3</sub> loading (% w/w)	Surface Area (m <sup>2</sup> g <sup>-1</sup> )
P2026	Condea M-1206	Incipient Wetness	12	164
P2023	Condea M-1206	Incipient Wetness	15	149
P2027	Condea M-1206	Incipient Wetness	18	167
P2019	Condea M-1206	Incipient Wetness	20	102
P2013	Engelhard AL-3992-E	Incipient Wetness	15	130
P2017	Engelhard AL-3992-E	Incipient Wetness	20	104

In relation to the surface area of alumina (taken to be ~200m<sup>2</sup>g<sup>-1</sup>) and assuming there to be 10-15 hydroxyl groups per nm<sup>2</sup> of alumina [77] then monolayer coverage was calculated to be within the range of 15±3%. It was found that 20% loading was greater than the weight required to achieve monolayer coverage and produced catalysts with low activity for the reaction.

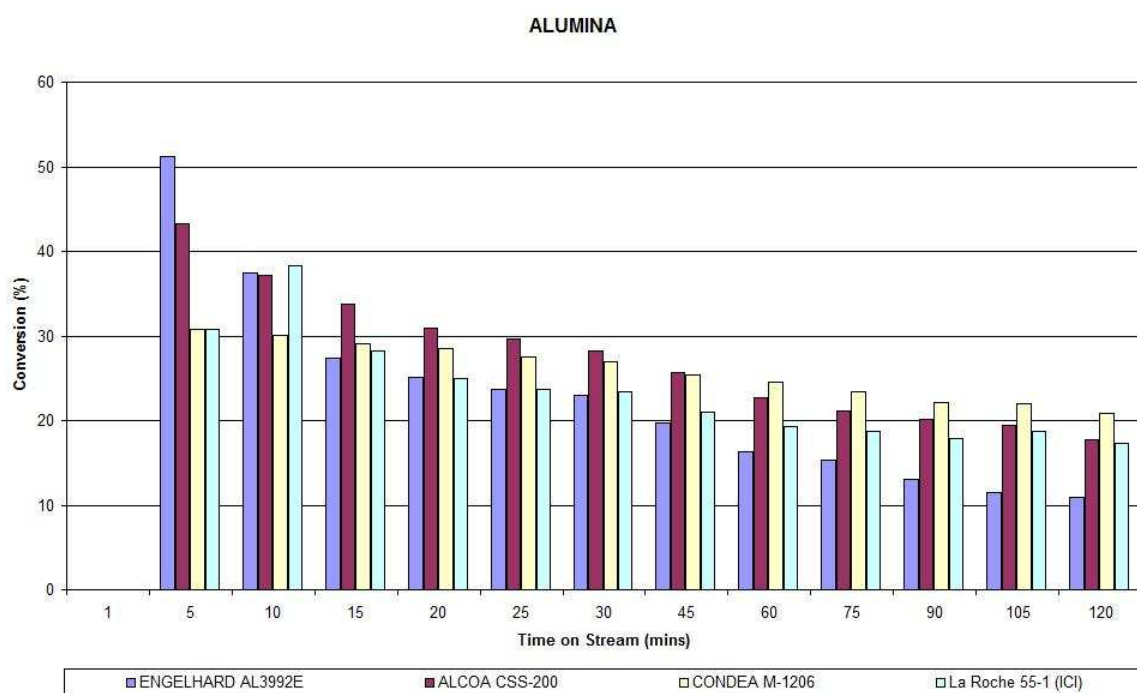
## 6.7 Alumina Supplier

Reactions were conducted to investigate the effect that the commercial alumina had on the activity of the catalyst. Table 6.8 shows the surface area measurements for catalysts and the alumina support, while figure 6.12 shows the conversion of allylbenzene against time on stream for each of the catalysts.

**Table 6.8: Surface area measurements for Alumina Supplier Catalysts**

Catalyst Code	Supplier Code	Appearance	Surface Area of catalyst ( $\text{m}^2\text{g}^{-1}$ )	Surface Area of alumina ( $\text{m}^2\text{g}^{-1}$ )
P2013	Engelhard AL-3992-E	3.2mm diameter extrudate pellet	130	186
P2014	Alcoa CSS-200	3.2mm diameter sphere	128	201
P2015	Condea M-1206	0.8mm diameter extrudate pellet	133	220
P2016	La Roche 55-1 (ICI)	3.2mm diameter sphere	188	313

**Figure 6.12: Conversion of Allylbenzene against time on stream**



The catalyst prepared using Engelhard AL-3992E (P2013) exhibited the greatest conversion of allylbenzene. The catalyst prepared using Alcoa CSS-200 exhibited the second highest initial conversion and the other catalysts showed lower but similar conversions.

If the surface area of the catalyst is considered in relation to the surface area of the alumina support the following ratios are determined.

**Table 6.9: Surface area catalyst: surface area of alumina**

Catalyst Code	Supplier Code	Surface Area of catalyst ( $\text{m}^2\text{g}^{-1}$ )	Surface Area of alumina ( $\text{m}^2\text{g}^{-1}$ )	Surface Area ratio
P2013	Engelhard AL-3992-E	130	186	0.70
P2014	Alcoa CSS-200	128	201	0.64
P2015	Condea M-1206	133	220	0.60
P2016	La Roche 55-1 (ICI)	188	313	0.60

The ratio of surface areas may serve as a crude indication of active phase dispersion. A monolayer dispersed catalyst should result in a minimum effect on surface area, hence giving a high ratio, whereas large particles have the potential to pore block and so a lower surface area would be measured. The results in figure 6.12 support this interpretation. Catalyst P2013 has the largest surface area ratio and hence should have the highest dispersion of active phase and so activity: this is indeed the case. In fact the activity and the surface area ratio fall in tandem suggesting a *prima facie* link between the ratio and activity. Further work on active phase dispersion would be needed to confirm this hypothesis.

The Engelhard Al-3992E (2013) catalyst exhibited the fastest deactivation whereas the other catalysts exhibited relatively low deactivation rates. This is also in keeping with the proposed relationship between activity and surface:bulk ratio as the more accessible the catalytic area, the faster it can become poisoned by adsorbed aromatic species.

Table 6.10 shows the product alkene selectivity for each catalyst.

**Table 6.10: Product Alkene selectivity for Alumina Supplier Catalysts**

Catalyst Code	Cis-isomer (%)	Trans-isomer (%)	Cis:trans ratio
P2013	8.2 ± 1.2	77.1 ± 2.1	1:9
P2014	4.2 ± 0.8	37.1 ± 10.9	1:8
P2015	3.5 ± 0.4	35.5 ± 4.9	1:10
P2016	4.0 ± 1.0	31.1 ± 9.8	1:7

Catalyst P2013 exhibited high product alkene selectivity (~80%), however all other catalysts exhibited a poor selectivity of below 40% and no other liquid products were detected through gc analysis. The lower product selectivity exhibited by catalysts P2014, P2015 and P2016 could be due to carbon transfer to alumina support, given that they do not show rapid deactivation even though they have significant carbon lay-down.

## 6.8 Caesium

The activity and selectivity of a 15% Cs<sub>2</sub>CO<sub>3</sub>/alumina catalyst was compared with a 15% K<sub>2</sub>CO<sub>3</sub>/alumina catalyst to investigate the effect of basicity of catalyst on the conversion of allylbenzene.

Caesium carbonate finds application as a base [106] and the strength of its basic sites are said to be stronger than those of potassium carbonate [18]. In a previous study [12], a direct relationship between the conversion of allylbenzene and the basicity of the catalyst followed the order Cs-X > Rb-X > K-X > Na-X. The order of basicity agreed with that reported by IR [107], XPS [108] and basicity spectra [109] for these solids.

The caesium carbonate on alumina catalyst used in this study showed significant activity for the isomerisation of allylbenzene, however an overall lower conversion of allylbenzene to cis/trans products. In addition, the caesium carbonate catalyst used was found to deactivate very quickly with time on stream. Deactivation constants suggest twice as quickly as the corresponding potassium carbonate catalysts.

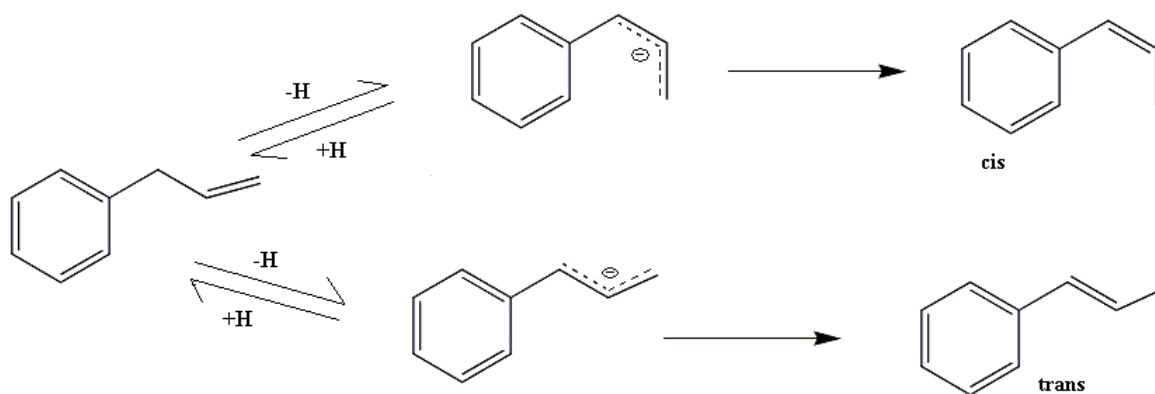
Caesium carbonate and potassium carbonate catalysts with 15% weight loading were compared however; this did not take into consideration the difference in atomic weight between potassium and caesium. In fact, caesium carbonate on alumina is a more active catalyst than potassium carbonate on alumina catalyst for the isomerisation of allylbenzene. Although the caesium catalyst in this study exhibited a much lower conversion and higher deactivation, than that of the potassium carbonate catalyst, it is more effective. If the catalysts are compared on the basis of conversion per number of atoms of potassium and caesium, then the caesium catalyst with less than a third of the atoms than that of the potassium catalyst, produces a higher conversion per atom than the potassium catalyst. The direct relationship between basicity and conversion is in agreement with previous studies [12] and analysis [107-109].

## **6.9 Product Distribution**

For all reactions, a mixture of cis- and trans- $\beta$ -methylstyrene was produced. Although product selectivity varied somewhat between catalysts the trans-isomer was formed predominantly over all catalysts.

Kishore and Kannan observed a similar tendency through the use of MgAl-4HT in the isomerisation of estragole to anethole [14]. It was reported that the trans-isomer was produced as it exhibits strong thermodynamic stability. However, in previous studies involving alkenes, such as butene [11, 70] and pentene [31] it is the cis-isomer that is the predominant product. It is therefore suggested that the presence of the aromatic ring has an effect on the product ratio. The isomerisation of an aromatic alkenyl involves double bond migration to a position conjugated to the benzene ring. This occurs via an anionic intermediate as shown in figure 6.13.

**Figure 6.13: Isomerisation of allylbenzene via anionic intermediate**



With aliphatic alkenes it has been proposed that the stability of the cis-form anionic intermediate promotes the formation of the cis-isomer product however this currently awaits theoretical confirmation [110.] The formation of the trans-isomer indicates that the thermodynamic stability of this isomer controls the outcome of the reaction, suggesting that conjugation of the benzene ring with the anionic intermediates brings their energy closer together to allow the final state thermodynamics to dominate.

Taskinen and Lindholm performed a study of the relative thermodynamic stabilities of the isomeric propenylbenzenes [111]. The composition of the equilibrium mixtures of allylbenzene, cis- $\beta$ -methylstyrene and trans- $\beta$ -methylstyrene showed a 3:97 ratio of cis:trans- $\beta$ -methylstyrene. A study by Ela and Cram [112] reported a cis:trans ratio of 5:95. During the course of this study a product ratio no lower than 1:6 and no higher than 1:10 cis:trans was obtained. Hence thermodynamic equilibrium was not reached during the reactions performed in this study.

## 6.10 Future Work

Many aspects of this study require further research and in this section some areas are highlighted and the method by which the area could be studied is suggested.

#### **i. Preparation Method**

There was significant carbon transfer during the reaction involving catalyst P2015; prepared by incipient wetness. More extensive study is required to investigate the apparent loss of carbon from the system.

#### **ii. Alumina Supplier**

There may be a relationship between surface area ratio and conversion of allylbenzene. Further study of this possible relationship is required including investigation of site density.

#### **iii. Caesium**

Further study is required into the relationship between basicity and conversion. A fairer comparison of catalysts on an atomic weight level would serve to further investigate the order of basicity and the conversion of allylbenzene.

#### **iv. Deactivation**

In depth study of the process of catalyst deactivation is another area of interest. Future work could involve distinguishing the aromatic poison involved in the isomerisation reaction. Further reactions involving firstly product feed stock used to wet the catalyst bed. After sufficient wetting, allylbenzene feed solution should be contacted with the catalyst bed. If the catalyst exhibits an activity similar to that of a catalyst that had only been in contact with allylbenzene then it is unlikely that the product material is acting as the poison.

## 7. CONCLUSIONS

Isomerisation of allylbenzene can be performed at 50°C over an activated  $K_2(CO_3)$ /alumina catalyst. The way in which the catalyst was prepared had a significant effect on the activity of the catalyst.

Wet impregnation was found to produce a catalyst that has a high surface area but the nature of the method allowed for active phase to penetrate to pores. Spray impregnation was found to give the highest conversion of allylbenzene however the available surface area rapidly became poisoned.

The optimum loading was ~ 15 % w/w  $K_2(CO_3)$  . This produced the highest conversion of allylbenzene whereas a lower loading produced a lower conversion of allylbenzene. Higher loadings led to pore blocking and low surface areas, which caused an overall low conversion and a fast deactivation.

Alumina supplier had a significant affect on the product selectivity. It was found that the highest product selectivity was obtained through the use of Engelhard AL-3992E alumina support material. All other support materials produced catalysts that exhibited low product selectivity (35-40%) however no other liquid phase products were detected. In addition it was found that there may be a relationship between surface area ratio and the conversion of allylbenzene.

It was found that the catalyst could be regenerated producing conversions close to that of the catalyst during first use. It was also found that aromatic reactant/products were acting as poisons restricting access to active sites. Identification of the specific aromatic species acting as the poison was not possible during this study and would require further study. There was also evidence for the formation of coke on the surface of the catalyst.

Calcination of the catalyst was found to cause firstly dehydration of the catalyst followed by the decomposition of some of the carbonate species. Similarly, activation caused dehydration and decomposition of carbonate producing potassium oxide on the surface. It is thought that this is the source of some of the basic sites involved in the catalytic process.

Investigation of the concentration of feed solution used allowed for the determination of fundamental kinetic parameters. It was found that the reaction exhibits a negative first order with respect to the concentration of allylbenzene.

It is well known that strong alkaline bases catalyse the double bond migration in alkenes [11, 18, 19, 25, 37]. The use of solid bases over the use of liquid bases, such as KOH solution [2-7], provides an environmentally benign method of obtaining a mixture of cis/trans products. Acid catalysis of this type of transformation is said to produce a cis:trans ratio of near one [21]. In cases where one isomer is industrially more useful, a method that produces predominantly one over the other is favourable [12]. The isomerisation of alkenes such as pentene [37] and butene [25] over solid base catalysts produces a ratio in favour of the kinetic product: the cis isomer [9]. Interestingly, the isomerisation of aromatic alkenyl compounds over solid base catalysts produces a cis:trans ratio in favour of the thermodynamically stable trans isomer [1].

As this is the first systematic study of the isomerisation of allylbenzene many aspects require further work. This could include surface density study, a more intensive study of caesium carbonate catalysts in comparison to potassium carbonate of equal atomic weights and the deactivation of these catalysts also requires more intensive research.

## 8. REFERENCES

- [1] C. M. Jinesh, Churchill A. Antonyraj, S. Kannan, *Catalysis Today*, 141, (2009), 176-181
- [2] T. F. West, *J. Soc. Chem. Ind.*, 59, (1940), 275
- [3] F. Tiemann, *Ber.*, 24, (1891), 2872
- [4] A. Eborn, C. Trey, *Ber.*, 27, (1891), 2455
- [5] M. Palgi, *zhur. Obsch. Khim.*, 28, (1958), 2239
- [6] R. Horiuchi, *J. Chem. Soc., Japan*, 45, (1925), 209
- [7] R. H. Boots, *Brit.* 271, (1926), 819
- [8] US Patent 5750457
- [9] K. Tanabe, M. Misono, Y. Ono, H. Hattori, *New Solid acids and Bases their catalytic properties*, Amsterdam: Elsevier, (1989), 28
- [10] T. Baba, *Catalysis Surveys from Japan*, 4, (2000), 17-29
- [11] M. G. Stevens, H. C. Foley, *Chem. Comm.*, (1997) 519-520
- [12] V. K. Srivastava, H. C. Bajaj, R. V. Jasra, *Catal. Comm.* 4 (2003) 543-548
- [13] Y. Li, Z. Sun, L. Zhao, Y. Xu, *Appl. Biochem. Biotech.* 125, 1 (2005), 1-10
- [14] D. Kishore, S. Kannan, *Appl. Catal. A: Gen.* 270, (2004), 227-235
- [15] C.H. Bartholomew, *Appl. Catal. A: Gen.*, 212, (2001), 17-60

- [16] K. Bauer, D. Garbe, H. Surberg, Ullmann Encyclopedia of Industrial Chemistry, Electronic Release, 6<sup>th</sup> Edition, (2002)
- [17] US Patent 4138411
- [18] H. Hattori, Chemical review, 95, (1995), 537-558
- [19] H. Pines, J. A. Vesely, V. N. Ipatieff, J. Am. Chem. Soc., 77, (1955), 347-348
- [20] W.O. Haag, H. Pines, J. Am. Chem. Soc., 82, (1960), 387-391.
- [21] A. Beres, I. Hannus and I. Kiricsi, React. Kinet. Catal. Lett. 56, 1, (1995), 55-61
- [22] R. A. Sheldon, Chem. Ind. 1 (1997) 12; R. A. Sheldon, in: R. A. Sheldon, H. van Bekkum (Eds.), Fine Chemicals through Heterogeneous Catalysis, Wiley-VCH, Weinheim, (2001)
- [23] W. F. Hoelderich, D. Heinz, Catalysis 14 (1999) 149; W. F. Hoelderich, M. Hesse, F. Navmann,, Angew. Chem. Int. Ed. Engl. 27 (1998) 226; W. F. Hoelderich, J. Rosler, G. Heitmann, A. T. Liebens, Catal. Today 37, (1997), 353
- [24] E.J. Dostkocil, S. Bordawekar, R.T. Davis. In: Catalysis 15, Royal Soc. of Chemistry, Cambridge, UK (2000), 40
- [25] G. Kuriakose, N. Nagaraju Journal of Molecular Catalysis A: Chemical 223, 1-2, (2004), 155-159
- [26] P.B. Venuto, Miropor. Mater. 2, (1998), 297
- [27] M. E. Davis, Miropor. Mesopor. Mater. 21, (1998), 12657
- [28] S. E. Sen, S.M. Smith, K.A. Salivan, Tetrahedron 55, (1998), 12657
- [29] G. J. Kelly, F. King, M. Kett Green Chemistry, 4, (2002), 392–399

- [30] Y. Ono, *J. Cat.*, 216, (2003), 406-415
- [31] H. Tsuji, H. Kabashima, H. Kita, H. Hattori, *React. Kinet. Catal. Lett.*, 56, 2, (1995), 363-369.
- [32] I. Al-Maskery, K. Girling, S. D. Jackson, L. Pugh, R. R. Spence, accepted for publication *Topics in Catalysis*, (2010)
- [33] G.C. Bond, *Heterogeneous catalysis principles and applications*, Oxford University Press, London, (1974), 6
- [34] <http://www.chemguide.co.uk/physical/basicrates/catalyst.html>
- [35] J.M. Thomas, W.J. Thomas, *The Principles and Practices of Heterogeneous Catalysis*, Wiley-VCH, Germany, (1997), 1
- [36] R.L. Augustine, *Catalytic Hydrogenation: techniques and applications in organic synthesis*, E Arnold, London, (1965), 23.
- [37] <http://www.spaceflight.esa.int/impress/text/education/Catalysis/index.html>  
6/07/10
- [38] R. L. Augustine, *Heterogeneous catalysis for the synthetic chemist*, CRC Press (1996), 241.
- [39] B. Chen, U. Dingerdissen, J.G.E. Krauter, H.G.J. Lansink Rotgerink, K. Moëbus, D.J. Ostgard, P. Panster, T.H. Riermeier, S. Seebald, T. Tacke, H. Trauthwein, *Applied Catalysis A: General* 280 (2005) 17–46
- [40] S. Nishimura, *Handbook of Heterogeneous Catalytic Hydrogenation for Organic Synthesis*, Wiley, New York, (2001)
- [41] US Patent 3692692
- [42] Fengyu. Zhao<sup>a,b,c</sup>, Rong Zhang<sup>b</sup>, Maya Chatterjee<sup>b</sup>, Yutaka Ikushima<sup>b,c</sup>, and Masahiko Araie<sup>d</sup> *Prepr. Pap.-Am. Chem. Soc., Div. Fuel Chem.* 49, (1), (2004), 14

- [43] A. S. Al-Ammar, G. Webb *J. Chem. Soc., Faraday Trans. 1*, 74, (1978), 195 - 205
- [44] US Patent 6841085
- [45] S. D. Jackson, G. J. Kelly, G. Webb, *J. Catal.*, 176, 1, (1998), 225-234
- [46] D. J. C. Yates, W. F. Taylor, J. H. Sinfelt, *J. Am. Chem. Soc.*, 86, 15, (1964), 2996–3001
- [47] J.H. Clark, *Catalysis of Organic Reactions by Supported Inorganic Reagents*, VCH Publishers Inc., Germany, (1994), 5, 29, 39
- [48] US Patent 5102855
- [49] J. M Thomas, *Sci. Am.* 266, (1992), 112
- [50] US Patent 4602119
- [51] H. R. Shaterian; F. Khorami; A. Amirzadeh; M. Ghashang; A. Hosseinian; Phosphorus, Sulfur, and Silicon and the Related Elements, 183, 10 (2008), 2584 – 2595
- [52] S.D. Jackson, J.S.J. Hargreaves, *Metal Oxides*, Vol. 1 Wiley-VCH (2009)
- [53] S. M. A. M. Bouwens, J. P. R. Vissers, V. H. J. de Beer and R. Prins, *J. Catal.* 112, 2, (1988), 401-410
- [54] <http://www.bza.org/zeolites.html> 14/6/10
- [55] C. Stefanadis, B. C. Gates, *J. Molec. Catal.* 67, 3, (1991), 363-367
- [56] W. W. Kaeding, C. Chu, L. B. Young, S. A. Butter *J. Catal.* 69, 2, (1981), 392-398
- [57] A. Corma, *Chem. Rev.* 95 (1995), 559
- [58] US Patent 6462247

- [59] C. N. Satterfield, *Heterogeneous Catalysis in Practice*, McGraw-Hill Inc. (1980), 1, 14
- [60] L. L. Hegedus, E. E. Petersen, J. Catal. 28, 1, (1973), 150-156
- [61] J. P. Giannetti, R. T. Sebulsky *Ind. Eng. Chem. Prod. Res. Dev.*, 8, 4, (1969), 356–361
- [62] J. Hagen, *Industrial catalysis: a practical approach*, Wiley-VCH (2006), 199
- [63] G.C. Bond, *Appl. Catal. A: General*, 149, (1997), 3-25
- [64] P.G. Menon, *J. Molec. Catal.* 59, (1990), 207-220
- [65] <http://herkules.oulu.fi/isbn9514269543/html/x546.html> 08/05/10
- [66] J. J. Spivey, *Catalysis*, Royal Society of Chemistry, (2000), 45-46
- [67] L. P. Hammett, *Physical Organic Chemistry*, McGraw-Hill, New York, (1940)
- [68] D. J. Cram, *Fundamentals of Carbanion Chemistry*, Academic Press, New York/London, (1965)
- [69] H. Handa, Y. Fu, T. Baba, Y. Ono, *Catal. Lett.* 59, (1999), 195-200
- [70] T. Yamaguchi, J-H. Zhu, Y. Wang, M. Komatsu, M. Ookawa, *Chem. Lett.* (1997), 898
- [71] L. Giroux, M. H. Back *Chemical Physics Letters*, 154, 6, (1989), 610-612
- [72] P. D. N. Svoronos, T. J. Bruno, *Ind. Eng. Chem. Res.* 41 (22), (2002), 5321–5336
- [73] Y. Amenomiya, G. Pleizier, *J. Catalysis*, 76, (1982), 345-353.
- [74] M. Kantschewa, E. V. Albano, Gerhard ERTL and Helmut Knozinger, *Applied Catalysis*, Elsevier Science Publishers B.V., Amsterdam, 8 (1983) 71-84.

- [75] R. Dotzel, M. Reif, E. Klemm, *Stud. Surf. Sci. Cat.* 130, (2000), 2243-2248
- [76] R. M Levy, D.J. Bauer, *J. Catalysis*, 9, (1967), 76-86.
- [77] I. Chorkendorff, J.W. Niemantsverdriet, *Concepts of Modern Catalysis and Kinetics*, WILEY-VCH Verlag GmbH & Co. KGaA, Germany, (2007), 194, 189.
- [78] US Patent 7341773B
- [79] H. Pines, W. M. Stalick, *Base-Catalysed Reactions of Hydrocarbons and related compounds*, Academic press, New York (1977)
- [80] M. Campanati, G. Fornasari, A. Vaccari, *Catalysis today*, 77, (2003), 299-314.
- [81] J. T. Richardson, R. Scates, M.V. Twigg, *Applied Catalysis A: General*, 246, (2003), 137-150.
- [82] M.H. Al-Dahhan, Y.Wu, M.P. Dudukovic., *Ind. Eng. Chem. Res.* 34 (1995), 741-747.
- [83] M.H. Al-Dahhan, M.P Dudukovic. *AIChE J.*, 42 (1996), 2594-2606
- [84] R. Dotzel, *Die heterogen katalysierte Isomerisierung von propadien zu Methylacetylen in der Flüssigphase*, Verlag Dr. Hut, München (2006) 137-139
- [85] D. H. Williams, I. Fleming, *Spectroscopic Methods in Organic Chemistry*, McGraw-Hill, London, (1995), 189
- [86] V. Švob, D. Deur-Šiftar, *J. Chromatography*, 91, (1974), 659-675
- [87] <http://webbook.nist.gov/cgi/cbook.cgi?Source=1951ROB/JES11-17&Units=SI&Mask=1EFF#Mass-Spec> 14/07/10
- [88] O. Knacke, baschewski, K. Hesselmann (Eds.), *Thermochemical Properties of Inorganic Substances*, I, 2nd edn., Springer-Verlag, Heidelberg, (1991)

- [89] R.E. Mills, R.T. Coyle, *Thermochim. Acta* 124, (1988), 89–98
- [90] A. Reisman, *J. Am. Chem. Soc.* 80(1958), 3558–3561
- [91] W.H.J. Stork, G.T. Pott, *J. Phys. Chem.*, 78, (1974), 2496-2506
- [92] <http://www.ijvs.com/volume2/edition3/section3.html#jackson> 12/6/10
- [93] A.R. Davis, B.G. Oliver, *Journal of Solution Chemistry*, 1, 4, (1972), 329-339.
- [94] B.G Oliver , A.R. Davis, *Can. J. Chem.* 51, (1973), 698-702.
- [95] J.B. Bates, M.H. Brooker, A.S. Quist, G.E. Boyd, *J. Phys. Chem.* 76, 11, (1972), 1565-1571.
- [96] H. Lee, J.K Wilmshurst, *Aust. J. Chem.* 17, (1964), 943-945.
- [97] S.C. Wait, A.T. Ward and G.J. Janz, *J. Chem. Phys.*, 4, (1966), 133-138.
- [98] J. D. Frantz, *Chemical Geology* 152, 3-4, (1988), 211-225
- [99] R. M. Levy and D. J. Bauer, *J. Catalysis*, 9, (1967), 76-86
- [100] US Patent 4721824
- [101] P.G. Menon, *J. Molec. Catal.* 59, (1990), 207
- [102] H. H. Voge, J. M. Good, B. J. Greensfelder, *Proc. World Pet. Congr.* 3<sup>rd</sup> 4 (1951), 124
- [103] B. C. Gates, J. R. Katzer, G.C. A. Schuit, *Chemistry of Catalytic Processes*, McGraw-hill, New York, (1979), 43
- [104] J. B. Butt, E. E. Petersen, *Activation, Deactivation and Poisoning of Catalysts*, Academic Press Inc. (1988), 97

- [105]** W. G. Appleby, J. W. Gibson, G. M. Good, *Ind. Eng. Chem. Process Des. Dev.* 1, (1962), 102-110,
- [106]** T. Flessner, S. Doye, *Journal für praktische Chemie*, 341, (1999), 186–190
- [107]** M. Huang, S. Kaliaguine, *J. Chem. Soc. Faraday Trans.* 88 (1992) 751
- [108]** L. Yang, Y. Aizhen, X. Qinhua, *Appl. Catal.* 67, (1991), 169
- [109]** M. Huang, S. Kaliaguine, A. Auroux, *Stud. Surf. Sci. Catal.* 97, (1995), 311-318
- [110]** S. Bank, A. Schriesheim and C. A. Rowe, Jr., *J Am Chem Soc.* 87, (1965), 3244
- [111]** E. Taskinen, N. Lindholm, *J. Phys. Org. Chem.* 7, (1994), 256-258
- [112]** S. W. Ela, D. J. Cram, *J. Am. Chem. Soc.* 1, (1966), 5791-5802